Applications in Energy and Combustion Science 16 (2023) 100201

Contents lists available at ScienceDirect

Applications in Energy and Combustion Science

journal homepage: www.elsevier.com/locate/jaecs

The reactor-based perspective on finite-rate chemistry in turbulent reacting flows: A review from traditional to low-emission combustion

Arthur Péquin [a,b,*], Michael J. Evans [c], Alfonso Chinnici [d], Paul R. Medwell [d], Alessandro Parente [a,b]

[a] Université Libre de Bruxelles, Aero-Thermo-Mechanics Laboratory, École Polytechnique de Bruxelles, Avenue F.D Roosevelt 50, Brussels, 1050, Belgium
[b] Université Libre de Bruxelles and Vrije Universiteit Brussel, Brussels Institute for Thermal-fluid Systems and Clean Energy (BRITE), Brussels, Belgium
[c] UniSA STEM, University of South Australia, Mawson Lakes, Australia
[d] School of Electrical and Mechanical Engineering, University of Adelaide, Adelaide, Australia

ARTICLE INFO

Keywords:
Reactor-based turbulence-chemistry models
Combustion modelling
Turbulence-chemistry interactions
Moderate or Intense Low-oxygen Dilution (MILD)
Eddy Dissipation Concept (EDC)
Partially Stirred Reactor (PaSR)

ABSTRACT

In flames, turbulence can either limit or enhance combustion efficiency by means of strain and mixing. The interactions between turbulent motions and chemistry are crucial to the behaviour of combustion processes. In particular, it is essential to correctly capture non-equilibrium phenomena such as localised ignition and extinction to faithfully predict pollutant formation. Reactor-based combustion models — such as the Eddy Dissipation Concept (EDC) or Partially Stirred Reactor (PaSR) — may account for turbulence-chemistry interactions at an affordable computational cost by calculating combustion rates relying upon canonical reactors of small fluid size and timescale. The models may include multiscale mixing, detailed chemical kinetic schemes and high-fidelity multispecies diffusion treatments. Although originally derived for conventional, highly turbulent combustion, numerous recent efforts have sought to generalise beyond simple empirical correlations using more sophisticated relationships. More recent models incorporate the estimation of scales based on local variables such as turbulent Reynolds and Damköhler numbers, phenomenological descriptions of turbulence based on fractal theory or specific events such as extinction. These modifications significantly broaden the effective range of operating conditions and combustion regimes these models can be applied to, as in the particular case of Moderate or Intense Low-oxygen Dilution (MILD) combustion. MILD combustion is renown for its ability to deliver appealing features such as abated pollutant emissions, elevated thermal efficiency and fuel flexibility. This review describes the development and current state-of-the-art in finite-rate, reactor-based combustion approaches. Recently investigated model improvements and adaptations will be discussed, with specific focus on the MILD combustion regime. Finally, to bridge the gap between laboratory-scale canonical burners and industrial combustion systems, the current directions and the future outlook for development are discussed.

1. Introduction

Future energy demands from fossil fuels will decrease according to the latest projections [1]. Such a scenario can be explained by high energy prices, concerns about energy security, and strengthened climate policies. Efforts in electrification and renewable energy sources will soon put non-renewable energies such as natural gas, oil and coal, into decline. Nevertheless, facing energy transition requires the development of clean and efficient combustion technologies as combustion will remain key for the industry sector, transportation, energy and heat production into the foreseeable future. Governmental policies make the reduction of emissions of carbon dioxide, CO_2, greenhouse gas such as methane, CH_4, and other pollutants, a priority. The deployment of renewable energy sources will continue to grow significantly. However, renewable energy production suffers from intermittency, i.e. periods of underproduction and overproduction. When the demand is fully covered, one option is for the excess energy to be used to produce synthetic fuels, i.e. synthetic chemical molecules, suitable for long term storage and transportation. The energy stored in from synthetic fuels can be released through clean combustion processes. Moderate or Intense Low-oxygen Dilution (MILD) combustion [2–4] is a promising combustion technology in terms of fuel flexibility, pollutant emissions,

* Corresponding author at: Université Libre de Bruxelles, Aero-Thermo-Mechanics Laboratory, École Polytechnique de Bruxelles, Avenue F.D Roosevelt 50, Brussels, 1050, Belgium.
E-mail addresses: Arthur.Pequin@ulb.be (A. Péquin), Alessandro.Parente@ulb.be (A. Parente).

https://doi.org/10.1016/j.jaecs.2023.100201
Received 16 April 2023; Received in revised form 25 July 2023; Accepted 1 September 2023
Available online 7 September 2023

and thermal efficiency. Traditional combustion systems rely on system-dependent solutions to ensure stability and reduce pollutant emissions, while fuel and load flexibility remains a difficult task. In MILD combustion, the thermo-chemical conditions are such that the formulation of pollutant species is prevented thanks to the intense internal recirculation of exhaust gases and the smoothed temperature and species gradients. Hot and recirculating combustion products preheat local reactant mixtures up to their auto-ignition temperature, leading to high thermal efficiencies and complete combustion. Relying on internal gas recirculation reduces the sensitivity of MILD systems to the type of fuel and operating conditions. A large variety of fuels, such as the synthetic fuels mentioned above, can be considered and so in a wide range of loads [5].

Combustion converts reactants to products and heat through chemical reactions. A prerequisite of combustion is mixing of fuel and oxidiser. Turbulent flames are usually preferred in practical applications as turbulence enhances mixing and flame surface augmentation by stretching. The complexity of turbulent motions may be represented as an energy spectrum composed of different length and time scales [6,7], such as the integral, the Taylor λ and the Kolmogorov η scales. When modelling flames, dealing with chemistry requires additional efforts as chemical processes are associated with timescales differing by several orders of magnitudes [8], i.e. from fast reactions of radicals species ($\sim 10^{-9}$ s) to the slow formation of nitrogen oxides NOx or soot ($\sim 10^{-2}$ s).

To help classify flames, non-dimensional numbers are introduced by comparing respective scales such as the Reynolds (Re) number that evaluates the turbulence intensity level, the Damköhler (Da) number that compares the respective scales of turbulence and chemistry or the Karlovitz (Ka) number that contrasts the characteristic scale for chemistry against the turbulent dissipating scales. As far as combustion modelling is concerned, assumptions can be made on the non-dimensional numbers to treat chemistry with reasonable efforts, as in the case of infinitely fast chemistry where all chemical scales are assumed to be smaller than the turbulent ones, e.g. typically $\mathrm{Ka} \ll 1$ for premixed flames. Similarly, the condition $\mathrm{Da} \gg 1$ indicates a mixing controlled regime, where turbulence-chemistry decoupling is also possible. Nevertheless, all real systems present a scale overlap.

With the advances in computer science, the industrial sector has benefited from the implementation of Computational Fluid Dynamics (CFD) to lower the cost of innovation. CFD applications range from laminar non reacting flows to complex industrial combustors. Dealing with all these applications is made possible by adapting the resolution of turbulence and chemistry. Three categories of CFD are identified, namely, Direct Numerical Simulation (DNS), Large Eddy Simulation (LES) and Reynolds-Averaged Navier–Stokes (RANS) simulations [9]. Whereas all the scales are resolved in DNS simulations, they are all modelled in RANS, thus considerably lowering the computational effort of RANS simulations. LES simulations solve the scales above a given threshold imposed on the turbulent energy spectrum, and model the scales smaller than the computational grid. When simulating turbulent reacting flows, combustion models are used to estimate the rates of consumption/production of the chemical species, i.e. the "mean" reaction rates in the context of RANS simulations, and the "filtered" reaction rates in LES. RANS simulations have been widely used in the industrial sector for their ability to provide a numerical solution to complex geometries and real systems with accessible computer power. As a major drawback, RANS simulations do not capture non-equilibrium phenomena such as local extinction and re-ignition which require a higher resolution level. DNS aim to address questions in fundamental problems by solving every scale of turbulence and chemistry. However, given the elevated computational cost of DNS, computational domains are limited to small and simple geometries. With the increasing availability of computational resources, LES has recently gained interest for its ability to provide accurate numerical solutions up to industrial scale problems. Unsteady phenomena can now be investigated in detail at acceptable computational costs. To support the decarbonisation of the industrial sector and a transition to a low-carbon economy, it is essential to develop accurate CFD models for combustion applications.

Reactor-based combustion modelling approaches have recently drawn interest for their ability to treat finite-rate chemistry at an affordable cost [8–10]. Notably, these models handle individual multi-species diffusion without requiring any Lewis (Le) number relationships. Continuously developed since the 1970's, reactor-based models are derived from the intermittency theory of turbulent reacting flows. Assuming that combustion takes place in a series of unique volumes allows each to be modelled using finite-rate chemistry. Originally assuming infinitely fast chemistry, these models have evolved to provide a valuable solution to any type of flame. Turbulence-chemistry interactions are naturally strengthened in MILD combustion [11,12] and classic combustion models based on time scale separation usually fail to accurately capture MILD features [13,14], such as local extinction and re-ignition [15].

Along with the features of reactor-based models, their recent numerical development is presented hereafter, from their origins to their adaptation to MILD combustion. The remainder of this paper is organised as follows. The underlying characteristics of reactor-based models are presented in Section 2. Models relying on fast chemistry are described in Section 3. Finite-rate reactor models are presented in Section 4. Section 5 reports numerical configurations on which reactor-based models have been used and developed, with a special focus on MILD combustion applications. The concluding points are discussed in the final section.

2. Underlying features of reactor-based models

2.1. Turbulence scales

To characterise flows, the Reynolds number indicates the ratio between inertial and viscous forces, and is used to distinguish laminar (low Reynolds number) from turbulent (high Reynolds number) flows. Turbulence is characterised by the entanglement of eddies, vortices, and complex structures of different scales [7]. Shear-induced fluidic instabilities make turbulence chaotic. Small-scale structures are deformed and advected by larger scales, resulting in tremendous structural complexity [16]. In addition, as the ratio between the small dissipative scales and the large scales is inversely proportional to the turbulent Reynolds number, increasing turbulence results in the production of finer structures.

Inspired by Richardson's work in 1922 [17], Kolmogorov [6,18] estimated the characteristics of the small dissipative scales by means of his theory of local similarity of turbulent motion at high Reynolds numbers. By self-similarity assumptions, the turbulent scales are then linked together, from the integral scale, of the same order of typical boundary layer thicknesses, to the Taylor scale, i.e. where viscous effects balance the inertial forces, and the Kolmogorov scale where viscous effects are dominant. Turbulent kinematic energy cascades from the biggest turbulent structures to the smallest eddies that are dissipated by viscosity. The statistical properties of the small-scale structures can be determined, based on local isotropy, via macro-fluidic properties such as the kinematic viscosity ν and the turbulent kinetic energy dissipation rate ε.

Batchelor and Townsend [19] summarised the implications of Kolmogorov's theory by advancing two major points: at high Reynolds numbers the large eddies are not affected by viscosity and the motion of the small scales is entirely laminar. Although the dissipative Kolmogorov scale is well-located in the turbulence energy spectrum, most of the cascade models [19–22] treated only the sub-inertial range, thus addressing the first point of Batchelor and Townsend [19]. This inertial portion of wave numbers k can be approximated by the relation $k^{-5/3}$, neglecting any effect of the kinematic viscosity ν [20].

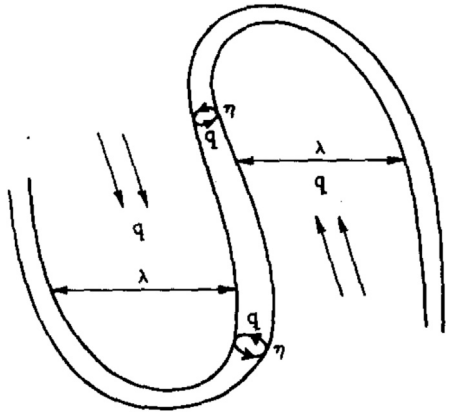

Fig. 1. Schematic representation of the fine structures proposed by Tennekes in 1968 [28].
Source: Reprinted from *Tennekes, H., 1968. Simple Model for the Small-Scale Structure of Turbulence. The Physics of Fluids 11, 669–671*, doi:10.1063/1.1691966, with the permission of AIP Publishing.

In contrast to inert flows, turbulent reacting flows are subject to turbulence-chemistry interactions. In other words, turbulence affects the chemical processes and combustion locally modifies the flow properties by means of heat release, hence affecting the energy distribution of turbulent motions. Whereas turbulence enhances mixing of fuel and oxidiser in diffusion flames, it preheats the fresh mixture in premixed flames. However, the main interrogation in the combustion community remained in whether turbulent flames could be considered ensembles of laminar flame fronts [23]. Advancements on the comprehension of the small-scales were needed to address that issue. Damköhler identified two regimes, of high and low intensity turbulence, respectively. Where the inner structure is kept laminar for the low turbulence intensity regime, the high intensity turbulence yields flame fronts much different with respect to a laminar structure. The role of relaminarisation, i.e. weakened turbulence due to elevated kinematic viscosity from higher temperature, and flame generated turbulence, i.e. enhanced turbulence intensity due to higher density ratios, in combustion have been widely assessed.

2.2. Fine structures

Batchelor and Townsend [19] introduced the notion of *spatial intermittency* or *spatial binary character* of highly turbulent flows. This approach states that for high Reynolds number flows, there are large regions of low density of fine structures and relatively small regions of intense fine structures where viscous dissipation occurs. After studying the spatial distribution quantities, the authors concluded that a spatial inhomogeneity of energy is produced early in the history of the turbulence by an intrinsic instability, and sustained by the action of energy transfer. As a result, the energy associated with large wave-numbers k is very unevenly distributed in space. Numerous studies [24,25] on probability distributions reinforced the notion of intermittency and Kuo and Corrsin [26,27] equated the intermittency factor γ with the fractional volume of space occupied by the fine structures.

Corrsin [29] modelled the fine structures as vortex sheets whereas Tennekes [28] revised the fine structures as dissipative vortex tubes of diameter η being stretched by eddies of Taylor microscale size λ, see schematic representation in Fig. 1. Kuo and Corrsin [26,27] represented the topological complexity of the fine structures as vortex sheets, ribbons and tubes. Chomiak [23,30] confirmed Tennekes' model of the vortex tubes by identifying transient chemiluminiscent reactive objects inside the combustion region with a characteristic dimension comparable to the Kolmogorov scale η. Owing to the dimension of the reactive spots, these objects could not be interpreted as laminar flame fronts.

High-fidelity DNS of high Reynolds numbers inert and reacting flows [31,32] demonstrated that small reactive structures can be of many types, such as isolated, partially stirred, strained or deformed, as turbulence promotes intermittency and shapes the fine structures in tubes, vortices, pockets or sheets, some examples of which are presented in Fig. 2. In particular, vortex tubes-like fine structures are concentrated into filaments, immersed in sheets of low-intensity vorticity. The small volume fraction of these isolated regions was estimated to be inversely proportional to the Reynolds number.

As chemical processes tend to be concentrated within small zones, affordable efforts in treating the chemistry with accuracy provides an approach for reproducing the global scale. The concentrated reactive structures are fed with fresh mixture by larger turbulent structures, hence it is important that turbulent scales are well captured. Reactor-based combustion models follow the fine structures concept and aim to describe the reacting pockets by ideal reactors surrounded by larger inert turbulent structures. The modelling complexity comes from the precise description of such reactors, their characteristics (reacting fraction, residence time, reactor type) and their interaction with the surroundings. Several modelling assumptions can be found in the literature to model the fine structures and their characteristics [33–37].

The estimation of the fine structures characteristics are generally available from turbulence modelling. As in RANS simulations, these quantities are intrinsically linked to the turbulence parameters such as the flow viscosity, the turbulent kinetic energy and its dissipation rate. As far as LES modelling is concerned, physical scales are extracted from the filter model and time scales are related to the mass transfer rate within the subgrid. Towards the DNS limit, the fine structures occupy the entire volume of the computational cells. The reactors have the characteristics of the grid elements and the timescale tends toward the inverse of the scalar dissipation rate. As fine structures characteristics rely on an accurate description of turbulence, these models are sensitive to turbulence modelling.

The reactor volume can be of the size of the computational grid, of filter width, or within a grid element. The residence time within the reactor is specified to allow micro mixing and reactions to occur. The reactors' microscale has to provide an accurate description of the reaction zone. To comply with the phenomenological description that combustion occurs at the dissipating scales, the microscale is often considered similar to either the Taylor scale, where the viscous effects begin to significantly dampen the inertial structures, or the Kolmogorov scale at which the flame exhibits laminar structures. Respectively, the two scales represent the onset or dominance of viscous effects over inertial forces. The choice of length scale for the microscale should be supported by a combination of qualitative arguments from experiments and numerical investigations. For the experimental contribution, instantaneous planar or tomographic laser-induced fluorescence (PLIF or Tomo-LIF) can provide high resolution imaging of the reaction zone [38]. From a numerical perspective, high-fidelity DNS must be considered.

2.3. Reaction scales

Reactor-based combustion models tend to accommodate phenomenological descriptions of both fluid mixing and chemistry (both characterised by associated time scales) through numerically simulating fine-structures within the flow-field. The non-dimensional numbers comparing turbulence and chemistry such as the Damköhler (turbulence time scale vs chemical time scale) or Karlovitz (chemical time scale vs Kolmogorov time scale) numbers are of interest. In premixed flames, where the notions of flame thickness and flame speed are well-defined, the Damköhler and Karlovitz numbers are inversely proportional. Identifying a turbulence time scale for the Damköhler number is challenging and impacts its interpretation. Generalisation for "high",

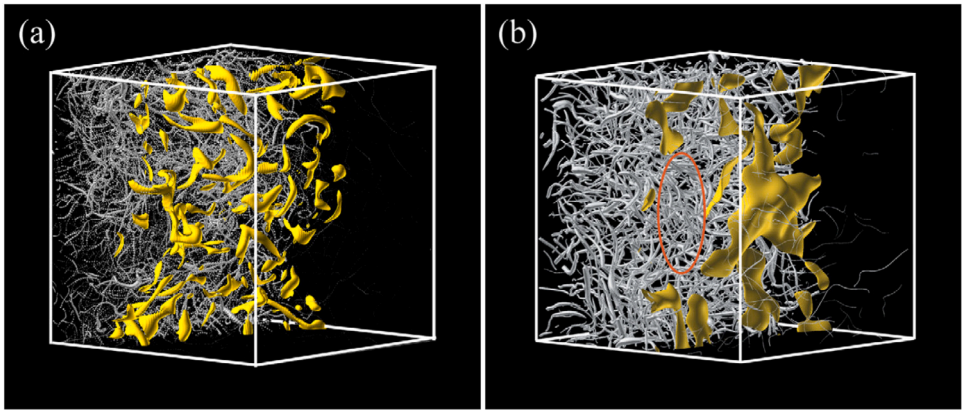

Fig. 2. DNS results of combustion in homogeneous isotropic turbulence at moderate turbulent Reynolds (a) $Re_t = 515$; (b) $Re_t = 141$, Damköhler (a) $Da = 21$; (b) $Da = 5$, and Karlovitz (a) $Ka = 1.3$; (b) $Ka = 2.8$, numbers from [31]. Iso-surfaces of heat release and vorticity are displayed in yellow and grey, respectively. (For interpretation of the references to colour in this figure legend, the reader is referred to the web version of this article.)

"low" or "order unity" Damköhler numbers may describe "fast" or "slow" chemistry relative to the flow. Above all, care must be taken to understand how the timescales are defined before directly comparing non-dimensional numbers.

By separating the reactor models from the flow iterations, i.e. operator-splitting [39,40], reactor-based models can incorporate chemical mechanisms of various complexity, ranging from simplified global mechanisms to detailed chemical mechanisms with hundreds of different chemical species and thousands of reactions. Considering only a few, e.g. 1 to 4, reactions may be limited at capturing the flame structure, as intermediate species are neglected but are crucial in ignition processes. Conversely, detailed mechanisms induce rapid growth of the computational expense. The selection of a chemical mechanism with finite-rate Arrhenius-type reactions may affect the calculation of the timescales both directly, i.e. by changing the means of calculating chemical time scales, and indirectly, by impacting the flame structure. Where a very simple, single-step reaction with a global reaction rate is chosen to represent combustion chemistry, the chemical timescale would simply be defined as the inverse of the reaction rate. Where more complex chemistry is implemented, the definition of an indicative chemical reaction rate becomes significantly more complex. Approaches may include the selection of a surrogate single-step reaction combining local concentrations of reactants and products calculated using more complex chemistry, the inverse of the formation rate of one or several pre-selected species which limit the local reaction rate [34], or a more sophisticated approach which may be employed to interpret eigenvalues of the chemical Jacobian matrix [8]. Reactor-based models can also benefit from mechanism reduction techniques to speed up the simulation from chemical kinetics reduction. Irrespective of the means of calculating the chemical time scale, it subsequently allows for the calculation of the Damköhler number [9].

By integrating finite-rate chemistry, reactor-based models can deal with various types of fuels from hydrogen to complex hydrocarbons. Along with fuel flexibility, such approaches can be used in various types of systems and configurations where the estimation of combustion products and pollutants such as nitric oxides (NOx) is of importance. Such features are required to support the development of future combustion technologies via CFD. Examples of applying reactor-based models with ammonia [41–43], ethylene [44–46], propane [47], *n*-heptane [48–52], diesel [34,48–50,53,54], coal [55,56], or plasma [57] can be found in the literature. These approaches have been validated on canonical flames [58], with the Eddy Dissipation Concept (EDC) [59–62] or the Partially Stirred Reactor (PaSR) model [63], on premixed flames [64], sprays [65,66], and flames with extinction such as the Sandia piloted jet flame F [67,68] or the highly swirling flames (DLR) as in [42,69–71], or on more complex systems such as hydrogen scramjets [66,72–79], gas turbines [80], engines [81,82] or combustors [83–87]. Reactor-based models have also been applied in non-conventional combustion regimes, notably to support the development of MILD combustion technologies.

2.4. MILD combustion

Moderate or Intense Low-oxygen Dilution (MILD) combustion [2–4] is a promising technology to face the energy and environmental challenges [88]. MILD combustion has demonstrated its ability to deliver abated pollutant emissions along with fuel flexibility and increased overall thermal efficiency. Such features are obtained by means of hot Exhaust Gases Recirculation (EGR) in the reactive zone that preheats and dilutes fresh reactants. A commonly used definition of MILD combustion states that this regime is achieved when the reactants temperature T_r is higher than the reference auto-ignition temperature T_{ign} and the temperature raise, expressed as $\Delta T = (T_b - T_r)$, satisfies the relation $\Delta T < T_{ign}$, T_b being the temperature of the burnt gases [3]. Analysing hysteresis behaviour, Sabia et al. [89] recently defined MILD combustion with the characteristic temperatures of the *unstable* branch, that may be lower than T_r or T_{ign}. The possibility to stabilise MILD combustion processes may be enlarged by accounting for conditions belonging to hysteresis branches. By preheating the reactants, the suitable homogeneous temperature conditions for limited pollutant production are met [90]. Although spatially distributed on the length scale of the combustion chamber, heat release rate from MILD combustion zones present spatial inhomogeneity at small scales [91,92]. Experimental studies demonstrated that auto-ignition and igni-diffusion processes are the dominant elementary processes in MILD flames [93]. Although expected to be fully characterised by auto-ignition dynamics, MILD combustion exhibits higher morphological complexity [94]. Understanding the topological features of MILD combustion is of importance. To this regard, high-fidelity DNS can provide physical insights of MILD combustion.

As reported by Swaminathan [97] and Doan [96], few DNS of MILD combustion have been performed so far. van Oijen and co-workers [98,99] performed a DNS of ignition in a temporally evolving mixing layer to mimic reacting flow characteristics of the Adelaide Jet in Hot-Coflow (AJHC) burner operating under MILD conditions [100]. Premixed [101] and non-premixed internal MILD combustion [12] configurations with exhaust gas recirculation (EGR) were investigated (Cases AZ1 and BZ1 with 3.5% (lower dilution) and 2.0% (higher dilution) maximum volume fraction of O_2, respectively), see Fig. 3. The EGR configurations yielded a number of communications on the intrinsic features of MILD combustion [11,15,94,95,102–106].

Physical insights gathered from DNS data demonstrated that MILD combustion features highly convoluted reaction zones with increased

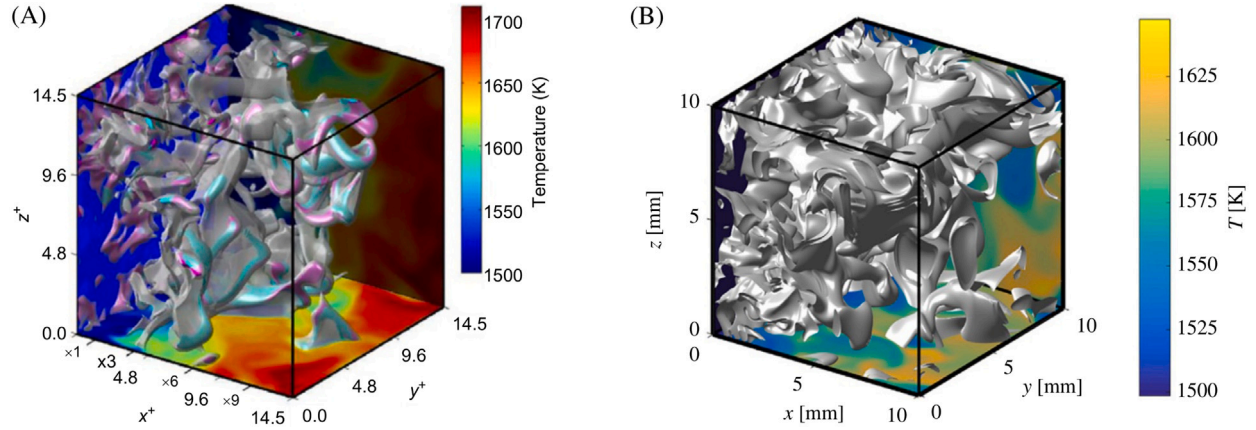

Fig. 3. DNS results of (a) premixed [95] and (b) non-premixed [12] MILD combustion. Typical isosurface of normalised heat release rate for (A) case A1 and (B) case AZ1 [96]. Temperature field is shown on the bottom and side surfaces.
Source: Reprinted from *Doan, N.A.K., 2022. Chapter 8 - Direct numerical simulations of flameless combustion, in: Hosseini, S.E. (Ed.), Fundamentals of Low Emission Flameless Combustion and Its Applications. Academic Press, pp. 221–260*. URL: https://www.sciencedirect.com/science/article/pii/B9780323852449000022, doi:10.1016/B978-0-323-85244-9.00002-2, with the permission from Elsevier.

interactions between flames and no clear front separations as in conventional combustion [12,95]. Iso-surfaces of heat release rate, depicted in Fig. 3, demonstrate the presence of inert flow pockets and the difficulty to characterise the reaction zones with the common fine structures shapes such as sheet, ribbon, tube, and blob [95]. Rather than sheet-like pockets, the topological complexity of MILD reaction zones in premixed conditions can be characterised by pancakes-like or blob-shaped reacting structures [97]. The structural complexity of MILD combustion challenges classical combustion models such as flamelets or geometrical based models, i.e. flame surface density approaches [102]. The role of radicals in the inception, i.e. auto ignition, in MILD combustion has been highlighted by comparing concentration levels of OH in non-premixed cases [105]. In regions of elevated heat release rate, the limited OH concentration differences question the capabilities of PLIF methods to investigate MILD combustion features [104]. Furthermore, a Beta analysis, comparing the convective–diffusive terms to the reaction sources in the transported balance equations, demonstrated the coexistence of flame-propagated and ignition dominated modes [11]. Tracking the Beta sign on Lagrangian particles demonstrated the ability of MILD combustion to switch from a flame propagation mode to an auto-ignition dominated behaviour [12]. Similarly, Dave et al. [107] computed the probability density function (PDF) of absolute ratio between the diffusion and the reaction terms on DNS data of non-premixed MILD combustion [12]. It was found that diffusion dominates over reaction in systems with high dilution, i.e. Case BZ1. In addition, the unsupervised VQPCA clustering algorithm was investigated in that work for the characterisation of structures of physical variables in MILD combustion. A quantitative comparison was developed based on Boolean logic and rank important features (or variables) within each cluster. Whereas heat release rate was found to be a leading variable for the distribution of VQPCA clusters in the lower diluted case (Case AZ1), no single leading system-level characterisation variable emerged from Case BZ1. Nevertheless, the characterisation of the latter case was performed through a combination of unsupervised clustering, feature extraction and domain expertise.

Besides having similar structural flame features as conventional flames, the locally preferred feature is related to the scalar fluxes. In contrast to conventional flames, where the scalar gradients of direction normal to the reaction zone are stronger than the tangential components, it has been demonstrated in both premixed [95,101] and non-premixed [12,15] conditions that they are of same amplitudes in MILD combustion. By means of the Takeno index, it was shown that premixed MILD combustion [11] combines rich and lean premixed zones and ignition front-like structure. In addition to these characteristics, non-premixed MILD combustion [12] also features premixed reaction zones. However, from the two EGR cases [11,12], it can be concluded that the MILD features are not heavily impacted by the premixed or non-premixed conditions as long as turbulence and mixture thermo-conditions are similar. From a modelling point of view, this is a strength for MILD combustion modelling as flexibility across the cases are naturally inherited by the nature of MILD combustion.

3. Fast chemistry reactor models

3.1. Reactor model background

Originally, combustion models considered that mixing was limiting and made the assumption of infinitely fast chemistry (as in the case of wrinkled flames), i.e. any scale describing chemistry is faster than the turbulent Kolmogorov scale. This results in small Karlovitz and high Damköhler numbers, independent of the turbulence. Consequently, the chemical reactions rates are governed by the turbulent mixing rate and in a way, "mixed is burnt" as a Burke-Schumann [108] flame analogy. Early studies [109–112] focused on the impact of turbulence on combustion rates. Howe [109] modelled the burning zone as the periphery of parcels of unburnt gas dispersed through burnt gas and investigated the quenching limits for confined turbulent flames. While Magnussen [111] disproved the application of simple laminar approach for soot formation estimation in turbulent flames, Chomiak [23] proposed a possible mechanism of propagation of high Reynolds number premixed flames by supposing that the chemical reactions take place mainly in the fine structures. Spalding [110] obtained fairly good predictions of reaction rates while taking the rate of break-up of the eddies into account and concluded that the eddy-break-up term is essential if the dominance of hydrodynamic processes is to be correctly simulated. Magnussen [112] confirmed the importance of accounting for the eddy break-up information to get good predictions of the combustion rates for soot formation. This led Magnussen to present its mathematical model of turbulent combustion closely related to the eddy break-up approach [109,110]: the Eddy-Dissipation combustion model [113]. The Eddy-Dissipation model relates the rate of combustion to the rate of dissipation of eddies by taking into account intermittent quantities of turbulent flames. The historical development of reactor-based models is graphically represented in Fig. 4. Originally derived in the context of RANS, as presented in the following, the models have been straightforwardly and successfully implemented in LES to provide closure to the filtered reaction rates.

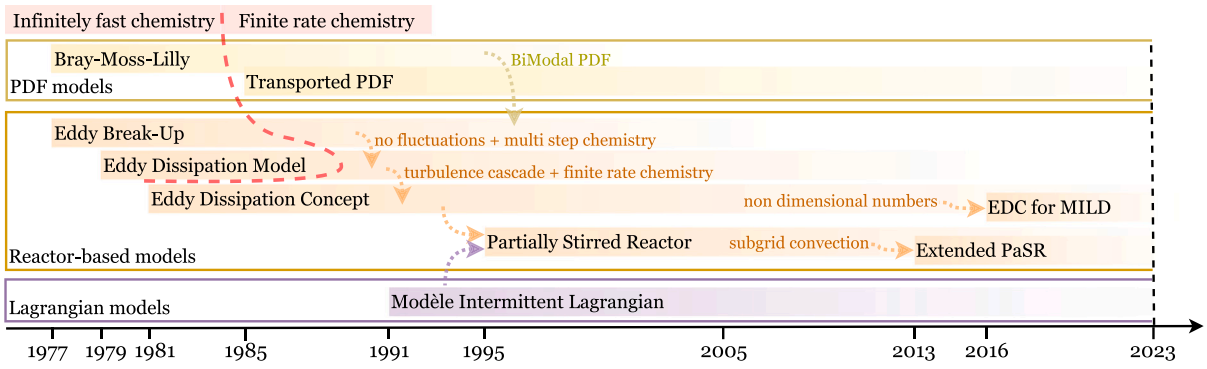

Fig. 4. Historical development of reactor-based models.

3.2. Eddy Break-Up model (EBU)

The Eddy Break Up (EBU) model is based on the phenomenological analysis of highly turbulent flows, i.e. high Reynolds numbers. Turbulent motions control the flow and chemistry does not play a significant role. The reaction layer is seen as a collection of fresh and burnt mixtures transported by turbulent motions. Chemical reaction rates are thus mixing rate controlled and the associated characteristic time scale is estimated [110,114]. The EBU model is attractive for its simplicity, i.e. no additional transport equations are required. As a major model drawback, any effect of chemical kinetics is neglected (EBU uses a simple global reaction rate as an approximation of real combustion kinetics). The rather limiting "mixed-is-burnt" hypothesis allows the formation of products in flammable mixtures with sufficiently long associated residence times. The EBU model does not capture complex dynamics of turbulent flames.

The mean of a non-dimensional progress variable, e.g. the reduced temperature Θ, is expressed as a variance term multiplied by a constant and the inverse of a time scale,

$$\bar{\dot{\omega}}_\Theta = C_{\mathrm{EBU}}\bar{\rho}\frac{\sqrt{\widetilde{\Theta''^2}}}{\tau_{\mathrm{EBU}}} \sim C_{\mathrm{EBU}}\bar{\rho}\frac{\epsilon}{k}\widetilde{\Theta}(1-\widetilde{\Theta}). \tag{1}$$

In the context of premixed combustion, the variance term can be simplified $\sqrt{\widetilde{\Theta''^2}} \sim \widetilde{\Theta}(1-\widetilde{\Theta})$ under the assumption of fast chemistry and infinitely thin reaction layer [9]. The term C_{EBU} is a model constant of the order of unity. As the integral length scales are assumed to be responsible for the largest turbulent motions, the integral time scale $\tau_{\mathrm{EBU}} = \tau_I = k/\varepsilon$ is selected. The estimation of the turbulent kinetic energy and its dissipation is then required. In the context of RANS simulations, the EBU model is usually associated to the $k-\varepsilon$ turbulence model where a set of transported equations provides both quantities. However, the choice of the time scale formulation is somewhat arbitrary and the Kolmogorov time scale is selected to replace the integral one, as in the Intermittent Turbulence Net Flame Stretch (ITNFS) Model [115]. Nicolleau and Mathieu [116] used arguments from fractal theory to change the time scale definition. Efforts were also made to include chemical information in the model, as in the ESCIMO (Engulfment, Stretching, Coherence, Interdiffusion, and Moving-Observer) model [117].

3.3. Eddy Dissipation Model (EDM)

The evaluation of the variable fluctuations in the EBU model [109,110] is rather complicated and this difficulty motivated Magnussen and Hjertager [113] to propose the Eddy Dissipation Model (EDM). The Eddy Dissipation Model (EDM) [113,118] is a direct extension of the EBU model to diffusion flames resulting in a unified model. Although still relying on the fast chemistry assumption, the model may feature multi-step chemistry without the need to compute statistical fluctuations of mixture fraction or progress variable. As fuel and oxidiser appear as fluctuating intermittent quantities, the EDM approach relates the fluctuations to the mean concentrations of the species. The EDM combustion rates are then limited by the local availability of fuel or oxidiser and the dilution effect of combustion products that would limit the overall combustion process. The fuel burning rate is expressed as,

$$\bar{\dot{\omega}}_F = \alpha\frac{\bar{\rho}}{\tau_I}\min\left(\tilde{Y}_F, \frac{\tilde{Y}_O}{r}, \beta\frac{\tilde{Y}_P}{1+r}\right), \tag{2}$$

where α and β are model parameters, $\tilde{Y}_F$, $\tilde{Y}_O$ and $\tilde{Y}_P$ are the filtered fuel, oxidiser and reaction products mass fractions and r is the stoichiometric ratio from a global one-step irreversible reaction,

$$1\ \mathrm{kg\ fuel\ (F)} + \mathrm{r\ kg\ oxidant\ (O)} \longrightarrow (1+\mathrm{r})\mathrm{kg\ product\ (P)}. \tag{3}$$

However, the artificial limiting of potential temperature and reaction rates over predictions can be viewed as a drawback. The EDM still relies on the estimation of a characteristic mixing time scale.

3.4. Historical note on the terminology of the "eddy dissipation concept"

Whereas the EDM makes the assumption of fast chemistry, as detailed in the present paper, the "Eddy Dissipation Concept" and the acronym "EDC" model refers to the model developed by Magnussen in 1981 [33] in which detailed, finite-rate kinetics are incorporated. Therefore, the term "Eddy Dissipation Concept" has been often misassigned to the EDM approach in a number of references from the literature. The "Eddy Dissipation Concept" (EDC) model [33] is presented hereafter.

4. Finite-rate reactor models

4.1. General model formulation

Characteristic timescales are crucial to understand Turbulence - Chemistry Interactions (TCI) in turbulent reacting flows. As turbulence is characterised by a wide spectrum of scales, complexity emerges when selecting the relevant scale to be used in a turbulent combustion model. Any simplified model based on time scale separation, as in infinitely fast chemistry approaches, would fail at capturing TCI. Conversely, when detailed kinetics are considered, characteristic chemical timescales may be of the same order of magnitude than the turbulence timescales. Evaluating non-dimensional numbers such as Damköhler or Karlovitz with precision becomes critical to accurately capture the salient physics.

As a first approach of including finite-rate chemistry in combination with the Eddy Dissipation Model, the Eddy Dissipation/ Finite-Rate (ED/FR) model estimates the mean reaction rate as the minimum between the EDM rates and the Arrhenius rates. This allows a switch from mixed to chemically controlled rates. However, this

approach is prone to computational instabilities, especially when large kinetic schemes are considered. Advancing research on soot modelling [113], Magnussen proposed in 1981 the Eddy Dissipation Concept (EDC) [33] model for chemical reaction treatment in turbulent flows. The novelty of EDC lies in the integration of the fine structures theory [6,19,23,25–30] in the determination of the chemical source terms. The continuum energy spectrum is considered via the stepwise energy cascade linking the large-scale eddies to the small-dissipative scales and characterises the fine structures with quantities of the large flow structures.

Chomiak [30] stated that a mass exchange between the fine structures and the surrounding fluids may play a crucial role for the flame propagation and that the fine structures can be considered well-stirred reactors due to turbulent mixing. The EDC model integrates this idea and embeds three key factors: the proportion of the total mass that is contained in the fine structures γ^* [113,118], the mass transfer rate between the fine structures and the surrounding fluids $\dot{m}^*$ [30,119] and the reacting fraction of the fine structures χ [113,118]. The net consumption rate of a certain chemical species i is then computed from the reaction rate of species i within the reacting fraction χ of the fine structures. From a general point of view, the chemical source terms in reactor-based models, to be returned to the solver, can be expressed as the contribution from all possible composition space,

$$\bar{\dot{\omega}}_i = \int_{\psi} \mathcal{P}(\psi)\dot{\omega}_i d\psi, \tag{4}$$

where $\mathcal{P}(\psi)$ expresses the joint scalar Probability Density Function (PDF) of associated domain of definition Ψ, and $\psi = [T, Y_i]^T$ the composition space. In the basic concept of the Bray-Moss-Libby (BML) formulation for turbulent premixed flames [120], three contributions are considered, from fresh, fully burnt and burning gases. Assuming large Reynolds and Damköhler numbers leads to a bimodal-shaped PDF, decomposed into the fine structures, denoted by $(.^*)$, and its surroundings, denoted by $(.^0)$ (assuming infinitely thin flame front). The mean quantities are defined for a given scalar $\phi \in \psi$ as,

$$\tilde{\phi} = \gamma^*\chi\phi^* + (1-\gamma^*\chi)\phi^0, \tag{5}$$

where ϕ^* and ϕ^0 are the fine structures and the surroundings scalar values, respectively, and the term $\gamma^*\chi$ identifies itself as the cell reacting volume fraction. Furthermore, it is assumed that most exothermic reactions occur within the fine structures, as they are characterised by high reaction rates due to favourable mixing conditions, i.e. $\dot{\omega}_i(\psi^0) \sim 0$. This idea is supported by theoretical [23] and numerical [31,121] arguments. The mean reaction rates are then evaluated at the fine structures conditions $\psi^* = [T^*, Y_i^*]^T$,

$$\bar{\dot{\omega}}_i = \gamma^*\chi\dot{\omega}_i(\psi^*) + (1-\gamma^*\chi)\dot{\omega}_i(\psi^0) \sim \gamma^*\chi\dot{\omega}_i(\psi^*). \tag{6}$$

4.2. Eddy dissipation concept model (EDC)

The EDC model extends the previously introduced EDM. Originally formulated in Magnussen [33,122] and later modified in Gran and Magnussen [123], Ertesvåg and Magnussen [124], and Magnussen [125], the assumption is made that combustion takes place at the smallest physical scales, of the order of Kolmogorov scales, in the so-called fine structures [33,122,124]. A step-wise self-similar energy cascade from the integral to dissipating scales leads to the evaluation of the characteristics of the fine structures [124], depicted in Fig. 5. The nth cascade scale is characterised by its velocity u_n, length scale L_n and strain rate $\omega_n = u_n/L_n$. The production w_n and dissipation q_n terms of the turbulent kinetic energy are expressed as

$$\begin{cases} w_n = \frac{3}{2}C_{D1}\omega_n u_n^2, \\ q_n = C_{D2}\nu\omega_n^2, \end{cases} \tag{7}$$

where C_{D1} and C_{D2} are model constants that can be assigned values of 0.135 and 0.5, respectively [124]. The $(n+1)$th level is characterised by

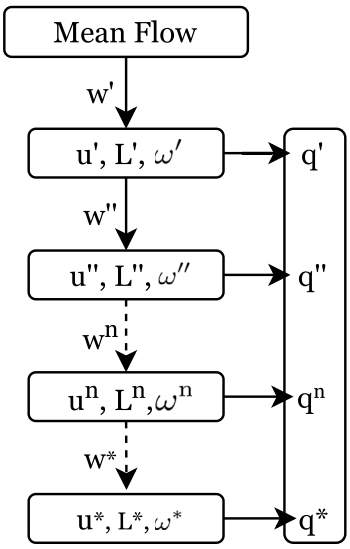

Fig. 5. Sketch of the transfer model of mechanical energy from larger to smaller turbulence structures in the EDC approach.

the nth scale properties under a quasi-steady assumption. By conservation of energy, the energy production is $w_{n+1} = w_n - q_n$ and the strain rate $\omega_{n+1} = C_\omega\omega_n$ with the constant C_ω generally set at a value of 2 (doubling frequency). At the fine structures level, all energy production is dissipated by viscosity, i.e. $q^* = w^*$. The sum of the dissipation terms q results in the evaluation of the dissipation rate of turbulence kinetic energy ε. From the large, energy-containing scale properties (u', L', ω', w', q'), the conservation of energy also yields $w' = \varepsilon$. The typical fine structures length scale [33,124]

$$L^* = \frac{2}{3}\left(\frac{3C_{D2}^3}{C_{D1}^2}\right)^{1/4}\left(\frac{\nu^3}{\varepsilon}\right)^{1/4}, \tag{8}$$

whereas the fine structures velocity is

$$u^* = \left(\frac{C_{D2}}{3C_{D1}^2}\right)^{1/4}(\nu\varepsilon)^{1/4}, \tag{9}$$

where ν is the kinematic viscosity and ε is the dissipation rate of the turbulent kinetic energy k. The fine structures Reynolds number is,

$$Re^* = \frac{u^*L^*}{\nu} = \frac{2C_{D2}}{3C_{D1}} = 2.5. \tag{10}$$

The previous fine structures characteristic scales are used to estimate the dimensionless fine structures length fraction [61],

$$\gamma_\lambda = \left(\frac{3C_{D2}}{4C_{D1}^2}\right)^{1/4}\left(\frac{\nu\varepsilon}{k^2}\right)^{1/4} = C_\gamma Re_\tau^{-1/4}. \tag{11}$$

It is to be noted that there is no clear distinction in the terminology between γ^* and γ_λ. From the pioneering work of Magnussen [33] to the recent review of Ertesvåg [126], both quantities are defined as the *mass fraction occupied by the fine structures* or the *ratio of mass in fine structures to the total mass*. Nevertheless, γ_λ may also be viewed as a dimensionless fine structures length fraction, as proposed in Bösenhofer et al. [61], which is related to γ^* by an exponent representing the topology of the fine structures [127].

The fine structures characteristic scales are also used to estimate the mean residence time within the fine structures,

$$\tau^* = \frac{1}{\dot{m}^*} = \left(\frac{C_{D2}}{3}\right)^{1/2}\left(\frac{\nu}{\varepsilon}\right)^{1/2} = C_\tau\left(\frac{\nu}{\varepsilon}\right)^{1/2}. \tag{12}$$

$Re_\tau = k^2/(\nu\varepsilon)$ is the turbulence Reynolds number, and the secondary model constants C_γ and C_τ are introduced for convenience with standard values of $C_\gamma = 2.1377$ and $C_\tau = 0.4083$, respectively [36].

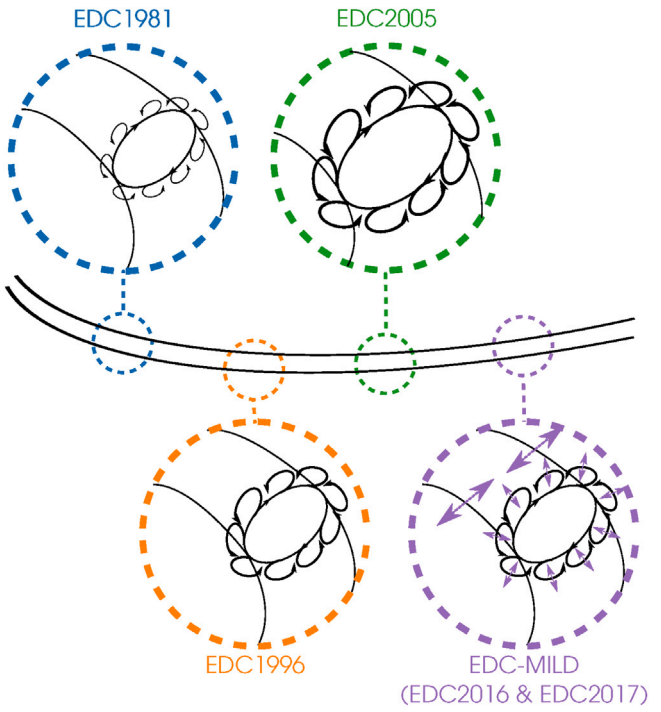

Fig. 6. Schematic view from Bösenhofer et al. [61] of the different Eddy Dissipation Concept (EDC) versions on the graphical representation of tube-like structures of Tennekes [28]. Mass transfers between the fine structures (circles) and the surroundings are represented with curved arrows. Additional straight arrows are added to the MILD modifications to illustrate the variable interaction intensities.

Originally based on empiricism, the EDC model constants may be tuned on a case-by-case basis to improve numerical predictions. The method of determining the fine structures characteristics, along with the numerical values of the model constants, are subject to discussion and have yielded multiple versions of the EDC model.

The classical cascade model described by the EDC model was developed in the context of highly turbulent flows, i.e. high Reynolds numbers, with clear separation between turbulent scales. In MILD combustion, the dilution and preheating of the reactants generate a distributed reaction zone associated with slower chemical reaction scales. The system tends towards perfectly mixed conditions and the reaction process is characterised by lower Damköhler numbers with respect to traditional combustion. As a consequence, it is likely that the flow yields smaller turbulent structures than the fine structures, i.e. of higher frequencies than those of the reacting structures. The energy cascade, based on the detailed description of energy from large motions being transferred to the smallest structures containing the fine structures needs revision. Therefore, Parente et al. [36] proposed to assimilate MILD combustion to the so called Distributed Reaction Regime of the classic theory of turbulent premixed flame (or Thick Flame Regime). Hence, the revised model features parameters clarifying the dependency of the energy cascade parameters on the flow and reaction structure characteristics, i.e. the dimensionless turbulence Reynolds and Damköhler ($Da_\eta = \tau_\eta/\tau_c$) numbers, yielding

$$C_\gamma \propto Da_\eta^{1/2}(Re_\tau + 1)^{1/2} \text{ and } C_\tau \propto Da_\eta^{-1}(Re_\tau + 1)^{-1/2}. \tag{13}$$

The coefficients in front of the dependencies have been discussed more in details in Evans et al. [128].

The conditions in the fine structures and surroundings are coupled by a subgrid set of quasi equilibrium equations for mass and energy,

$$\begin{cases} \bar{\rho}(Y_i^* - Y_i^0)/\tau^* = \dot{\omega}_i(\psi^*), \\ \bar{\rho}\sum_{i=1}^{N_s}(Y_i^* h_i^* - Y_i^0 h_i^0)/\tau^* = \sum_{i=1}^{N_s} h_{i,f}^\theta \dot{\omega}_i(\psi^*), \end{cases} \tag{14}$$

where $\bar{\rho}$ is the Reynolds-averaged density, h_i are the species enthalpies and $h_{i,f}^\theta$ are the enthalpies of formation of species. From Eqs. (6) and (14), the historical mean reaction rates in the EDC model are expressed as [33],

$$\bar{\omega}_i = \gamma^* \chi \dot{\omega}_i(\psi^*) = \gamma^* \chi \frac{\bar{\rho}(Y_i^* - Y_i^0)}{\tau^*}. \tag{15}$$

At the grid resolution level, both the fine structures ψ^* and the surroundings ψ^0 states remain unknown. From Eq. (5), the mass fractions difference in Eq. (15) can be replaced by the term $(Y_i^* - Y_i^0) = (Y_i^* - \tilde{Y}_i)/(1 - \gamma^* \chi)$,

$$\bar{\omega}_i = \frac{\gamma^* \chi}{(1 - \gamma^* \chi)} \frac{\bar{\rho}(Y_i^* - \tilde{Y}_i)}{\tau^*} = \mathbf{g}_{EDC} \frac{\bar{\rho}(Y_i^* - \tilde{Y}_i)}{\tau^*}, \tag{16}$$

where the term $\mathbf{g}_{EDC}$ is used as the EDC factor in [37] to ease the presentation of the many EDC model versions. From Eq. (16), various final expressions of the chemical source terms have been developed. Originally [33], the total mass fraction of the fine structures over a given control volume γ^* is given by the Corrsin's topological sheet-like representation of the fine structures [29], hence $\gamma^* = \gamma_\lambda^3 = (u^*/u')^3$, where u' and u^* are the respective turbulent and fine structures velocity scales. The reacting fraction of the fine structures χ is expressed by Magnussen [33] as $\chi = \chi'/\gamma_\lambda$ resulting in

$$\mathbf{g}_{EDC}^{1981} = (\gamma_\lambda^2 \chi')/(1 - \gamma_\lambda^2 \chi'). \tag{17}$$

As reported by Ertesvåg [37], the 1981 version of the EDC factor has been approximated by the expression $(\gamma_\lambda^3)/(1 - \gamma_\lambda^3)$ in some works [61,129] (imposing $\chi' = \gamma_\lambda$, i.e. $\chi = 1$). Considering the reciprocal γ_λ in the mean reaction rate expression, separated from χ, the version presented in [122] yields

$$\mathbf{g}_{EDC}^{1989} = (\gamma_\lambda^2 \chi)/(1 - \gamma_\lambda^3 \chi). \tag{18}$$

Assuming $\chi = 1$ as in the work of Gran from 1994 [130], the previous formulation simplifies into

$$\mathbf{g}_{EDC}^{1994} = (\gamma_\lambda^2)/(1 - \gamma_\lambda^3). \tag{19}$$

The consideration of the topological tube-like representation of the fine structures from Tennekes [28] led Magnussen [125] to revise the fine structures mass fraction as $\gamma^* = \gamma_\lambda^2 = (u^*/u')^2$, the 2005 factor version is written as

$$\mathbf{g}_{EDC}^{2005} = (\gamma_\lambda^2 \chi)/(1 - \gamma_\lambda^2 \chi). \tag{20}$$

Furthermore, the reacting fraction χ needs to be determined. In the original EDC formulation, a global one-step irreversible reaction was used, defined in Eq. (3). Posing $\tilde{Y}_F$, $\tilde{Y}_O$ and $\tilde{Y}_P$ the filtered fuel, oxidiser and reaction products mass fractions, and their respective normalised forms: $\hat{Y}_F = (\tilde{Y}_F/1)$, $\hat{Y}_O = (\tilde{Y}_O/r)$ and $\hat{Y}_P = \tilde{Y}_P/(1 + r)$, the 1981 version of the reaction fraction χ reads as

$$\chi = \frac{1}{\gamma_\lambda} \frac{\hat{Y}_P}{(\hat{Y}_P + \tilde{Y}_F)} = \frac{1}{\gamma_\lambda} \chi'. \tag{21}$$

However, dividing by γ_λ does not ensure that χ, supposed to be a mass fraction, does not exceed unity. In [122,123,130], a combination of three components was formulated $\chi = \chi_1 \cdot \chi_2 \cdot \chi_3$ to account for the limiting effects of the probability of coexistence of the reactants χ_1, the degree of heating χ_2 and the lack of reactants χ_3. With the minimum normalised mass fraction defined as $\hat{Y}_{min} = \min(\hat{Y}_F, \hat{Y}_O)$ and an artificial χ maximum of unity, the three compounds of the 1989 version of χ are formulated as

$$\chi_1 = \frac{(\hat{Y}_{min} + \hat{Y}_P)^2}{(\hat{Y}_F + \hat{Y}_P)(\hat{Y}_O + \hat{Y}_P)}, \tag{22}$$

$$\chi_2 = \min\left\{ \frac{1}{\gamma_\lambda} \frac{\hat{Y}_P}{(\hat{Y}_P + \hat{Y}_{min})}, 1 \right\}, \tag{23}$$

$$\chi_3 = \min\left\{ \frac{\gamma_\lambda(\hat{Y}_P + \hat{Y}_{min})}{\hat{Y}_{min}}, 1 \right\}. \tag{24}$$

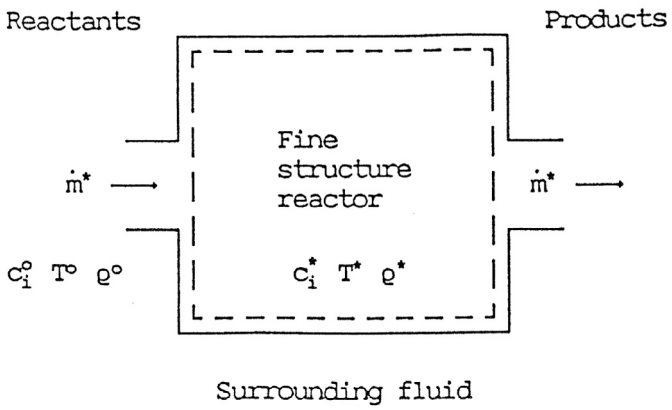

Fig. 7. Schematic illustration of a fine structures reactor.
Source: Adapted from Magnussen [122].

In addition, the simpler 2005 version used in [125] expresses the reacting fraction as

$$\chi = \frac{\hat{Y}_P}{(\hat{Y}_P + \hat{Y}_{min})}. \tag{25}$$

For the sake of simple modelling, some works [123] considered $\chi = 1$. A thorough comparison of all the EDC factors, along with the role of the reacting fraction χ is presented in [37] where the EDC approach from 2005 is considered to be the most complete version as it settles both the topological interpretation of the fine structures and the above unity χ definition issue. Parente's modification for MILD combustion was based on the 1994 model version from [123,130] although the local evaluation of the EDC model parameters is independent from the EDC factor formulation. Bösenhofer et al. [61] graphically represented the interactions between the fine structures and their surroundings in the different EDC model versions, see Fig. 6. The mass transfers between the fine structures (circles) and the surroundings are represented with curved arrows whose size depends on their relative intensity, i.e. on the definition of $\mathbf{g}_{EDC}$. In addition, straight arrows are added to the MILD modifications to illustrate the variable interaction intensities.

In Eq. (16), the species mass fractions from the fine structures Y_i^* are still to be evaluated. The terms Y_i^* are obtained through the time integration of subgrid equations. The fine structures are viewed as a reacting zone fed with fresh mixture by its surroundings [122], see Fig. 7. As they are considered perfectly mixed, a Perfectly Stirred Reactor (PSR) was originally considered but some computational arguments highlighted the numerical benefits of Plug-Flow-Reactors (PFR). A discussion is dedicated to the choice of the reactors in Section 4.3.

4.3. Ideal reactor treatment

4.3.1. Perfectly Stirred Reactor (PSR)

Perfectly Stirred Reactors (PSR) or Continuously Stirred Tank Reactors (CSTR) are characterised by continuous inflow and outflow at a constant mass flow rate $\dot{m}$, see Fig. 8(a) [8,131]. Such reactors are assumed to be rigorously stirred so that any concentration gradient within the vessel can be neglected. As a consequence, the outlet composition is identical to the reactor concentrations, i.e. $\psi^{\text{outlet}} \equiv \psi$. The PSR balance equations for the chemical mass fractions are as follows [40],

$$\frac{dY_i}{dt} = \frac{Y_i^{\text{inlet}} - Y_i}{\tau} + \frac{\dot{\omega}_i}{\rho}, \; i = 1, \dots, N_S, \tag{26}$$

where Y_i^{inlet} is the composition at the inlet of the reactor, ρ is the density within the reactor. The characteristic residence time within the reactor τ is provided by the ratio of the reactor density ρ and volume V over the inflow rate $\dot{m}$. The reactor can be considered adiabatic, isothermal, or interacting with its external environment by means of heat exchange [40]. In addition, both unsteady or steady-state solutions from PSRs can be solved. Assuming steady-state in Eq. (26), i.e. $d./dt = 0$, the PSR model reduces in a set of non-linear algebraic equations that can be solved for $Y \equiv Y^{\text{outlet}}$. The resolution to these equations is obtained using the Newton's method or modified Newton's methods [40,132]. In the case of large chemical mechanisms, numerical problems may arise as the Newton's methods are not sufficiently robust and require a good first-guess solution to converge. Such an initial guess can be provided from the time integration of the unsteady set of equations over a relatively short time. If the first guess is not sufficiently precise, the latter operation can be iterated and may lead to the final solution in case no steady state solution is found.

4.3.2. Plug flow reactors (PFR)

Plug flow reactors (PFR), also called Continuous Tubular Reactor (CTR) or Piston Flow Reactors (PFR), are one-dimensional, steady-state reactors that are commonly used in chemical reaction engineering [8], including to validate chemical kinetic mechanisms [40]. Although the composition and temperature may vary along the reactor, i.e. in the flow direction, complete radial homogeneity is assumed, see Fig. 8(b). In addition, diffusion transport along the direction of the reactor is neglected. In this regard, no mixing is presumed in the flow direction (no "back-mixing") and a PFR can be regarded as an infinite sequence of infinitesimal stirred reactors [131]. Reactions occur across time scales according to chemical kinetics. As with the PSR, a PFR can be considered adiabatic, isothermal or with external interactions. The balance equations for the chemical concentrations Y are written along the longitudinal coordinate ζ as follows [40],

$$v\frac{dY_i}{d\zeta} = \frac{\dot{\omega}_i}{\rho}, \; i = 1, \dots, N_S, \tag{27}$$

where v is the mean axial fluid velocity. The reactor residence time τ is estimated as the ratio between the characteristic reactor length L and v. Given the composition at the inlet ψ^{inlet} and the chemical source terms $\dot{\omega}$, the PFR model is solved using numerical methods for initial-value problems to find the outlet composition ψ^{outlet}. In the case that flow velocity, area, and pressure are constant, the governing equations may be turned into transient equations as,

$$\frac{dY_i}{dt} = \frac{\dot{\omega}_i}{\rho}, \tag{28}$$

that can be integrated in time from the initial $Y(t = 0) = Y^{\text{inlet}}$ to the final concentrations $Y(t = \tau) = Y^{\text{outlet}}$. Sharing similarities with PFRs, i.e. leading to the same solution if the kinetic energy effects are negligible, batch reactors can also be employed [40].

4.3.3. Discussion on the choice of the reactor

Although a PSR was originally used to deal with the fine structures integration, they are subject to convergence issues and high computational costs [40,132]. As a solution, a PFR is generally preferred to alleviate the computational expense of the chemical kinetics integration as in [14,43,61,129,133] and CFD codes [134]. While comparing the reaction rates obtained from a PSR and a PFR solutions, Bosenhöfer et al. [61] stated that the results deviate, especially when a short residence time scale is considered. Higher reactions rates were obtained while treating the ideal reactor with a PSR approach [124]. In their investigation of the AJHC burner [100], Li et al. [129] demonstrated that the fine structures can be modelled by means of PFR without loss of prediction accuracy. More recently, Lewandowski and Ertesvåg [127] discussed the impact of treating the fine structures differently on the EDC formulation, with special regards to the inlet reactor composition ψ^{inlet}. It is well established that PSRs depart from the surrounding composition, i.e. $\psi^{\text{inlet}} = \psi^0$ to model the continuously feed of fresh mixture to the fine structures. However, PFRs do not allow exchanges

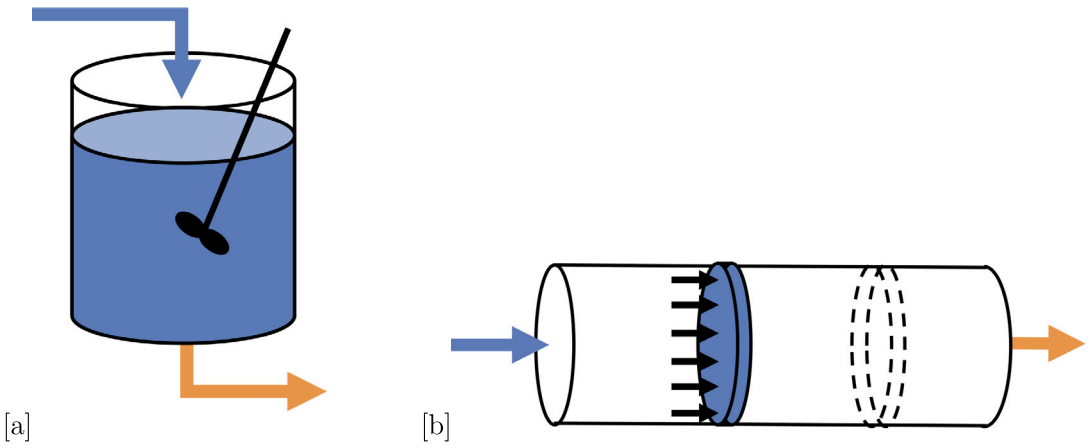

Fig. 8. Sketches of ideal reactors (a) Perfectly Stirred Reactor (PSR); (b) Plug Flow Reactor (PFR). The blue and orange arrows represent the inlet and outlet conditions of the reactors, respectively. The blue zones are where the chemical processes take place. (For interpretation of the references to colour in this figure legend, the reader is referred to the web version of this article.)

between mixtures and such an interaction between the surroundings and a chemically evolving environment is neglected. Hence, the mean composition is generally considered at the inlet of PFRs, i.e. $\psi^{\text{inlet}} = \tilde{\psi}$, as in commercial codes [134]. From the resolution of Eqs. (26) and (28), and the use of Eq. (5) that yields a factor $(1 - \gamma^* \chi)$, the fine structures mass fractions from the two reactors are expressed as in [127],

$$Y^*_{i,\text{PSR}} = (1 - \gamma^* \chi)(\dot{\omega}_i \tau)/\rho + \tilde{Y}_i, \tag{29}$$

$$Y^*_{i,\text{PFR}} = (\dot{\omega}_i \tau)/\rho + \tilde{Y}_i. \tag{30}$$

As the term $(1 - \gamma^* \chi)$ is below unity, the differences between the fine structures and the mean mass fractions from the PFR are higher than those from a PSR, $(Y^*_{i,\text{PFR}} - \tilde{Y}_i)/(Y^*_{i,\text{PSR}} - \tilde{Y}_i) = 1/(1 - \gamma^* \chi)$. Re-injected in Eq. (16), it results that considering the mean composition as inlet instead of the surroundings quantities, as in a PFR, implies an over prediction by a factor $1/(1 - \gamma^* \chi)$. To compensate this rate over estimation, one should consider multiplying the original mean reaction rates expression in Eq. (16) by a factor $(1-\gamma^* \chi)$ when modelling the fine structures with PFRs departing from mean compositions. Comparing the modelling approaches of the fine structures as ideal reactors is of interest for reactor-based models as it directly impacts the final estimation of the chemical source terms. The residence time scale within the reactors remains an important parameter that is discussed along with the combustion models.

4.4. Partially Stirred Reactor model (PaSR)

To account for imperfect mixing and scalar fluctuations at a molecular level within a reactor, Vulis suggested in 1961 [135] to calculate the mean chemical source terms from a *virtual* thermo-chemical state space ψ^v. Assuming quasi-equilibrium between molecular mixing and chemical sources, transient and convection effects are neglected. The model solves stationary balance equations for a PSR with modified chemical source terms. An additional set of balance equations, linking the virtual state to the mean quantities and including a characteristic time scale for micro mixing, was used to close the modified source terms. Golovitchev et al. noted in [53] "this model [135], when applied to turbulent reactive flows, introduced for the first time the concept of micro-mixing in a form which is equivalent to the turbulent dissipation (or eddy break-up) concept, later on, extensively exploited in the turbulent combustion modeling".

The Partially Stirred Reactor (PaSR) combustion model, as the extension of Vulis' model [135], is first described in the works of Karlsson [136], Chomiak [34] and Golovitchev [53,137,138]. The model takes inspiration from the concept of micro-mixing of Vulis, the fine structures theory and the pioneering works of Magnussen [33] on the EDC model, and Gonzales and Borghi [139] who developed the Modèle Intermittent Lagrangian (MIL) model, an extension of the Interaction-by-Exchange-with-the-Mean (IEM) model.

The PaSR model is motivated by the need for a robust model independent of combustion type (premixed, non-premixed and partially premixed) and covering broad ranges of characteristic time scales to handle the slow chemistry of the distributed zones and the fast chemistry from the turbulent mixing controlled regions. A local stirred reactor approximation is assumed as an evident solution to account for species segregation, micro-mixing and complex chemistry effects. The molecular fluxes calculations are omitted at first but finally considered by including the mixing Kolmogorov time scale and random turbulent motion of the reacting regions.

As in the EDC model, it is assumed in the PaSR approach that combustion takes place in the fine structures of typical length scale smaller than the control volumes. Each cell of the computational grid is partitioned into two locally uniform regions, i.e. a non-reacting surroundings solely driven by turbulent mixing and a reacting part referring to the fine structures. The virtual composition state space, suggested by Vulis, refers in fact to the composition space within the fine structures so that $\psi^v \equiv \psi^*$. All interactions between fluid elements within a cell follow the *interactions by exchange with the mean* principle, whereas the mean cell values are obtained as weighted sum of the fine structures and surroundings quantities, as in Eq. (5). The mean reaction rates, contributing to the transport equations of the chemical species, are estimated as the reaction rates from the fine structures multiplied by the cell reacting fraction, i.e. the volume fraction of the cell occupied by the fine structures, see Eq. (6). The PaSR model differs from the EDC model on the estimation of the cell reacting fraction and the characteristic time of the fine structures but the general form of the chemical reaction rates, see Eq. (16), is conserved. In addition, the PaSR approach features chemical information through the estimation of a characteristic time for chemistry. Since combustion is assumed to be a sequential process where finite-rate chemistry proceeds after turbulent mixing, the total conversion time is assumed to be the sum of the characteristic timescales for mixing and chemistry. The cell reacting fraction in the PaSR model is then estimated as the ratio between the chemical time scale and the total conversion time. To the authors' knowledge, the PaSR model has never been thoroughly reviewed. The various existing versions of the PaSR model in the literature lead to several points of discussions. The original mathematical development of the PaSR combustion model, along with its different adaptations, are presented hereafter.

The determination of the reaction rates within the fine structures is a crucial point. From the stationary balance equations of a modified

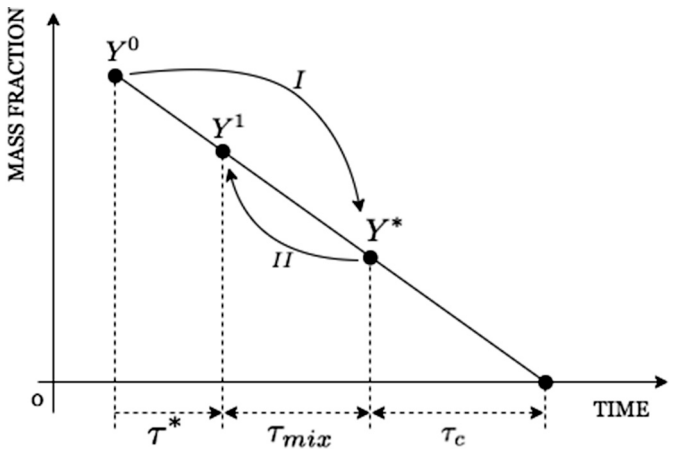

Fig. 9. Simplified chart of the PSR rate balances.
Source: Adapted from Golovitchev [138].

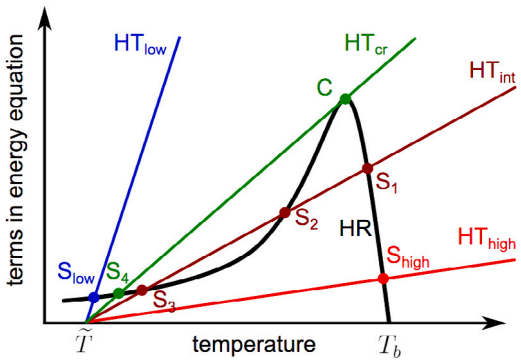

Fig. 10. Steady-state solutions of well-stirred reactors [86,132,146]. HR — Heat Release, HT — Heat Transfer, S — Solution, C — Critical conditions.

PSR representing the reaction zone and interacting with its surroundings, see Fig. 9, the Vulis equations [135] read as

$$\frac{\dot{\omega}(\psi^*)}{\rho} = \frac{Y^1 - Y^0}{\tau^*} = \frac{Y^* - Y^1}{\tau_{mix}} = -\frac{Y^*}{\tau_c}, \tag{31}$$

where Y^0 and Y^1 are the inflow and outflow mass fractions, τ^* is the mean residence time within the reactor, and τ_{mix} and τ_c are the characteristic timescales for mixing and chemistry, respectively. The reactor quantities Y^* may be expressed in terms of inflow and outflow parameters from Eq. (31) by posing the reduced variable $x = \tau^*/\tau_{mix}$, i.e. the dimensionless ratio between the mean residence and mixing time scales,

$$Y^* = (1 + \frac{1}{x})Y^1 - \frac{1}{x}Y^0 \Longleftrightarrow Y^1 = \kappa^* Y^* + (1 - \kappa^*)Y^0, \tag{32}$$

where $\kappa^* = \tau^*/(\tau^* + \tau_{mix})$ is the definition of the reactive volume fraction introduced in the works of Karlsson [136] and Golovitchev et al. [137]. In the case of fast mixing, i.e. the mixing time scale is much faster that the reactor residence time, the PSR conditions are recovered and the fine structures quantities tend to be the mean values $\psi^* \approx \tilde{\psi}$. From Fig. 9, one can also write

$$\frac{\dot{\omega}(\psi^*)}{\rho} = -\frac{Y^1}{\tau_c + \tau_{mix}} = -\frac{Y^1}{\tau_c + \tau_{mix}}\frac{\tau_c}{\tau_c} = -\frac{Y^1}{\tau_c}\kappa, \tag{33}$$

with the rate multiplier introduced by Chomiak and Karlsson in [34] defined as

$$\kappa = \frac{\tau_c}{\tau_c + \tau_{mix}}. \tag{34}$$

Chomiak and Karlsson explicitly described the term κ as the molecularly mixed fraction of the cell volume available for chemical processes, hence bringing confusion with the previously defined term κ^* (no clear distinction between the two quantities). From the literature, the term κ in Eq. (34) is the dominant expression for the cell reacting volume fraction and replaces the term $\gamma^*\chi$ in Eqs. (5) and (6) in the context of the PaSR model. A direct relation between the two modelled terms can be made. Assuming fast chemistry $\tau_c \ll \tau_{mix}$ in Eq. (34) with mixing and chemical time scales associated with the integral length and Kolmogorov-like flame sheets, respectively, i.e. $\tau_{mix} \sim k/\varepsilon$ and $\tau_c \sim \tau_\eta = (\nu/\varepsilon)^{1/2}$, yields the relation $\kappa \approx (\nu\varepsilon/k^2)^{1/2} \sim \gamma_\lambda^2$. The PaSR model makes fewer assumptions about the combustion process than the EDC approach.

By considering the term $-Y^1/\tau_c$ of Eq. (33) as the first-order approximation of the Arrhenius reaction source terms calculated using the exit reactor parameters $\dot{\omega}(\psi^1)/\rho$ [53,138], the model may be considered a corrected quasi-laminar expression. Under the simplistic assumption that in most combustion regions, the fine structures composition may be approximated by the mean quantities $\psi^* \approx \tilde{\psi}$ [47,54,140–143], the mean PaSR reaction rates, to be returned to the solver, directly read as

$$\bar{\dot{\omega}} = \kappa\dot{\omega}(\tilde{\psi}), \tag{35}$$

where the terms $\dot{\omega}(\tilde{\psi})$ are given by calculating the Arrhenius reaction source terms at the mean quantities. This is the version of the PaSR model that is available by default in most of the combustion CFD codes such as ANSYS Fluent [134] and OpenFOAM [144]. While further considering that the mixing time scale is much faster than the chemical time scale, i.e. assuming $\tau_{mix} \ll \tau_c$, it results that the term κ is approximated as unity. This version of the model simplifies itself to the Quasi-Laminar (QL) approach [145], also referred as the Implicit-LES (ILES) in the LES framework [72,142].

While Eq. (35) may be sufficient for extinction problems, Moule et al. [146] noted the limitations of this expression in self-ignition mixtures scenarios, where ψ^* may greatly vary with respect to $\tilde{\psi}$. The algebraic equations of a PSR achieving steady state from Eqs. (14) may yield multiple solutions, such as the two stable 'hot' and 'cold' solutions, respectively depicted as S_1 and S_3 solutions in Fig. 10, and pose problems with convergence due to potential hysteresis behaviours [132]. In particular, the importance of the initial conditions was stressed on the converging behaviour of the intermediate and unstable S_2 solution, hence calling for a need of a more comprehensive approach. Revoking the limiting assumption $\psi^* \approx \tilde{\psi}$, the PaSR model may solve subgrid balance equations for the fine scale quantities, as in [35,72,132,147]. As a solution to this problem, Moule et al. [132,148,149] proposed the Unsteady-PaSR (UPaSR) model. The UPaSR subgrid equations consider the transient terms in the subgrid set of balance equations of Eqs. (14). These are equivalent to unsteady PSR equations departing from the surroundings composition, i.e. $\psi^{\text{inlet}} = \psi^0$, see Eq. (26). Eq. (5) is employed to express the balance equations of the subgrid mass fractions in terms of known quantities $\tilde{\psi}$ and yields a factor $1/(1-\kappa)$,

$$\begin{cases} \dfrac{dY_i^*}{dt} + \dfrac{1}{1-\kappa}\dfrac{Y_i^* - \tilde{Y}_i}{\tau_{mix}} = \dfrac{\dot{\omega}_i(\psi^*)}{\tilde{\rho}}, \\ h(\psi^*) = h(\tilde{\psi}), \end{cases} \tag{36}$$

with κ defined as in Eq. (34) and the residence time scale estimated as $\tau^* = (1-\kappa)\tau_{mix}$. The resolution of Eqs. (36) provides the fine structures conditions ψ^* and the mean reaction rates are then obtained similarly to Eq. (6) as

$$\bar{\dot{\omega}} = \kappa\dot{\omega}(\psi^*). \tag{37}$$

Further considering subgrid effects, Sabelnikov and Fureby [35,65] developed the Extended-PaSR approach in the LES framework — later derived in the context of RANS simulations by [86]. Rooted in the mathematical modelling of multiphase flows, the EPaSR model extends

the PaSR approach by accounting for the unsteady convective and diffusive terms in the balance equations of the fine structures quantities. An exchange term is added to the fine structures balance equations to account for the exchange rate of mass and molecular diffusion at the immaterial interface between the fine structures volume and the surrounding fluid. The multiphase flow approach leads to consider dual energy, pressure and density for the mean values and the fine structures, hence complicating the EPaSR implementation. The subgrid equations for the fine structures mass fractions can be found in Sabelnikov and Fureby [35,65]. Once the fine structures conditions from the EPaSR solution are known, the mean reaction rates are calculated similarly as in the UPaSR model, see Eq. (37).

More recently, some authors [129,150] benefited from the numerical advantages of PFRs [61] to estimate the fine structures conditions ψ^*. Considering Eqs. (16) in a PaSR framework using a PSR, the mean reaction rates write as

$$\bar{\dot{\omega}}_i = \frac{\kappa}{1-\kappa}\frac{\bar{\rho}(Y^*_{i,\mathrm{PSR}} - \tilde{Y}_i)}{\tau^*}. \tag{38}$$

The cell reacting fraction κ is estimated as Eq. (34) and the residence time scale τ^* is assumed to be equal to the mixing time scale. As discussed in Section 4.3.3 and in Lewandowski and Ertesvåg [127], $(Y^*_{i,\mathrm{PFR}} - \tilde{Y}_i) = (Y_{i,\mathrm{PSR}} - \tilde{Y}_i)/(1-\kappa)$, from modelling the fine structures with a PFR departing from the mean composition $\tilde{\psi}$. In this context, the rates equivalent to those obtained from a PSR approach are recovered by

$$\bar{\dot{\omega}}_i = \kappa\frac{\bar{\rho}(Y^*_{i,\mathrm{PFR}} - \tilde{Y}_i)}{\tau^*}. \tag{39}$$

This form of the chemical source terms has been widely employed in recent numerical investigations [129,151–154].

Originally, the residence time within the fine structures τ^* was calculated from the characteristic mixing time scale. Chomiak and Karlsson [34] estimated the characteristic mixing time scale with a compromise between a single scale, i.e. the eddy break-up time scale which was considered much too long, and the integration of the whole spectrum of time scales as in the MIL model of Gonzalez and Borghi [139]. The formulation includes the geometrical mean of the two most important turbulent scales, namely the eddy-break-up time scale $\tau_I = k/\varepsilon$ leading from large-scale to Kolmogorov-scale non uniformities, and the Kolmogorov time scale $\tau_\eta = (\nu/\varepsilon)^{1/2}$ determining the local molecular interaction for the reactions,

$$\tau_{mix} = \sqrt{\tau_I\tau_\eta} = \sqrt{\frac{k}{\varepsilon}\left(\frac{\nu}{\varepsilon}\right)^{1/2}}. \tag{40}$$

In the context of the LES framework, Sabelnikov and Fureby [35] suggested adapting Eq. (40) by replacing the integral mixing time scale with the subgrid velocity stretch time scale $\tau_{v'} = (\Delta/v')$ where Δ is the LES grid size and v' are the velocity fluctuations, i.e.

$$\tau_{mix} = \sqrt{\tau_{v'}\tau_\eta} = \sqrt{\frac{\Delta}{v'}\left(\frac{\nu}{\varepsilon}\right)^{1/2}}. \tag{41}$$

Kärrholm and Nordin [48,54] also estimated the mixing time scale as a certain fraction of the integral time scale,

$$\tau_{mix} = C_{mix}\tau_I = C_{mix}\frac{k}{\varepsilon}, \tag{42}$$

where C_{mix} the mixing constant, typically ranging from 0.001 to 0.3 [150,151]. Another approach [150] is based on arguments from the fractal theory of turbulent structures,

$$\tau_{mix} = \left(\frac{C_\mu}{Re_\tau}\right)^{\frac{1-\alpha}{2}}\frac{k}{\varepsilon}, \tag{43}$$

where $\alpha = 3(D-3)/(1+D)$ with D the fractal dimension, $C_\mu = 0.09$ is the constant of the turbulent $k-\varepsilon$ model and $Re_\tau = \nu_t/\nu$ is the turbulent Reynolds number. The term $\left(C_\mu/Re_\tau\right)^{\frac{1-\alpha}{2}}$ in Eq. (43) can be viewed as a way to express the model constant C_{mix} as a function of the local turbulent Reynolds number. Still, all previous formulations can be regarded as global approaches. In particular, the wide variability of the constants C_{mix} and D motivated the development of a more comprehensive approach. Senouci et al. [155] developed a local formulation for τ_{mix} involving the scalar mixing time scale τ_ϕ from Raman and Pitsch [156],

$$\tau_{mix} = \tau_\phi = \frac{\widetilde{\phi^{\varepsilon 2}}}{\widetilde{\epsilon_\phi}}, \tag{44}$$

where $\widetilde{\phi^{\varepsilon 2}}$ is the filtered scalar variance and $\widetilde{\epsilon_\phi}$ the filtered scalar dissipation rate. In the LES framework, the transported scalar equations based on mixture fraction $[\widetilde{Z}, \widetilde{Z^{\varepsilon 2}}, \widetilde{\chi}_{sgs}]$ write as in [157],

$$\frac{\partial(\bar{\rho}\widetilde{Z})}{\partial t} + \frac{\partial(\bar{\rho}\widetilde{u}_j\widetilde{Z})}{\partial x_j} = \frac{\partial}{\partial x_j}\left[\bar{\rho}(D + D_{sgs})\frac{\partial\widetilde{Z}}{\partial x_j}\right], \tag{45}$$

$$\frac{\partial(\bar{\rho}\widetilde{Z^{\varepsilon 2}})}{\partial t} + \frac{\partial(\bar{\rho}\widetilde{u}_j\widetilde{Z^{\varepsilon 2}})}{\partial x_j} = \frac{\partial}{\partial x_j}\left[\bar{\rho}(D + D_{sgs})\frac{\partial\widetilde{Z^{\varepsilon 2}}}{\partial x_j}\right] + 2\bar{\rho}D_{sgs}\left(\frac{\partial\widetilde{Z}}{\partial x_j}\right)^2 - \bar{\rho}\widetilde{\chi}_{sgs}, \tag{46}$$

$$\frac{\partial(\bar{\rho}\widetilde{\chi}_{sgs})}{\partial t} + \frac{\partial(\bar{\rho}\widetilde{u}_j\widetilde{\chi}_{sgs})}{\partial x_j} = \frac{\partial}{\partial x_j}\left[\left(\frac{\mu}{Sc} + \frac{\mu_{sgs}}{Sc_{sgs}}\right)\frac{\partial\widetilde{\chi}_{sgs}}{\partial x_j}\right] - C_1\bar{\rho}\frac{\widetilde{\chi}^2_{sgs}}{\widetilde{Z^{\varepsilon 2}}} - C_2C_D\bar{\rho}|\widetilde{S}|\widetilde{\chi}_{sgs} + C_3C_D\frac{\mu_{sgs}}{Sc_{sgs}}|\widetilde{S}|\left(\frac{\partial\widetilde{Z}}{\partial x_j}\right)^2 + C_4C_D\bar{\rho}|\widetilde{S}|\widetilde{\chi}_{sgs}, \tag{47}$$

where $D_{sgs} = \nu_{sgs}/Sc_{sgs}$ is the Subgrid Scale (SGS) diffusivity and $Sc_{sgs} = 0.4$ is the Subgrid Scale (SGS) Schmidt number. $C_D = 0.17$ and C_1, C_2, C_3 and C_4 are model constants of standard values 2.0, 1.8, 1.7 and 1.4, respectively [157]. Other sets of constant values can be found in [151,157,158].

In contrast to the EDC model, the PaSR approach allows the integration of chemical information through the estimation of a characteristic time scale for chemistry. As a wide range of time scales is present in chemical dynamics, the selection of a unique characteristic time τ_c is a significant simplification. Chomiak and Karlsson [34] employed a species limited approach, i.e. the chemical species which is consumed first. The estimation of the chemical time scale is based on the formation rates of the species acting as fuel and oxidiser which are deemed to best represent the changes in the reacting system,

$$\frac{1}{\tau_c^{\mathrm{Ch.}}} = \max\left(\frac{-\dot{\omega}_F}{Y_F}, \frac{-\dot{\omega}_O}{Y_O}\right)/\rho, \tag{48}$$

where $\dot{\omega}$ is the global conversion rate, Y is the species mass fraction, and the subscripts F and O stand for fuel and oxidiser respectively. Fox [8] considered all the reacting species and their individual chemical time scales calculated as the inverse of the eigenvalue λ_i of the Jacobian matrix $J_{jk} = \partial\dot{\omega}_j/\partial Y_k$, where $\dot{\omega}_j$ is the jth species net production rate and Y_k the kth species mass fraction. After removing the dormant species, characterised by infinite time scale values, the maximum chemical time scale is then assigned to τ_c,

$$\tau_c = \max\left(\frac{1}{|\lambda_i|}\right). \tag{49}$$

Although accurate, the method yields a higher computational cost with respect to other chemical time scale formulations due to the decomposition of the Jacobian matrix of the species source terms. As a compromise between accuracy and computational cost, other works [128,129,152,154,159–161] considered the Slowest Formation Rate (SFR) time scale as the leading one (after removing the N_D dormant species that are characterised by an absolute formation rate $|\dot{\omega}_i|$ lower than a given threshold $\varepsilon = 10^{-16}$),

$$\tau_c^{\mathrm{SFR}} = \max_{i=[1,N_S-N_D]}\left(\frac{Y_i}{|\dot{\omega}_i|/\rho}\right). \tag{50}$$

Sabelnikov and Fureby [35] also considered using a timescale $\tau_c \approx \delta_u/s_u \approx \nu/s_u^2$ based on the laminar flame thickness δ_u and speed s_u. The evaluation of the characteristic time scales in the PaSR model is still an open question and will be discussed in the following Section 5.

4.5. Clarification of the PaSR terminology

As underlined by Marzouk and Huckaby [141], the PaSR model, described above, is to be differentiated with a class of stochastic partially stirred reactor models that can also be found in the literature [162–165]. Although resembling the reactor-based models described in previous sections, these stochastic approaches have been developed in the Lagrangian framework. Originally, Correa [162] developed a stochastic PaSR approach suitable for particle tracking in probability density functions (PDF) transport equations. The stochastic steady state of unmixedness is maintained in the reactor by considering the inlet composition is different from the one inside the reactor, i.e. $\psi^{\text{inlet}} \neq \psi$. Assuming spatial homogeneity in the flow, the joint velocity-composition PDF degenerates into a PDF on composition scalars ψ only. For a given variable, the PDF is expressed from the values taken by each among the N_P individual particle. The general equations for the N_S species mass fractions and energy of a particle n are calculated as

$$\begin{cases} \dfrac{dY_i^n}{dt} = -C_\phi \omega (Y_i^n - \tilde{Y}_i) + \dfrac{\dot{\omega}_i(\psi^n)}{\rho^n}, \\ \bar{C}_p \dfrac{dT^n}{dt} = \dfrac{dH^n}{dt} - \sum_{i=1}^{N_S} h_i \dfrac{dY_i^n}{dt}, \end{cases} \tag{51}$$

with the species $i = 1, \ldots, N_S$ and particle $n = 1, \ldots, N_P$ indexes, yielding a coupled system of $(N_S + 1) \times N_P$ first-order ordinary differential equations (ODEs) in time. C_ϕ is a model constant, ω is the mixing frequency, H^n is the enthalpy of particle n and h_i are the species enthalpies [162]. In Eq. (51), the first term of the right-hand-side represents scalar mixing and identifies itself as the linear deterministic relaxation to the mean, also referred to as the Interaction by Exchange with the Mean (IEM) model [166,167] The Lagrangian IEM model was designed by Villermaux [166] where a set of Lagrangian equations is solved to study the composition evolution of fluid particles. The change of concentration in a point is caused by chemical reactions and diffusion. The diffusion term is modelled as a mass exchange between the point and its inert environment represented by a statistical mean value. Exchanges between fluid particles are expected to happen over a unique turbulence time scale, proportional to k/ε, describing the local conditions of the reactor. The environment concentration can be evaluated with the two-environment concept. In the case of a Perfectly Stirred Reactor, the mean value is the average concentration in the volume. If a Plug-Flow Reactor is considered, the mean is the average concentration of the fluid of the same age. Details about the IEM model and its extensions can be found in Borghi [167].

The Modèle Lagrangian Intermittent (MIL) model [168] extends the Lagrangian (IEM) model by allowing the exchange time to capture a distribution of turbulence timescales rather than being unique. Gonzalez and Borghi [139] present the theoretical development of the MIL model in the context of diffusion flames although premixed flames can also be considered with limited model modifications. In addition, the model features "sudden combustion" happening after an ignition delay, i.e. fast reactions but taking place after a given chemical time interval (slow chemistry due to unmixedness), which relaxes the assumption of infinitely fast chemistry. On a phase plane (mixture fraction-like/oxidiser mass fraction for diffusion flames), the trajectories of fluid particles are affected by mixing before suddenly jumping from mixing lines to chemical equilibrium lines. In combination with the IEM equations, this allows an expression of the mean reaction rate as a combination of the chemical contributions from the jump and in the vicinity of the equilibrium lines (remnant reactions). The chemical contributions are evaluated from time integrals containing the distribution of turbulence timescales and are null along the mixing lines. The ignition delay time is estimated as the inverse of the instantaneous consumption rate of oxidiser given by an Arrhenius law from mixtures on the mixing lines. When comparing the model to experimental results, difficulty in predicting reignition arose. An accurate estimation of the turbulent scales and the integration of more detailed chemistry for the estimation of the ignition delay were suggested for model improvement [139].

5. Modelling MILD flames with reactor-based models

5.1. Introduction

From a fluid-dynamic point of view, industrial systems operating under MILD conditions are characterised by high flow recirculation within the combustion zone [88,97]. This allows diluted oxygen concentrations and homogeneous temperature fields to be achieved in practical systems. Such conditions are challenging for combustion models that have originally been developed for conventional combustion. Efforts were put to adapt the numerical models to cope with the specific MILD combustion features. Canonical test cases were considered in the first place. In particular, lab-scale configurations with simple geometries have been designed to provide high-fidelity experimental data for numerical model validation. Towards more complex cases, the models were then validated on lab-scale burners operating under more realistic conditions. Industrial furnaces, of nominal firepower of the order of megawatts (MW), can be investigated with confidence. In addition to the *a posteriori* validation of combustion models, DNS data of turbulent combustion can supply key information to turbulence-chemistry interactions models [169].

The closure of the chemical source terms in MILD combustion has been widely investigated in both RANS and LES frameworks [13]. In particular, reactor-based models have succeeded in proving their modelling capabilities and advantages over other combustion models for MILD applications [14,158]. Reactor-based modelling in the context of MILD combustion consists of addressing modelling issues such as constant tuning, fine structures interpretation, reactor type treatment or sub-modelling choices. The modelling insights, gathered through the investigation of test cases of various scales, are presented and discussed hereafter.

5.2. Jet-in-Hot-Coflow burners

5.2.1. Experimental configurations

Among canonical configurations, Jet-in-Hot-Coflow (JHC) burners emulate MILD conditions by means of hot and highly oxygen diluted co-flows, as in Adelaide Jet-in-Hot-Coflow [100] or the Delft Jet-in-Hot-Coflow [93,170]. The Adelaide Jet-in-Hot-Coflow burner is composed of a central fuel jet and an annulus pipe for a hot coflow formed by a secondary burner mounted upstream of the jet exit plane with surrounding air in a wind tunnel [100], see Fig. 11(a). The jet nozzle feeds the burner with blends of methane CH_4 and hydrogen H_2 [171], or more complex fuels such as ethylene C_2H_4 [45,172] or *n*-heptane C_7H_{16} [52,173]. Configurations of the flames with changing inlet velocities are available with resulting Reynolds numbers ranging from 5000 to 20,000. In addition, the oxygen level in the coflow has been varied between 3% or 9%. While the 9% case is typically transitional between conventional and MILD combustion regime, the 3% configuration yields MILD conditions. The two cases of different dilution level provide Damköhler numbers of 4.76×10^{-1} and 2.82×10^{-2}, respectively [174]. Experimental measurements of temperature, mixture fraction and species mass fractions are available. The Delft Jet-in-Hot-Coflow (DJHC) configuration is similar to the AJHC but features a partially premixed coflow [93,170], see Fig. 11(b). The jet stream Reynolds number, the maximum coflow temperature and the coflow oxygen mass fraction are the variable parameters of the DJHC burner.

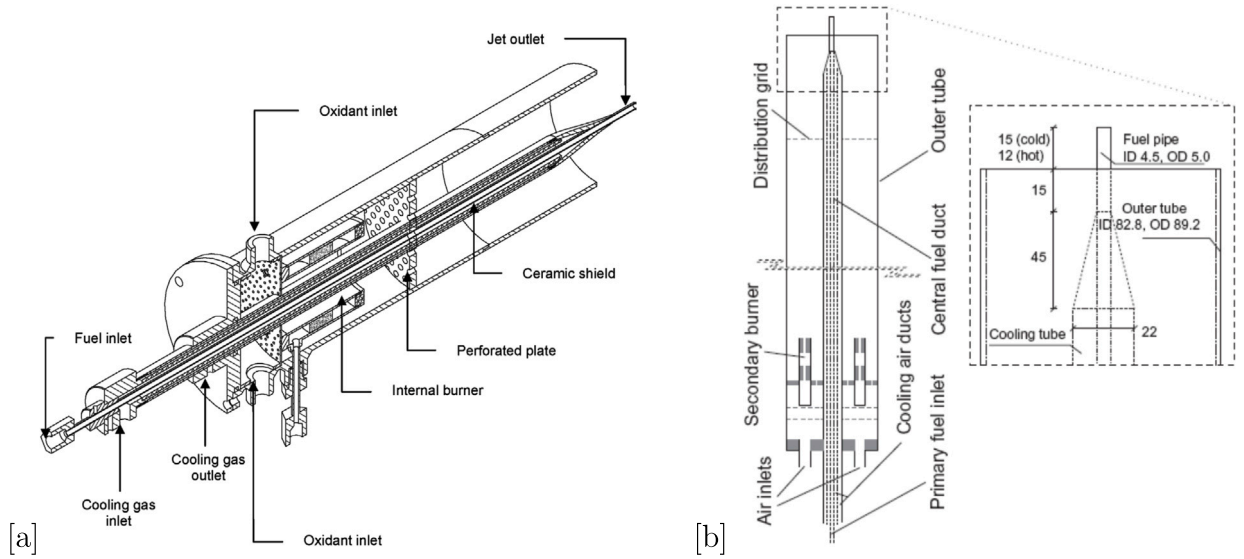

Fig. 11. Sketches of the Adelaide Jet-in-Hot-Coflow [100] and the Delft Jet-in-Hot-Coflow [170] .
Source: Reprinted from *Dally, B.B., Karpetis, A.N., Barlow, R.S., 2002. Structure of turbulent non-premixed jet flames in a diluted hot coflow. Proceedings of the Combustion Institute 29, 1147–1154*, doi:10.1016/S1540-7489(02)80145-6 and *Oldenhof, E., Tummers, M.J., van Veen, E.H., Roekaerts, D.J.E.M., 2011. Role of entrainment in the stabilisation of jet-in-hot-coflow flames. Combustion and Flame 158, 1553–1563*, doi:10.1016/j.combustflame.2010.12.018., with permission from Elsevier.

Particle Image Velocimetry (PIV) and/or Laser Doppler Anemometry (LDA) [93] are available as experimental data. The affordability of investigating such test cases numerically allows the validation of model hypotheses. Rather complete sets of experimental data are available, suitable for model development.

5.2.2. Modified EDC models

Anchored in empiricism, the EDC model is subject to model constant tuning. Various authors [129,175–178] modified the original values of the primary $[C_{D1}; C_{D2}]$ and secondary $[C_\gamma; C_\tau]$ model constants, obtaining improved prediction levels. The adjustments of the EDC constants in the MILD combustion context have been thoroughly discussed [127,178] and are summarised in reviews on the EDC approach [14,37]. Attempts have been made to revise the EDC model more in depth, with more sophisticated solutions than constant tuning.

Aminian et al. [179] proposed an extended EDC extinction model for MILD combustion where finite-rate chemistry effects are considered. In the EDC extinction model, extinction within the fine structures occurs when the local fine structures residence time is lower than a given critical time. To alleviate the computational cost of the EDC model when dealing with detailed chemistry, Farokhi and Birouk [180] proposed a hybrid EDC/flamelet approach using tabulated chemistry from steady laminar flamelet calculations. The approach was validated against the experimental measurements from the piloted Sandia flames [58,67,68,181]. Furthermore, Farokhi and Birouk [182] proposed a modification of the EDC model based on arguments from fractal theory. The modelling of the fine scales is revised and no longer depends solely on the turbulent fields but also considers the combustion regime. A fractal-based flame surface density (FSD) approach is adopted in the case of premixed flames whilst the turbulent intermittency of velocity field is used for diffusion flames. The AJHC configuration was considered as a validation case and better results were obtained with respect to a standard EDC approach.

Some recent modified EDC models for MILD combustion can be found for the AJHC [183,184], the DJHC [184–186] and on other configurations [43,187]. Furthermore, the EDC model has been revised for low turbulence combustion in an attempt of generalisation [36,128,188,189]. A summary is given in Ertesvåg [126].

5.2.3. PaSR sub-models

Works can be found using the PaSR combustion model in both RANS [52,129,150,152,190] and LES [159,191] frameworks on the JHC configurations. Various time scale sub-models for the PaSR model have been investigated in canonical cases of MILD combustion.

Li et al. [129] investigated the AJHC configuration with Reynolds number 10,000 and 3% O_2 by means of RANS and reactor-based models. Three versions of the EDC model were compared to a PaSR approach employing a combination of the mixing geometrical mean formulation, see Eq. (40), and the slowest formation rate chemical time scale, see Eq. (50). The PaSR model provided great improvement in the results, notably by reducing temperature over-predictions at axial position 60 mm and 120 mm and accurately predicting mass fraction fields for CO_2 and NO. Along with the influence of the combustion model, various effects have been investigated such as turbulence model parameters, boundary conditions or chemical mechanisms. In particular, the impact of the reactor treatment, between a PSR and a PFR, was found to have a limited impact on the results. The accurate predictions from the PaSR approach motivated Li et al. [192] and Ferrarotti et al. [150] to extend the discussion on the sub-models selection. Both investigated configurations of the AJHC burner operating with different Reynolds numbers and oxygen dilution levels. Li et al. [192] compared the accurate but expensive Jacobian matrix chemical time scale to the fast formation rates approach. It was concluded that the formation rate approach provides the best compromise between accuracy and computational cost. Ferrarotti et al. [150] investigated the role of the mixing time scale in the PaSR model while fixing the chemical time scale formulation. The results yield a wide variability in the predictions of temperature and species profiles by modifying the values of C_{mix} from 0.1 to 0.9 in Eq. (42) and D from 3.5 to 4.4 in Eq. (43). By increasing the model constants, a temperature peak reduction was observed. It was concluded that a constant value of $C_{mix} = 0.5$ led to improved results for the $Re = 10000$ and 3% O_2 AJHC configuration. Allowing a non constant C_{mix} equivalent value, the fractal model did not provide a significant improvement of the results with respect to the integral formulation. In addition to global approaches, the local formulation of the mixing time scale was studied with different sets of coefficients for the scalar dissipation rate equation. Both works [150,192] reported that the local methods outperformed the global formulations, especially at predicting the mean temperature and species mass fractions of CO

and OH. The effect of the four constants, $[C_1, C_2]$ for dissipation rate production and $[C_3, C_4]$ for dissipation rate sinking and embedded in Eq. (44), appeared to be limited in this case. Amaduzzi et al. [193] applied Uncertainty Quantification (UQ) [194,195] to assess the sensitivity effect of the constant parameters on numerical simulations of the Cabra flame [196], which shares similar physics to the JHC burner. While the production parameters showed minimal importance, the largest contribution to the uncertainty in the flame temperature was estimated to come from the dissipation parameters.

Towards LES, Li et al. [159] compared the PaSR approach with two implicit combustion models, namely Quasi Laminar Finite-Rate (QLFR) model and Laminar Finite-Rate (LFR) model, to assess the role of the combustion subgrid closure. Originally estimated from the mixing time scale, the residence time scale τ^* in Eq. (39) may equal the simulation step time in the LES context [159,191]. A combination of the SFR time scale and the subgrid velocity stretch mixing time scale was employed. Limited changes were found in the results of an AJHC configuration from the three approaches. On fine enough LES grids, implicit models can be used without critical loss of accuracy. Computational Singular Perturbation (CSP) and Tangential Stretching Rate (TSR) analysis [197–200] were carried out in [191] on the LFR-LES results [159] to investigate the nature of turbulence–chemistry interactions in MILD combustion. Local flame extinction and re-ignition were observed for the 10,000 Reynolds number and 3% O_2 case. Regions of equilibrium, within the coflow region, and intense chemical activity, where fuel and coflow mix, were identified by means of fast-slow system modes identification. An extended TSR validated the importance of both auto-ignition and diffusion-controlled ignition under MILD conditions [11,15,97].

5.2.4. Uniqueness of the cell reacting fraction

In the EDC model, the uniqueness of the cell reaction fraction $\gamma^*\chi$ emerges from the consideration of a single global step chemistry [123]. Although it is a common modelling practice, the set of equations Eqs. (22),(23),(24) may yield several χ values in the context of multi-step chemistry [37]. In the PaSR approach [34], a single pair of characteristic timescales allows a unique cell reacting fraction κ. While the assumption of a unique fraction is questionable from a physical standpoint, since multiple reacting layer thicknesses exist as a consequence of the multi-scale nature of reacting flows [201], closing the species transport equations with arbitrary species dependent in reactor-based models may not assure mass balance, as:

$$\sum_{i=1}^{N_S} \bar{\omega}_i = \frac{\bar{\rho}}{\tau^*} \sum_{i=1}^{N_S} (\gamma_\lambda \chi_i \text{ or } \kappa_i)(Y_i^* - Y_i^0) \stackrel{?}{=} 0 \tag{52}$$

is satisfied only if $\gamma_\lambda\chi_i \equiv \gamma_\lambda\chi$ or $\kappa_i \equiv \kappa$, or if $\{\gamma_\lambda\chi_i\}_{i=1,\dots,N_s}$ or $\{\kappa_i\}_{i=1,\dots,N_s}$ are exactly a solution of Eq. (52). This difficulty has been discussed by Iavarone et al. [152] and further extended by Péquin et al. [154]. The uniqueness of the cell reacting fraction is a general limitation of reactor-based models and applies to other combustion regimes than MILD combustion.

Simulating the AJHC burner, Iavarone et al. [152] proposed two or multiple-κ PaSR solutions, obtained by adaptive chemical time scales, to improve the source term predictions of selected species, such as NO. In particular, the local peak productions of N-containing species were correctly captured by introducing a specific κ that takes close to unity values, i.e. by using slow chemical time scales representative of certain nitrogen oxides (NO_x) formation pathways. Although resulting in small mass imbalances, estimated at 1.6% of the total mass as a volume integral over the whole CFD domain [152], the proposed solutions showed great improvement in the prediction of small chemical species for the AJHC burner. Going further, Péquin et al. [154] highlighted the difficulty of finding a physically meaningful family of fractions by performing a PaSR model decomposition using a DNS dataset of CO/H_2 with moderate turbulence [202]. While evaluating the sources of errors from each model layer, the authors motivated the need to develop a more comprehensive model able to integrate multiple reacting fractions for individual or group of species. To tackle the problem, Quadarella et al. [203] proposed a revision of the PaSR approach using CSP modal decomposition [197–200]. The eigenvalues of the Jacobian matrix of the chemical source terms were used to retrieve characteristic time scales for chemistry [8]. Although strongly deviating from the original PaSR formulation, abandoning the fine structures concept, the obtained results demonstrated the benefits of accounting for multiple reacting fractions. These promising results still need validation on challenging points such as larger chemical mechanisms, *a posteriori* testing or in the context of MILD combustion.

5.3. Lab-scale combustors

5.3.1. Experimental configurations

Open flame configurations are suitable for thorough optical measurements, while optical access is rather limited in enclosed flames devices [151,204–207]. More complex lab-scales systems achieve MILD regime aerodynamically by means of internal recirculation [151,204–207]. Four burners were selected to broaden the spectrum of MILD burner configurations. More lab-scale combustion devices can be found in the literature [13,55,208].

A small-scale combustion burner with internal recirculation was presented by Castela et al. [207] with a fuel thermal input of 8 kW. In this case, a reverse flow configuration is employed to achieve MILD conditions where the inlets and the exhaust gases outlet are mounted at the top of the combustion chamber, see Fig. 12(a) [204]. Fuel is fed into the chamber through a central orifice whilst preheated air is supplied through an annular orifice. This configuration is surrounding by an additional annular orifice for exhaust gases exit and ensures intense reactants/products mixing and a high residence time, suitable to reach complete combustion. The combustion chamber is made of a quartz-glass cylinder with a stainless steel plate closing the bottom end of the chamber. Probes can be inserted through a central hole in the steel plate for experimental measurements. Veríssimo et al. [204] presented a 10 kW lab-scale combustor running under MILD and conventional combustion modes. The details of the operational, combustion, and emission characteristics of the burner can be found in Veríssimo et al. [204]. From the configuration presented by Castela et al. [207], the bottom of the combustion chamber is made open by an outlet convergent nozzle of angle 15° and length 150 mm. A strong recirculation region with hot flue gases is achieved aerodynamically because of the converging section.

Chinnici et al. [205,209,210] developed a 20 kW annulus Hybrid Solar Receiver Combustor (HSRC) burner operated in the MILD combustion regime with internal recirculation, using multiple, inclined jets, see Fig. 12(b). MILD combustion can be achieved for a wide range of fuels, including H_2, syngas, and fossil fuels, and for different energy sources, including hybrid solar-MILD combustion operations. Four coils allow to assess the impact of heat load on stability and performance of MILD combustion. PIV data of non-reacting flows, temperature, thermal efficiency, and pollutant emissions for both MILD and MILD-solar modes are available for this furnace.

Sorrentino et al. [92,206,211] proposed the Laboratory Unit CYclonic (LUCY) burner, see Fig. 12(c). Two sets of fuel and pre-heated oxidiser (composed of oxygen and diluent) streams are fed into the combustion chamber from diagonally opposed locations inducing a cyclonic flow field. Burnt gases exit the chamber from a central position. The burner operates at a nominal thermal power of 2 kW. For experimental measurements, two thermocouples are placed at the mid-plane of the combustion chamber. A quartz window composes one of the chamber wall allowing side-view observations.

Ferrarotti et al. [151] presented a semi-industrial MILD furnace operating with a nominal power of 20 kW, see Fig. 12(d). The experimental setup allows for the variation of the inlet nozzle configurations, air excess, fuel and air velocity, and internal load. Fuel and air are

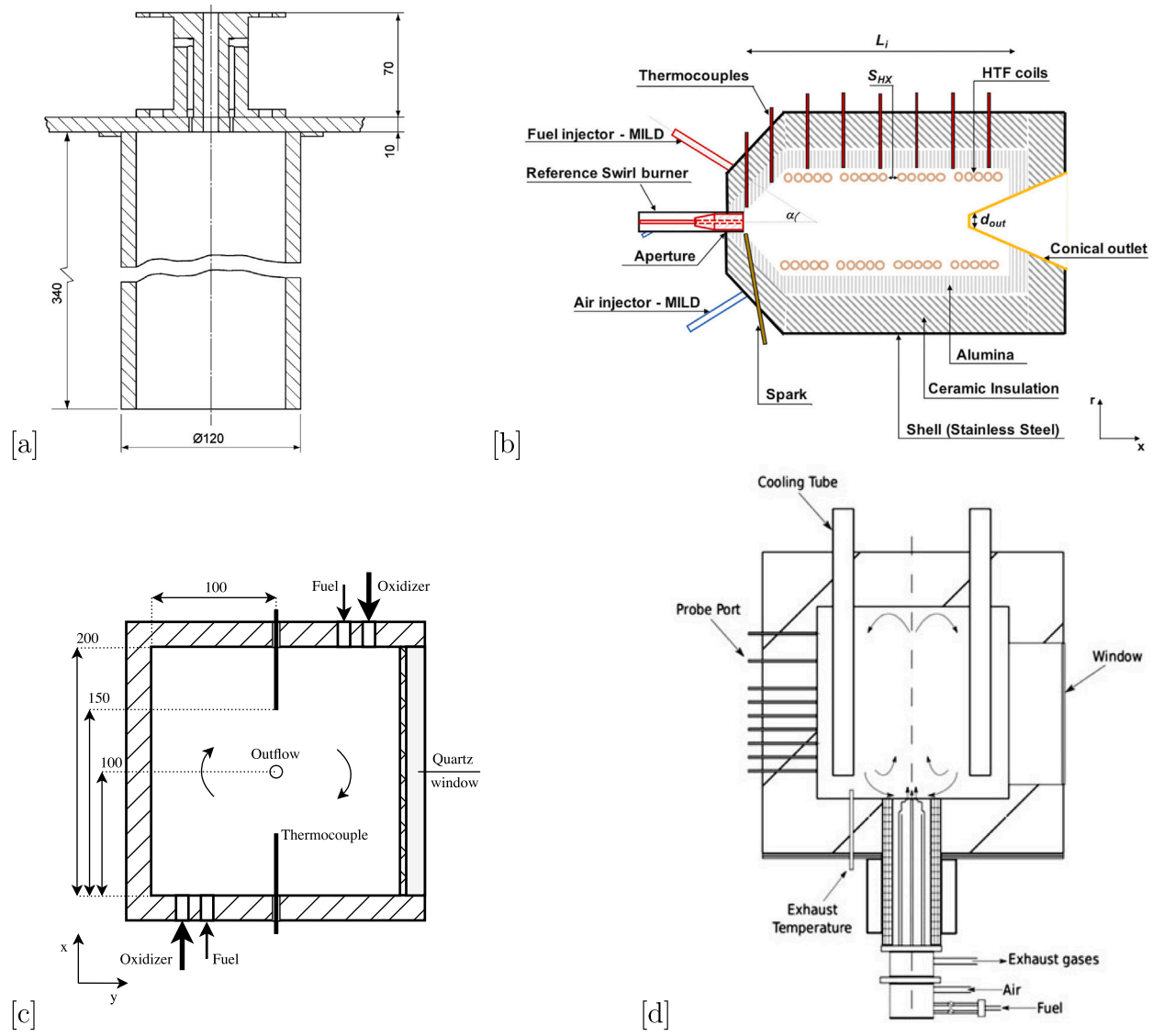

Fig. 12. Sketches of lab-scale combustors: (a) reverse-flow [204]; (b) HSRC [205]; (c) cyclonic [206]; (d) semi-industrial [41] .
Source: Reprinted from *Veríssimo, A.S., Rocha, A.M.A., Costa, M., 2011. Operational, Combustion, and Emission Characteristics of a Small-Scale Combustor. Energy & Fuels 25, 2469–2480,* doi:10.1021/ef200258t. *publisher: American Chemical Society*. Copyright 2023 American Chemical Society. Reprinted from *Chinnici, A., Nathan, G.J., Dally, B.B., 2018. Combined solar energy and combustion of hydrogen-based fuels under MILD conditions. International Journal of Hydrogen Energy 43, 20086–20100*, doi:10.1016/j.ijhydene.2018.09.027, with permission from Elsevier.

fed coaxially into the combustion chamber through separated jets. The standard configuration yields a fuel jet Reynolds number of 6000 and uses natural gas as fuel. Experimental Measurements are available from a combination of a side-view quartz window and OH* chemiluminescence imaging, thermocouple for in-flame temperature profiles and electrochemical sensors for the exhaust gas composition. An integrated heat exchanger recovers heat from the exhaust gases and preheats the combustion air. The unit is also equipped with an internal air cooling system.

5.3.2. Numerical studies

Graça et al. [212] investigated the reverse flow small-scale combustor [207], Fig. 12(a), by means of RANS simulations with two combustion models, namely the EDC and the composition-PDF (C-PDF) approaches. A case of MILD combustion regime was achieved by increasing the air flow rate [207]. Numerical flow patterns revealed an extended recirculation zone in which the fuel is engulfed. Both models under predicted the temperature field at the centreline and close to the burner inlets/outlets. With respect to experimental studies, combustion was delayed further downstream. None of the effects from the turbulence models, the boundary conditions or heat transfer phenomena between the air and fuel supplies were found responsible for this temperature discrepancy. Only a modification of the EDC constant C_γ value from 2.13 to 5, combined with a modified constant of the realisable $k-\varepsilon$ turbulence model, provided an amelioration in the results. Graça et al. [212] suggested an LES study should be conducted to focus on the mixing and chemical processes happening in the near burner region. Li et al. [213] conducted LES of the convergent nozzle configuration by Veríssimo et al. [204] using a modified 2005 EDC version with $\chi = 1$ and a PaSR model with similar settings as in Li et al. [159]. The analysis of streamline profiles revealed the existence of a relatively small recirculation zone at the side corner of the burner and a larger one in the middle of the combustion chamber, responsible for the preheating of fresh mixtures by hot burnt gases. The main recirculation zone was shifted upstream when using the PaSR model and resulted in better predictions of mean temperature and species mole fractions. Similarly to Li et al. [191], LES data were analysed using advanced post-processing methods such as the chemical Tangential

Stretching Rate (TSR) [198–200], balance analysis [11,15,97] and local Principal Component Analysis (PCA) [107,214,215] analysis. It was found that both auto-ignition and flame-like structures play equally important roles in MILD combustion.

Chinnici et al. [205] investigated the HSRC burner, see Fig. 12(b), operated in combustion-only mode, by means of RANS simulations. The numerical study investigated the effects of varying the type of fuel (natural gas (NG), liquefied petroleum gas (LPG), hydrogen) on the heat transfer mechanisms in a MILD combustion process. As combustion closure, the EDC model was used with simplified chemistry (6-step mechanism) for the oxidation of different fuels, namely, methane, propane and hydrogen, as in Evans et al. [177]. Key simulation variables such as the sensible heat in the exhaust and the maximum cavity temperature were calculated and compared with experimental measurements, yielding errors of around 3%. The numerical analysis revealed that the higher performance when burning hydrogen under MILD conditions is due to a higher radiative heat transfer rate. The EDC model was also employed in Chinnici et al. [210] where the MILD HSRC burner was fuelled with syngas at varying ratios of H_2/CO and nitrogen N_2 dilution levels.

Amaduzzi et al. [216] compared RANS simulations of the LUCY burner, see Fig. 12(c), using a flamelet generated manifold (FGM) approach and a PaSR model as combustion closures. Three values of the model constant $C_{mix} = [0.01, 0.1, 0.5]$ were considered along with the local mixing time scale formulation with standard parameter values [157]. The combustion chamber was fed with pure methane as fuel and different degrees of diluted air with pure N_2. The increase of the dilution level resulted in slower combustion processes and more homogeneous temperature field. For the non-diluted case, a strong temperature over prediction in the reacting zone was observed from the FGM solution. The value $C_{mix} = 0.5$ yielded the best agreement with the experimental measurements among the global PaSR solutions. From the diluted case, the impact of the combustion model on the predictions was reduced. Greater accuracy was obtained while employing the PaSR approach with the local definition on both cases. The numerical simulations were analysed by means of flame index and revealed dissimilarities in the combustion regimes from the two approaches. In particular, the FGM solution yielded a non-premixed behaviour whilst the PaSR model was mostly characterised by a premixed combustion regime, much aligned with the strong flow recirculation induced by the cyclonic configuration.

Ferrarotti et al. [151] numerically studied the semi-industrial furnace configuration, see Fig. 12(d), with both reactor-based models. The modified 2016 version of the EDC model [36] failed to capture the ignition region of the furnace. Results from PaSR solutions were also investigated with special attention given to the mixing time scale formulation. Two mixing definitions, namely the integral and the local approaches were employed along with the SFR chemical time scale definition. The C_{mix} constant value between 0.5 and 0.7 was found to provide the best predictions. Some variation in the results was observed in this case by modifying the four parameters of the scalar dissipation rate transported equation. The standard set of values, originally derived for homogeneous turbulence and two-dimensional configurations, may be optimised to obtain better agreement with the experiments. The comparison of 2D axisymmetric and 3D computational domains enabled the assessment of complex turbulent flow patterns. A temperature peak over estimation in the 2D case was corrected by means of a more homogeneous temperature field in the 3D configuration. Streamlines from the 3D case demonstrated the existence of three main vortices responsible for the dilution and the preheating of fresh reactants by the hot burnt exhaust gases. Additional vortices of smaller length scale were observed interacting with side walls and cooling tubes hence further complicating the internal flow pattern.

5.3.3. Development of Digital Twins

For their ability to cope with different operating conditions, reactor-based combustion models are ideal at providing numerical data for the development of Digital Twins (DT) [217]. DT may be defined as a predicted digital representation of a physical object that can closely simulate its behaviour in real time and environment, and have recently been applied to combustion systems [218–221]. The elevated computational expense of 3D CFD simulations of practical systems limits the exploration of new operating conditions. Reduced-Order Models (ROMs) [218] can be used to predict combustion data at unexplored operating conditions and with reasonable accuracy and abated computational cost. ROMs are obtained by means of two sequential steps, data compression and interpolation. For dimensionality reduction, several methods can be employed such as Principal Component Analysis (PCA)-based approaches [218,222,223], or modal Proper Orthogonal Decomposition (POD) [219]. The Kriging method [218] is of common use for interpolation. Aversano et al. [218] developed a methodology for Reduced Order Model (ROM) generation by means of PCA and Kriging. Drastic dimensionality reduction was obtained from a local form of PCA (LPCA). The Kriging method enabled the prediction of new-observed system states by weaving the non-linear relation between the reduced set of coefficients and the input parameters. Once trained, ROMs allow sensitivity analysis of the system parameters at a reduced cost even for very CPU-intensive systems. In Aversano et al. [218], datasets of 1D and 2D flames were used to train and validate the generated surrogate models. Satisfactory predictions were obtained in terms of temperature and species molar mass fractions. Aversano et al. [218] aimed at applying the method on more realistic combustion systems as to expose the full potential of ROMs and DTs.

Aversano et al. [219] built the first-of-its-kind digital twin of a furnace operating in MILD combustion conditions, namely the semi-industrial furnace [151] displayed in Fig. 12(d). An ensemble of forty-five three-dimensional CFD simulations of the furnace operating at different conditions were employed for ROM training and validation. The simulations used the PaSR model as combustion closure and were spread out on the design space made of three input parameters: air injector diameter, global equivalence ratio (from 0.7 to 1) and fuel composition (mixtures ranging from pure methane to pure hydrogen). A combination of POD for data compression and Kriging for the interpolation of the POD coefficients in the unexplored regions of the design space was used. The trained ROM exhibited satisfactory prediction capabilities at unseen input conditions. In particular, key combustion assets such as wall temperatures, pollutants and minor species spatial distribution and exhaust gas composition were predicted with errors below 5%. The ensemble of PaSR simulations were also employed in Procacci et al. [220] for the development of a hybrid numerical–experimental Digital Twin of the semi-industrial furnace. The objective was to accurately reconstruct 3D fields from a limited number of experimental measurements. The optimal number (14) of sensors and their ideal placement within the furnace were found by means of sparse sensing — a QR decomposition with column pivoting (QRCP) was combined to POD. The features to be measured at each location were also given. From sensor inputs at unseen operating conditions, the hybrid DT yielded better prediction accuracy with respect to the experimental measurements, when compared with CFD simulations and the purely numerical DT [219]. The generalisation capabilities of the hybrid DT were further explored by Procacci et al. [221]. The design space was modified to account for the addition of benzene C_6H_6 in H_2-rich fuel mixtures to mimic Coke Oven Gas (COG) industrial mixtures. Although feeding the system with heterogeneous and sparse datasets, obtained from experimental measurements, satisfactory accuracy was obtained while comparing the DT predictions to reference solutions. Having a ROM providing reliable and instantaneous predictions of expensive simulations outcome is paramount for the development of digital twins for real systems, which can be employed for system control and visualisation.

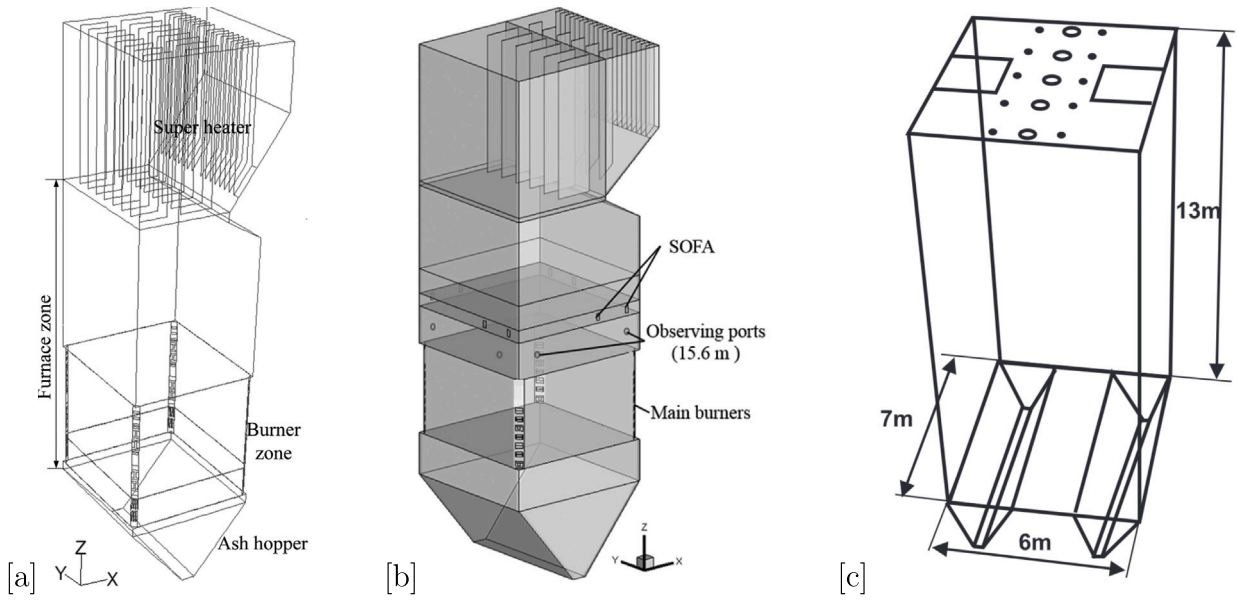

Fig. 13. Schematic diagrams of industrial tangentially-fired utility boilers and their burner nozzle arrangements with nominal powers (a) 200 MW [229] and (b) 100 MW [228] and (c) a HiTAC burner operated at 130 MW [231].
Source: Reprinted with permission from *Fang, Q., Musa, A.A.B., Wei, Y., Luo, Z., Zhou, H., 2012. Numerical Simulation of Multifuel Combustion in a 200 MW Tangentially Fired Utility Boiler. Energy & Fuels 26, 313–323*, doi:10.1021/ef201149p. *publisher: American Chemical Society*. and *Tan, P., Ma, L., Fang, Q., Zhang, C., Chen, G., 2016. Application of Different Combustion Models for Simulating the Co-combustion of Sludge with Coal in a 100 MW Tangentially Coal-Fired Utility Boiler. Energy & Fuels 30, 1685–1692*, doi:10.1021/acs.energyfuels.5b02236. *publisher: American Chemical Society*. Copyright 2023 American Chemical Society. Reprinted from *Schaffel-Mancini, N., Mancini, M., Szlek, A., Weber, R., 2010. Novel conceptual design of a supercritical pulverised coal boiler utilising high temperature air combustion (HTAC) technology. Energy 35, 2752–2760*, doi:10.1016/j.energy.2010.02.014, with permission from Elsevier.

5.4. Industrial furnaces

5.4.1. Towards industrial-scale burners

The fundamental aspects of MILD combustion with special attention on industrial applications were discussed by Weber et al. [224,225] in a series of experiments. A semi-industrial furnace, of thermal input 580 kW, was operated with different fuels, namely, methane, oil and coal. In-furnace measurements reported uniformly distributed fields for temperature and gas composition, and no-visible flame. While lab-scale burners offer the opportunity to inform modelling approaches in more realistic conditions, larger applications from the industry are the ultimate target of modelling development. Industrial furnaces [226–230] are characterised by nominal powers of order of tens or hundreds of megawatts such as industrial boilers and reheat furnaces. Examples of industrial applications, simulated by means of reactor-based combustion models, are given hereafter.

5.4.2. Coal-fired utility boilers

Byproducts of the iron and steel industries such blast furnace gas (BFG) and coke oven gas (COG) represent a valuable secondary energy source. Processing these gaseous fuels reduces the need for external fuels. To increase the thermal efficiency of industrial boilers, multiple fuels are jointly fed. Pulverised coal is of common use in combination with COG and BFG. This introduces complex geometries in practical systems which need to feature multiple separated inflows. Two examples of tangentially-fired utility boilers, operating with nominal powers of 200 MW [229] and 100 MW [228], are presented in Fig. 13. In three-stream configurations [228–230], combustion closures based on mixture fraction would likely fail and reactor-based models represent a modelling alternative. The case study in Fang et al. [229] is a 200 MW boiler of size 10.8 × 11.9 × 44.6 m, see Fig. 13(a), co-firing pulverised coal with BFG and COG. A total of 16 burner nozzles are placed at each corner. Three groups of super-heaters are mounted on top of the furnace. Fang et al. [229] simulated the 200 MW boiler by means of RANS simulations and EDM. The reasonable computational cost of EDM allowed the assessment of the BFG and COG flow rates effect on the boiler performance. It was found beneficial to increase the COG flow rate to gain thermal efficiency, as opposed to increasing the BFG flow rate. From the numerical study, an optimal operating condition was determined to maximise the boiler performance at 180 MW load.

Co-combustion of sludge with coal is a promising sludge disposal approach [232]. Tan et al. [228] investigated a 100 MW tangentially coal-fired utility boiler with separated over-fire air (SOFA) of dimensions 10 × 10 × 34.4 m, see Fig. 13(b). Different modelling approaches, namely a double mixture fraction/probability density function model, the EDM and the ED/FR model, were employed to simulate the addition of sludge into the co-firing process. In combination with a multiple-surface-reaction sub-model for char decomposition, the ED/FR model was able to capture the features of coal-sludge co-combustion (ignition, char burnout, NO_x emissions). The mixture fraction based approach failed at providing good estimates of NO_x emissions and unburnt carbon proportion in fly ash. The inclusion of sludge delayed fuel ignition and reduced char burnout. In addition, the high moisture and nitrogen composition in sludge were found responsible for promoting NO_x emissions.

Existing boiler configurations would face fluid slag when burning Zhundong (ZD) coal, a particular type of coal abundant in China whose composition varies from regular coal [230]. Notably, ZD coal features high amount of volatile compounds, low sulphur and ash content, along with elevated sodium content which significantly limits its widespread in the power generation industry. Generally blended with low sodium coal, i.e. negatively impacting coal processing cost, efforts are made to burn ZD coal on its own. For this purpose, Kang and Ding [230] investigated a 660 MW supercritical face-fired boiler of dimensions 25.8 × 16.6 × 79.5 m for the combustion of pure ZD coal. When reaching a critical temperature, pulverised coal particles release volatile matters, along with sodium and sulphur products. For its ability to cope with detailed kinetics, the EDC model was selected in combination with an optimised 32-step elemental reaction mechanism. Such attention was critical to understand the role of sodium-containing substances decomposition in the slagging process on heat-absorbing surfaces.

As far as non-conventional combustion regimes are concerned, Schaffel-Mancini et al. [231] conceptualised an original large-scale pulverised coal fired boiler design to enable high temperature air combustion (HiTAC) technology, which differs from MILD combustion regime by satisfying the condition $(\Delta T - T_{ign}) > 0$ (negative in the case of MILD combustion [97]). Three key points drove the HiTAC burner design, namely, the existence of an intense recirculation zone within the burner, homogeneous scalar fields and uniform heat fluxes. The burner shape and dimensions were optimised using CFD-based numerical simulations employing the EDC model as combustion closure. The study yielded a down-fired boiler configuration of dimensions $6 \times 7 \times 13$ m with nozzles placed on the top wall: two square flue gas outlets and five burners composed of a central injector of hot air and two coal guns positioned on both sides. This arrangement promotes strong internal flow patterns with limited zones of low-intense turbulence. Combustion products recirculation participates at diluting and heating up both air and fuel jets. For a total thermal input of 130 MW, the HiTAC boiler provided abated NO_x emissions with respect to other pulverised coal fired boilers technologies. The down-fired boiler configuration was further explored by Perrone et al. [233] in an attempt to combine HiTAC and oxy-combustion technologies. Due to the absence of N_2 in the oxidiser stream, replacing air with a mixture of O_2/CO_2, NO_x emissions were reduced from 135 in the HiTAC example to 75 mg/MJ in the HiTAC-oxy case according to CFD simulations using the ED/FR combustion model.

5.4.3. Reheating furnaces

In the steel industry, fossil fuels are largely consumed in reheating furnaces to heat steel billet, tubes or slabs [234]. In particular, pusher [227] or walking beam [226] type reheating furnaces consist of an assemble of separated heating zones, namely the convective, preheating, heating and soaking zones. Steel plates are loaded and unloaded from opposite ends of the burner. The clear separation between each individual zone allows reheating furnaces to be modelled as a sequential process, i.e. with a multi-block approach [226]. Each part of the domain can be characterised by local fuel and oxidiser conditions enabling the use of the steady flamelet model (SFM). Landfahrer et al. [226] compared the numerical performance of the SFM approach with EDM and EDC results of a walking beam type reheating furnace of dimensions $13 \times 24 \times 1.66$ m and maximum thermal power 34.8 MW. Although providing fairly good results in the air-fired part, i.e. preheating, heating and soaking zones, the SFM approach failed at capturing the thermal features of the oxy-fired part (convective part). Noticeable differences in the spatial species distribution were observed while comparing the tabulated chemistry approach with the reactor-based models. The EDM over-predicted the oxy-fuel flame temperature peak whilst EDC provided the best results. Eventually, the multi-block approach showed its limitations in case of noticeable backflow, i.e. flow transfer in between the part of the furnace. Capturing the turbulent flow patterns developing in the whole domain becomes mandatory for improved accuracy of the CFD simulations. Such a modelling consideration would make the application of the SFM approach unfeasible without modification. Reheating furnaces are an illustration of the application range of reactor-based models. Other types of conditions, e.g. poorly defined inlet streams, multiple inhomogeneous fuels, recirculating and flame–flame interactions, are other examples where reactor-based models may provide a numerical solution at a reasonable computational cost.

5.5. High-fidelity DNS data

5.5.1. A priori testing

By resolving all scales, DNS data of turbulent combustion can supply key information to turbulence-chemistry interactions models using both RANS and LES frameworks. As modelled terms must be expressed as a function of known quantities, high-fidelity DNS data is particularly appealing for the development and validation of combustion models [235]. *A posteriori* testing challenges the model within an integrated simulation framework, which is required to quantify realistic model errors [169]. However, the potential discrepancies observed in the results between simulation and the reference data may not be caused only by the tested model. Furthermore, the availability of DNS data of MILD combustion represents a real opportunity to develop efficient combustion models [169]. *A priori* testing is an example of modelling routes where filtered DNS values of the quantities of interest are compared with the modelled values. This allows the direct validation of model assumptions and has been extensively employed for the development of reactor-based models in the context of non-premixed flames [154,203,236], premixed flames [237,238], rocket combustors [239] or MILD combustion [160,240].

5.5.2. Validation of model assumption

Shamooni et al. [236] compared the EDC approach against scale similarity (SS) based combustion models on a temporally evolving non-premixed jet flame. Two DNS snapshots, characterised by maximum local extinction and re-ignition, were selected to assess the predictive capabilities of the combustion models. To mimic the LES framework, two filter widths were employed, respectively, in the inertial (coarse) and in the near dissipation (fine) range of the energy spectrum. The EDC model was adapted to the LES context by assuming the EDC factor as $\mathbf{g}_{EDC} = \gamma^*_{\text{LES}}/(1-\gamma^*_{\text{LES}})$ with $\gamma^*_{\text{LES}} = (u^*/u_{sgs})^2$ where u_{sgs} is the subgrid level based on the subgrid turbulent kinetic energy. It was shown that the term $\gamma^*_{\text{LES}} \approx 0.5$ yielded very small variation across mixture fraction values, i.e. $\mathbf{g}_{EDC} \approx 1$. As far as the chemical source terms of CO are concerned, all approaches were able to accurately reproduce the target values from the fine grid at extinction time. Aiming at coarser resolution, prominent discrepancies were observed in the EDC case whilst all other approaches, including a 'no-model' or QL approach, matched the filtered DNS values. A similar conclusion could be drawn from the H_2 and CO_2 rates at low grid resolution and re-ignition time. The developed SS models showed limited improvement for radical species predictions.

In MILD combustion, Iavarone et al. [160] performed an *a priori* testing of the PaSR model on non-premixed MILD combustion DNS data of Doan et al. [12], see Fig. 3(b). Both the characteristic timescales τ_c, τ_{mix} were assessed by comparing modelled net production and heat release rates with the corresponding quantities directly filtered from the DNS. Among many sub-model formulations, the most accurate predictions for CH_4, CO_2 and CO, were obtained while combining the local estimation of the mixing time scale of Eq. (44) with the SFR approach for the chemical time scale of Eq. (50). The slightly worse predictions of the OH rates were further discussed. The highest overestimation of the OH source terms was attributed to zones of low reactivity with extremely small values of τ_{mix} yielding an elevated term $\kappa\bar{\rho}/\tau^*$. Better OH results were obtained by considering the standard geometrical mean formulation of the mixing time scale, see Eq. (40). It was showed that the mixing time scale is the leading scale within the PaSR model.

5.5.3. Applications of data-driven techniques and machine-learning

As employing a unique time scale in the PaSR model was found sub-optimal, Péquin et al. [241] proposed a methodology based on supervised partitioning algorithms to provide local optimal sub-models. Guided by a heat release rate-based function, clustered versions provided modelling solutions with significant error cut-offs, and so independently of the combustion regime considered.

Leveraging the increased availability of high-fidelity DNS data, Machine Learning (ML) [242] has been widely applied in combustion [243,244]. Besides being difficult to interpret, Neural Networks (NN) based models face generalisation problems [245] and thus require

training data with a broad range of conditions. Due to their non-linear behaviour, chemical reaction rates are good candidates for machine learning applications and have been investigated with Convolutional Neural Networks (CNN) [246] and Deep Neural Network (DNN) [247–249].

As far as reactor-based models are concerned, Jigjid et al. [240] proposed an ML-aided PaSR approach in the context of a transported progress variable. DNS data of MILD combustion from the EGR based configurations [11,12], see Fig. 3, were used for training and validation. In particular, the prediction capabilities of the trained models were assessed on cases with higher dilution level (more intense MILD condition) and higher Karlovitz numbers. Inspired by the PaSR closure, the modified mean reaction rate of a progress variable was written as $\bar{\dot{\omega}}_c = \kappa \dot{\omega}_c^*$. The fraction of the reactive structure was predicted through a combination of Neural Networks (NNs), i.e. $\kappa = \kappa_{NN} f_{NN}$ with f_{NN} considered as an adjustment term to account for different mixing modes. Prior to the study, a first NN was trained at differentiating the local combustion regime between ignition/interaction mode. The trained combustion mode identifier $\bar{\boldsymbol{\Phi}}_{NN}$ served as input variable for two additional NNs for the respective prediction of κ_{NN} and f_{NN}. In a transported progress variable framework, the fine structures progress variable source term would be evaluated as $\dot{\omega}_c^* = \bar{\rho}(c^* - c^0)/\tau^*$ although c^* is still unknown. A first-order approximation $\dot{\omega}_{c,0_{\text{th}}}$, i.e. considering an infinitely fast mixing time scale, was used to estimate the term $\dot{\omega}_c^*$ from the grid scale quantities $\tilde{\psi}$, yielding the final expression of the progress variable source term $\bar{\dot{\omega}}_c = \kappa_{NN} f_{NN} \dot{\omega}_{c,0_{\text{th}}}$. The NN-aided model provided higher prediction capabilities with respect to the 0-th order approximation, and so for both premixed and non-premixed validation cases. In addition, the results were consistent across a range of LES grid resolutions. Although convoluted, the ML-aided modelling approach used by Jigjid et al. [240] demonstrated the potential benefits of applying machine learning tools within the reactor-based combustion model framework.

Notwithstanding the benefits, deep learning tools suffer from a lack of interpretability which prevents the understanding of the underlying physics of the resulting models. Machine learning and sparse-promoting techniques have recently been combined to discover parsimonious models [250] to cope with model interpretability. Leveraging sparse symbolic regression, Freitas et al. [237] explored a library of functional forms for the cell reacting fraction κ in the PaSR model. In addition to candidates supported by prior knowledge, the library was over-parameterised with arbitrary non-linear functions, e.g. sigmoid or error-based functions, to show the robustness of the proposed approach. Among the solutions, the results showed that data mostly supported the model form $\kappa = 1/(1 + Da)^{1/3}$ as a suitable balance between predictions accuracy and modelling complexity.

6. Concluding remarks

Reactor-based combustion models — the Eddy Dissipation Concept (EDC) and the Partially Stirred Reactor (PaSR) models — are derived from the fine structures theory, where combustion takes place in reacting pockets, of size similar to the Kolmogorov scale, embedded in larger turbulent structures. To accurately describe turbulent reacting flows, the characteristics of the fine structures are to be estimated. In the EDC model, a stepwise energy cascade model is employed to link the small-dissipative scales with the large-scale eddies by scale-similarity. The energy transfer rate and key modelling quantities such as the mass fraction and the mean residence time of the fine structures are parameterised by flow variables and model constants. The evaluation of the fine structures characteristics, along with the numerical values of the model constants, are subject to discussion and have yielded multiple versions of the EDC model. In the PaSR model, the volume fraction of each computational cell available for chemical processes is estimated from the ratio between characteristic timescales for mixing and chemical processes. Numerous time scale definitions and PaSR model versions can be found in the literature.

The gas composition within the reacting structures is also to be evaluated. The fine structures are assumed to be reacting zones fed with fresh mixture by larger turbulent structures, and can be modelled as ideal reactors evolving in time. PSR, PFR and batch reactors were employed to handle finite-rate chemistry. Reactor-based models are fuel flexible and computationally affordable combustion closures for all kind of flames. This class of models has been successfully investigated thoroughly in both RANS simulations and LES frameworks. The present work reviewed the development of these combustion models on applications ranging from canonical flames to industrial burners, and can be summarised in the following points.

- Featuring finite-rate chemistry, reactor-based models may provide a valuable solution to any type of flame. With respect to conventional regimes, MILD combustion can ensure abated pollutant emissions along with high overall thermal efficiency. Modelling efforts were put to cope with the strong interplay between turbulence and chemistry under MILD combustion.
- Tuning procedures may be employed to adapt the models to specific conditions. In particular, EDC model constants and PaSR time scale submodels have been calibrated on a case-by-case basis from RANS computations. To assess the impact of model constants on numerical results, techniques such as uncertainty quantification should be employed in future investigations.
- Reactor-based models were extended in the effort of capturing unconventional combustion regimes such as MILD combustion. Recent studies generalised reactor-based models making the model parameters function of local flow and reaction scales.
- Being flexible across operating conditions, reactor-based models have been selected to provide numerical data for the development of digital twins and reduced-order-models.
- The increasing availability of DNS data has pushed the *a priori* development and assessment of advanced combustion models. Machine learning techniques such as neural networks can efficiently handle large datasets and be used to improve specific model components and broaden the range of applicability of reactor-based models. Moreover, techniques such as sparse regression may also support the discovery of new model forms.

The choice of a combustion model is driven by the relative contribution of chemistry and mixing, and on the quantities of interest. Models with simple chemical descriptions are generally selected for industrial cases with complex geometries and numerical grids. More comprehensive chemical mechanisms should be employed if minor species and pollutants are of interest. Adaptive chemistry approaches that seek a local comprehensiveness over a global one can be of use [215,251]. The EDC model, assuming that chemistry happens at a scale close to the Kolmogorov one, provides a viable numerical solution for a large variety of fuels and blends. When this implicit assumption does not hold, the model may lead to extinct solutions or large over-predictions. This justified the development and the use of different EDC variants to obtain improved results. Relaxing such hypothesis, the PaSR model generally outperforms other reactor-based solutions, even for low turbulence and various O_2 dilution levels in the system. For well resolving grids only, model simplifications such as the LFR and the QLFR approaches may be considered.

As for future directions, it is of interest to continue investigating the predictive capabilities of reactor-based models on more complex, alternative, diluted, fuels and blends, and aim to simulate combustion systems up to the industrial-scale. DNS will continue to provide numerical insights and support combustion model development. Machine learning tools, as many techniques exist, may also be considered to further explore new modelling frameworks.

Declaration of competing interest

The authors declare that they have no known competing financial interests or personal relationships that could have appeared to influence the work reported in this paper.

Data availability

No data was used for the research described in the article.

Acknowledgements

A. Péquin acknowledges the financial support of the Fonds National de la Recherche Scientifique (FRS-FNRS). Funding and support from The University of Adelaide and the Australian Research Council (ARC) is gratefully acknowledged. This work has received funding from the European Research Council (ERC) under the European Union's Horizon 2020 research and innovation programme under grant agreement No 714605 and Marie Skłodowska-Curie grant agreement No 801505.

References

[1] IEA. World energy outlook 2022. Technical report, 2022, URL https://www.iea.org/reports/world-energy-outlook-2022.
[2] Wünning JA, Wünning JG. Flameless oxidation to reduce thermal no-formation. Prog Energy Combust Sci 1997;23(1):81–94. http://dx.doi.org/10.1016/S0360-1285(97)00006-3.
[3] Cavaliere A, de Joannon M. Mild combustion. Prog Energy Combust Sci 2004;30(4):329–66. http://dx.doi.org/10.1016/j.pecs.2004.02.003.
[4] de Joannon M, Sorrentino G, Cavaliere A. MILD combustion in diffusion-controlled regimes of hot diluted fuel. Combust Flame 2012;159(5):1832–9. http://dx.doi.org/10.1016/j.combustflame.2012.01.013.
[5] Sabia P, Sorrentino G, Bozza P, Ceriello G, Ragucci R, De Joannon M. Fuel and thermal load flexibility of a MILD burner. Proc Combust Inst 2019;37(4):4547–54. http://dx.doi.org/10.1016/j.proci.2018.09.003.
[6] Kolmogorov A. The local structure of turbulence in incompressible viscous fluid for very large Reynolds' numbers. Akademiia Nauk SSSR Doklady 1941;30:301–5, ADS Bibcode: 1941DoSSR..30..301K.
[7] Pope SB. Turbulent flows. Cambridge University Press; 2000.
[8] Fox RO. Computational models for turbulent reacting flows. Cambridge University Press; 2003, Google-Books-ID, aIW6ECRlDDoC.
[9] Poinsot T, Veynante D. Theoretical and numerical combustion. R.T. Edwards, Inc.; 2005, Google-Books-ID, cqFDkeVABYoC.
[10] Bilger R, Pope S, Bray K, Driscoll J. Paradigms in turbulent combustion research. Proc Combust Inst 2005;30(1):21–42. http://dx.doi.org/10.1016/j.proci.2004.08.273.
[11] Minamoto Y, Swaminathan N, Cant RS, Leung T. Reaction zones and their structure in MILD combustion. Combust Sci Technol 2014;186(8):1075–96. http://dx.doi.org/10.1080/00102202.2014.902814, Publisher: Taylor & Francis _eprint.
[12] Doan NAK, Swaminathan N, Minamoto Y. DNS of MILD combustion with mixture fraction variations. Combust Flame 2018;189:173–89. http://dx.doi.org/10.1016/j.combustflame.2017.10.030.
[13] Perpignan AAV, Gangoli Rao A, Roekaerts DJEM. Flameless combustion and its potential towards gas turbines. Prog Energy Combust Sci 2018;69:28–62. http://dx.doi.org/10.1016/j.pecs.2018.06.002.
[14] Li Z, Parente A. A review of the numerical investigations of jet-in-hot-coflow burner with reactor-based models. Front Mech Eng 2020;6.
[15] Doan NAK, Swaminathan N. Autoignition and flame propagation in non-premixed MILD combustion. Combust Flame 2019;201:234–43. http://dx.doi.org/10.1016/j.combustflame.2018.12.025.
[16] Bürger K, Treib M, Westermann R, Werner S, Lalescu CC, Szalay A, et al. Vortices within vortices: Hierarchical nature of vortex tubes in turbulence. 2013, http://dx.doi.org/10.48550/arXiv.1210.3325, arXiv arXiv:1210.3325 [physics].
[17] Richardson LF. Weather prediction by numerical process. University Press; 1922.
[18] Kolmogorov AN. A refinement of previous hypotheses concerning the local structure of turbulence in a viscous incompressible fluid at high Reynolds number. J Fluid Mech 1962;13(1):82–5. http://dx.doi.org/10.1017/S0022112062000518, Publisher: Cambridge University Press.
[19] Batchelor GK, Townsend AA. The nature of turbulent motion at large wave-numbers. Proc R Soc Lond Ser A. Math Phys Sci 1949;199(1057):238–55. http://dx.doi.org/10.1098/rspa.1949.0136, Publisher: Royal Society.
[20] Obukhov AM. On the distribution of energy in the spectrum of turbulent flow. Bull Acad Sci USSR Geog Geophys 1941;5:453–66.
[21] Onsager L. The distribution of energy in turbulence. Phys Rev ONE Phys Ellipse Coll Pk, Md 20740-3844 Usa: Am Phys Soc 1945;68(11–1).
[22] Batchelor GK. Kolmogoroff's theory of locally isotropic turbulence. Math Proc Camb Phil Soc 1947;43(4):533–59. http://dx.doi.org/10.1017/S0305004100023793, Publisher: Cambridge University Press.
[23] Chomiak J. A possible propagation mechanism of turbulent flames at high Reynolds numbers. Combust Flame 1970;15(3):319–21. http://dx.doi.org/10.1016/0010-2180(70)90014-3.
[24] Gurvich AS, Yaglom AM. Breakdown of eddies and probability distributions for small-scale turbulence. Phys Fluids 1967;10(9):S59–65. http://dx.doi.org/10.1063/1.1762505, Publisher: American Institute of Physics.
[25] Saffman PG. Dependence on Reynolds number of high-order moments of velocity derivatives in isotropic turbulence. Phys Fluids 1970;13(8):2193–4. http://dx.doi.org/10.1063/1.1693217, Publisher: American Institute of Physics.
[26] Kuo AY-S, Corrsin S. Experiments on internal intermittency and fine-structure distribution functions in fully turbulent fluid. J Fluid Mech 1971;50(2):285–319. http://dx.doi.org/10.1017/S0022112071002581, Publisher: Cambridge University Press.
[27] Kuo AY-S, Corrsin S. Experiment on the geometry of the fine-structure regions in fully turbulent fluid. J Fluid Mech 1972;56(3):447–79. http://dx.doi.org/10.1017/S0022112072002459, Publisher: Cambridge University Press.
[28] Tennekes H. Simple model for the small-scale structure of turbulence. Phys Fluids 1968;11(3):669–71. http://dx.doi.org/10.1063/1.1691966, Publisher: American Institute of Physics.
[29] Corrsin S. Turbulent dissipation fluctuations. Phys Fluids 1962;5(10):1301–2. http://dx.doi.org/10.1063/1.1706518, Publisher: American Institute of Physics.
[30] Chomiak J. Application of chemiluminescence measurement to the study of turbulent flame structure. Combust Flame 1972;18(3):429–34. http://dx.doi.org/10.1016/S0010-2180(72)80194-9.
[31] Tanahashi M, Sato M, Shimura M, Miyauchi T. DNS and combined laser diagnostics of turbulent combustion. J Therm Sci Technol 2008;3(3):391–409. http://dx.doi.org/10.1299/jtst.3.391.
[32] Woodward PR, Porter DH, Sytine I, Anderson SE, Mirin AA, Curtis BC, et al. Very high resolution simulations of compressible, turbulent flows. In: Computational fluid dynamics. WORLD SCIENTIFIC; 2001, p. 3–15. http://dx.doi.org/10.1142/9789812811592-0001.
[33] Magnussen B. On the structure of turbulence and a generalized eddy dissipation concept for chemical reaction in turbulent flow. In: 19th aerospace sciences meeting. American Institute of Aeronautics and Astronautics; 1981, http://dx.doi.org/10.2514/6.1981-42, _eprint: https://arc.aiaa.org/doi/pdf/10.2514/6.1981-42.
[34] Chomiak J, Karlsson A. Flame liftoff in diesel sprays. In: Symposium (International) on Combustion, Vol. 26, no. 2. 1996, p. 2557–64. http://dx.doi.org/10.1016/S0082-0784(96)80088-9.
[35] Sabelnikov V, Fureby C. Extended LES-PaSR model for simulation of turbulent combustion. In: Progress in propulsion physics, Vol. 4. EDP Sciences; 2013, p. 539–68. http://dx.doi.org/10.1051/eucass/201304539.
[36] Parente A, Malik MR, Contino F, Cuoci A, Dally BB. Extension of the eddy dissipation concept for turbulence/chemistry interactions to MILD combustion. Fuel 2016;163:98–111. http://dx.doi.org/10.1016/j.fuel.2015.09.020.
[37] Ertesvåg IS. Analysis of some recently proposed modifications to the Eddy dissipation concept (EDC). Combust Sci Technol 2020;192(6):1108–36. http://dx.doi.org/10.1080/00102202.2019.1611565, Publisher: Taylor & Francis _eprint.
[38] Evans MJ, Sidey JAM, Ye J, Medwell PR, Dally BB, Mastorakos E. Temperature and reaction zone imaging in turbulent swirling dual-fuel flames. Proc Combust Inst 2019;37(2):2159–66. http://dx.doi.org/10.1016/j.proci.2018.07.076.
[39] Cuoci A, Frassoldati A, Faravelli T, Ranzi E. A computational tool for the detailed kinetic modeling of laminar flames: Application to C2H4/CH4 coflow flames. Combust Flame 2013;160(5):870–86. http://dx.doi.org/10.1016/j.combustflame.2013.01.011.
[40] Cuoci A, Frassoldati A, Faravelli T, Ranzi E. OpenSMOKE++: An object-oriented framework for the numerical modeling of reactive systems with detailed kinetic mechanisms. Comput Phys Comm 2015;192:237–64. http://dx.doi.org/10.1016/j.cpc.2015.02.014.
[41] Ferrarotti M, Bertolino A, Amaduzzi R, Parente A. On the influence of kinetic uncertainties on the accuracy of numerical modeling of an industrial flameless furnace fired with NH3/H2 blends: A numerical and experimental study. Front Energy Res 2020;8.
[42] Zhang J, Sui C, Zhang L, Jiang J, Zhang B. Effects of ammonia addition on combustion characteristics in partially-premixed swirling ammonia/methane/air flame. Therm Sci 2022;(00):13.
[43] Mousavi SM, Sotoudeh F, Jun D, Lee BJ, Esfahani JA, Karimi N. On the effects of NH3 addition to a reacting mixture of H2/CH4 under MILD combustion regime: Numerical modeling with a modified EDC combustion model. Fuel 2022;326:125096. http://dx.doi.org/10.1016/j.fuel.2022.125096.
[44] Han X, Yang J, Mao J. LES investigation of two frequency effects on acoustically forced premixed flame. Fuel 2016;185:449–59. http://dx.doi.org/10.1016/j.fuel.2016.08.005.

[45] Evans MJ, Chinnici A, Medwell PR, Ye J. Ignition features of methane and ethylene fuel-blends in hot and diluted coflows. Fuel 2017;203:279–89. http://dx.doi.org/10.1016/j.fuel.2017.04.113.

[46] Peterson DM. Simulation of a round supersonic combustor using wall-modeled large eddy simulation and partially-stirred reactor models. Proc Combust Inst 2022. http://dx.doi.org/10.1016/j.proci.2022.08.120.

[47] Baudoin E, Yu R, Bai, Nogenmur KJ, Bai X-S, Fureby C. Comparison of LES models applied to a bluff body stabilized flame. In: 47th AIAA aerospace sciences meeting including the new horizons forum and aerospace exposition. Orlando, Florida: American Institute of Aeronautics and Astronautics; 2009, http://dx.doi.org/10.2514/6.2009-1178.

[48] Nordin PAN. Complex chemistry modeling of diesel spray combustion. 2001.

[49] Tao F, Chomiak J. Numerical investigation of reaction zone structure and flame liftoff of DI diesel sprays with complex chemistry. SAE Trans 2002;111:1836–54, Publisher: SAE International.

[50] Tao F, Golovitchev VI, Chomiak J. A phenomenological model for the prediction of soot formation in diesel spray combustion. Combust Flame 2004;136(3):270–82. http://dx.doi.org/10.1016/j.combustflame.2003.11.001.

[51] Shah YG, Brasseur JG, Xuan Y. Assessment of disparities in estimating filtered chemical reaction rates in LES using DNS of turbulent premixed flames. Combust Theory Model 2020;24(6):1179–94. http://dx.doi.org/10.1080/13647830.2020.1831616, Publisher: Taylor & Francis _eprint.

[52] Li Z, Evans MJ, Ye J, Medwell PR, Parente A. Numerical and experimental investigation of turbulent n-heptane jet-in-hot-coflow flames. Fuel 2021;283:118748. http://dx.doi.org/10.1016/j.fuel.2020.118748.

[53] Golovitchev VI, Nordin N, Jarnicki R, Chomiak J. 3-D diesel spray simulations using a new detailed chemistry turbulent combustion model. SAE Trans 2000;109:1391–405, Publisher: SAE International.

[54] Kärrholm FP. Numerical modelling of diesel spray injection, turbulence interaction and combustion [Ph.D. thesis], Göteborg, Sweden: Department of Applied Mechanics, Chalmers University of Technology; 2008.

[55] Saha M, Dally BB, Chinnici A, Medwell PR. Effect of co-flow oxygen concentration on the MILD combustion of pulverised coal. Fuel Process Technol 2019;193:7–18. http://dx.doi.org/10.1016/j.fuproc.2019.04.033.

[56] Wartha E-M, Haugen NE, Karchniwy E, Bösenhofer M, Harasek M, Løvås T. The effect of turbulence on the conversion of coal under blast furnace raceway conditions. Fuel 2023;331:125840. http://dx.doi.org/10.1016/j.fuel.2022.125840.

[57] Dong M, Cui J, Jia M, Shang Y, Li S. Large eddy simulation of plasma-assisted ignition and combustion in a coaxial jet combustor. Energy 2020;199:117463. http://dx.doi.org/10.1016/j.energy.2020.117463.

[58] Barlow R, Frank J. Piloted CH4/Air flames C, D, E, and F – release 2.1. Technical report, Livermore, CA 94551-0969: Sandia National Laboratories; 2007, p. 12.

[59] Lysenko DA, Ertesvåg IS, Rian KE. Numerical simulation of non-premixed turbulent combustion using the eddy dissipation concept and comparing with the steady Laminar flamelet model. Flow Turbul Combust 2014;93(4):577–605. http://dx.doi.org/10.1007/s10494-014-9551-7.

[60] Lysenko DA, Ertesvåg IS, Rian KE. Numerical simulations of the Sandia flame D using the eddy dissipation concept. Flow Turbul Combust 2014;93(4):665–87. http://dx.doi.org/10.1007/s10494-014-9561-5.

[61] Bösenhofer M, Wartha E-M, Jordan C, Harasek M. The eddy dissipation concept—Analysis of different fine structure treatments for classical combustion. Energies 2018;11(7):1902. http://dx.doi.org/10.3390/en11071902, Number: 7 Publisher: Multidisciplinary Digital Publishing Institute.

[62] He D, Yu Y, Ma H, Liang H, Wang C. Extensive discussions of the eddy dissipation concept constants and numerical simulations of the sandia flame d. Appl Sci 2022;12(18):9162. http://dx.doi.org/10.3390/app12189162, Number: 18 Publisher: Multidisciplinary Digital Publishing Institute.

[63] Lu H, Chen W, Zou C, Yao H. Large-eddy simulation of sandia flame f using structural subgrid-scale models and partially-stirred-reactor approach. Phys Fluids 2019;31(4):045109. http://dx.doi.org/10.1063/1.5087078, Publisher: American Institute of Physics.

[64] Liu H, Yin Z, Xie W, Zhang B, Le J, Liu H. Numerical and analytical assessment of finite rate chemistry models for LES of turbulent premixed flames. Flow Turbul Combust 2022;109(2):435–58. http://dx.doi.org/10.1007/s10494-022-00329-7.

[65] Sabelnikov V, Fureby C. LES combustion modeling for high Re flames using a multi-phase analogy. Combust Flame 2013;160(1):83–96. http://dx.doi.org/10.1016/j.combustflame.2012.09.008.

[66] Huang Z-w, He G-q, Qin F, Wei X-g. Large eddy simulation of flame structure and combustion mode in a hydrogen fueled supersonic combustor. Int J Hydrogen Energy 2015;40(31):9815–24. http://dx.doi.org/10.1016/j.ijhydene.2015.06.011.

[67] Barlow RS, Frank JH. Effects of turbulence on species mass fractions in methane/air jet flames. In: Symposium (international) on combustion. Twenty-seventh sysposium (international) on combustion volume one, vol.27, (no.1):1998, p. 1087–95. http://dx.doi.org/10.1016/S0082-0784(98)80510-9.

[68] Barlow RS, Frank JH, Karpetis AN, Chen JY. Piloted methane/air jet flames: Transport effects and aspects of scalar structure. Combust Flame 2005;143(4):433–49. http://dx.doi.org/10.1016/j.combustflame.2005.08.017.

[69] Fedina E, Fureby C, Bulat G, Meier W. Assessment of finite rate chemistry large eddy simulation combustion models. Flow Turbul Combust 2017;99(2):385–409. http://dx.doi.org/10.1007/s10494-017-9823-0.

[70] Zhang K, Shen Y, Duwig C. Finite rate simulations and analyses of wet/distributed flame structure in swirl-stabilized combustion. Fuel 2021;289:119922. http://dx.doi.org/10.1016/j.fuel.2020.119922.

[71] Qian X, Zou C, Lu H, Yao H. Large-eddy simulation of cambridge-sandia stratified flames under high swirl. Combust Flame 2022;244:112241. http://dx.doi.org/10.1016/j.combustflame.2022.112241.

[72] Berglund M, Fedina E, Fureby C, Tegnér J, Sabel'nikov V. Finite rate chemistry large-eddy simulation of self-ignition in supersonic combustion ramjet. AIAA J 2010;48(3):540–50. http://dx.doi.org/10.2514/1.43746, Publisher: American Institute of Aeronautics and Astronautics _eprint.

[73] Fulton JA, Edwards JR, Cutler A, McDaniel J, Goyne C. Turbulence/chemistry interactions in a ramp-stabilized supersonic hydrogen–air diffusion flame. Combust Flame 2016;174:152–65. http://dx.doi.org/10.1016/j.combustflame.2016.09.017.

[74] Wang Z, Cai Z, Sun M, Wang H, Zhang Y. Large eddy simulation of the flame stabilization process in a scramjet combustor with rearwall-expansion cavity. Int J Hydrogen Energy 2016;41(42):19278–88. http://dx.doi.org/10.1016/j.ijhydene.2016.09.012.

[75] Qin F, Huang Z-w, He G-q, Wang S, Wei X-g, Liu B. Flame stabilization mechanism study in a hydrogen-fueled model supersonic combustor under different air inflow conditions. Int J Hydrogen Energy 2017;42(33):21360–70. http://dx.doi.org/10.1016/j.ijhydene.2017.06.237.

[76] Zhao M, Zhou T, Ye T, Zhu M, Zhang H. Large eddy simulation of reacting flow in a hydrogen jet into supersonic cross-flow combustor with an inlet compression ramp. Int J Hydrogen Energy 2017;42(26):16782–92. http://dx.doi.org/10.1016/j.ijhydene.2017.04.250.

[77] Huang Z-w, He G-q, Wang S, Qin F, Wei X-g, Shi L. Simulations of combustion oscillation and flame dynamics in a strut-based supersonic combustor. Int J Hydrogen Energy 2017;42(12):8278–87. http://dx.doi.org/10.1016/j.ijhydene.2016.12.142.

[78] Vincent-Randonnier A, Sabelnikov V, Ristori A, Zettervall N, Fureby C. An experimental and computational study of hydrogen–air combustion in the LAPCAT II supersonic combustor. Proc Combust Inst 2019;37(3):3703–11. http://dx.doi.org/10.1016/j.proci.2018.05.127.

[79] Xiang Z, Yang S, Xie S, Li J, Ren H. Turbulence–chemistry interaction models with finite-rate chemistry and compressibility correction for simulation of supersonic turbulent combustion. Eng Appl Comput Fluid Mech 2020;14(1):1546–61. http://dx.doi.org/10.1080/19942060.2020.1842248, Publisher: Taylor & Francis _eprint.

[80] Fooladgar E, Tóth P, Duwig C. Characterization of flameless combustion in a model gas turbine combustor using a novel post-processing tool. Combust Flame 2019;204:356–67. http://dx.doi.org/10.1016/j.combustflame.2019.03.015.

[81] Hou XS, Zhang X, Hu ZQ. Experimental and numerical study on engine fueled with different fractions of natural gas–carbon dioxide-hydrogen blends. Int J Hydrogen Energy 2019;44(11):5599–606. http://dx.doi.org/10.1016/j.ijhydene.2018.08.013.

[82] Xu L, Treacy M, Zhang Y, Aziz A, Tuner M, Bai X-S. Comparison of efficiency and emission characteristics in a direct-injection compression ignition engine fuelled with iso-octane and methanol under low temperature combustion conditions. Appl Energy 2022;312:118714. http://dx.doi.org/10.1016/j.apenergy.2022.118714.

[83] Petrova N. Turbulence-chemistry interaction models for numerical simulation of aeronautical propulsion systems [Ph.D. thesis], Ecole polytechnique X; 2015.

[84] Lysenko DA, Ertesvåg IS. Reynolds-averaged, scale-adaptive and large-eddy simulations of premixed bluff-body combustion using the eddy dissipation concept. Flow Turbul Combust 2018;100(3):721–68. http://dx.doi.org/10.1007/s10494-017-9880-4.

[85] Ivankin M, Nikolaev A, Sabelnikov V, Shiryaeva A, Talyzin V, Vlasenko V. Complex numerical-experimental investigations of combustion in model high-speed combustor ducts. Acta Astronaut 2019;158:425–37. http://dx.doi.org/10.1016/j.actaastro.2018.11.046.

[86] Petrova N, Sabelnikov V, Bertier N. Numerical simulation of a backward-facing step combustor using reynolds-averaged navier–stokes / extended partially stirred reactor model. In: Progress in propulsion physics – volume 11, Vol. 11. EDP Sciences; 2019, p. 625–56. http://dx.doi.org/10.1051/eucass/201911625.

[87] Williamson AJ, Srivastava S, Sallam KA. Validating confined flame noise simulation using external sensor. Sensors 2022;22(20):8039. http://dx.doi.org/10.3390/s22208039, Number: 20 Publisher: Multidisciplinary Digital Publishing Institute.

[88] Hosseini SE. Fundamentals of low emission flameless combustion and its applications. Elsevier; 2022, http://dx.doi.org/10.1016/C2020-0-02292-9.

[89] Sabia P, Manna MV, Ariemma GB, Sorrentino G, Ragucci R, de Joannon M. Novel insights into mild combustion processes through analyses of hysteresis behavior. Proc Combust Inst 2022. http://dx.doi.org/10.1016/j.proci.2022.08.011.

[90] Iavarone S, Parente A. NOx formation in MILD combustion: Potential and limitations of existing approaches in CFD. Front Mech Eng 2020;6. http://dx.doi.org/10.3389/fmech.2020.00013.

[91] de Joannon M, Langella G, Beretta F, Cavaliere A, Noviello C. Mild combustion: Process features and technological constrains. Combust Sci Technol 2000;153(1):33–50. http://dx.doi.org/10.1080/00102200008947249, Publisher: Taylor & Francis _eprint.

[92] Sorrentino G, Sabia P, de Joannon M, Cavaliere A, Ragucci R. The effect of diluent on the sustainability of MILD combustion in a cyclonic burner. Flow Turbul Combust 2016;96(2):449–68. http://dx.doi.org/10.1007/s10494-015-9668-3.

[93] Oldenhof E, Tummers MJ, van Veen EH, Roekaerts DJEM. Ignition kernel formation and lift-off behaviour of jet-in-hot-coflow flames. Combust Flame 2010;157(6):1167–78. http://dx.doi.org/10.1016/j.combustflame.2010.01.002.

[94] Minamoto Y, Swaminathan N, Cant SR, Leung T. Morphological and statistical features of reaction zones in MILD and premixed combustion. Combust Flame 2014;161(11):2801–14. http://dx.doi.org/10.1016/j.combustflame.2014.04.018.

[95] Minamoto Y, Dunstan T, Swaminathan N, Cant R. DNS of EGR-type turbulent flame in MILD condition. Proc Combust Inst 2013;34(2):3231–8. http://dx.doi.org/10.1016/j.proci.2012.06.041.

[96] Doan NAK. Chapter 8 - direct numerical simulations of flameless combustion. In: Hosseini SE, editor. Fundamentals of low emission flameless combustion and its applications. Academic Press; 2022, p. 221–60. http://dx.doi.org/10.1016/B978-0-323-85244-9.00002-2.

[97] Swaminathan N. Physical insights on MILD combustion from DNS. Front Mech Eng 2019;5:59. http://dx.doi.org/10.3389/fmech.2019.00059.

[98] van Oijen JA. Direct numerical simulation of autoigniting mixing layers in MILD combustion. Proc Combust Inst 2013;34(1):1163–71. http://dx.doi.org/10.1016/j.proci.2012.05.070.

[99] Göktolga MU, van Oijen JA, de Goey LPH. 3D DNS of MILD combustion: A detailed analysis of heat loss effects, preferential diffusion, and flame formation mechanisms. Fuel 2015;159:784–95. http://dx.doi.org/10.1016/j.fuel.2015.07.049.

[100] Dally BB, Karpetis AN, Barlow RS. Structure of turbulent non-premixed jet flames in a diluted hot coflow. Proc Combust Inst 2002;29(1):1147–54. http://dx.doi.org/10.1016/S1540-7489(02)80145-6.

[101] Minamoto Y, Swaminathan N. Scalar gradient behaviour in MILD combustion. Combust Flame 2014;161(4):1063–75. http://dx.doi.org/10.1016/j.combustflame.2013.10.005.

[102] Minamoto Y, Swaminathan N. Modelling paradigms for MILD combustion. Int J Adv Eng Sci Appl Math 2014;6(1):65–75. http://dx.doi.org/10.1007/s12572-014-0106-x.

[103] Minamoto Y, Swaminathan N. Subgrid scale modelling for MILD combustion. Proc Combust Inst 2015;35(3):3529–36. http://dx.doi.org/10.1016/j.proci.2014.07.025.

[104] Doan N, Swaminathan N. Analysis of markers for combustion mode and heat release in MILD combustion using DNS data. Combust Sci Technol 2019;191(5–6):1059–78. http://dx.doi.org/10.1080/00102202.2019.1610746, Publisher: Taylor & Francis _eprint.

[105] Doan NAK, Swaminathan N. Role of radicals on MILD combustion inception. Proc Combust Inst 2019;37(4):4539–46. http://dx.doi.org/10.1016/j.proci.2018.07.038.

[106] Doan NAK, Bansude S, Osawa K, Minamoto Y, Lu T, Chen JH, et al. Identification of combustion mode under MILD conditions using chemical explosive mode analysis. Proc Combust Inst 2021;38(4):5415–22. http://dx.doi.org/10.1016/j.proci.2020.06.293.

[107] Dave H, Swaminathan N, Parente A. Interpretation and characterization of MILD combustion data using unsupervised clustering informed by physics-based, domain expertise. Combust Flame 2022;240:111954. http://dx.doi.org/10.1016/j.combustflame.2021.111954.

[108] Burke SP, Schumann TEW. Diffusion flames. Ind Eng Chem 1928;20(10):998–1004. http://dx.doi.org/10.1021/ie50226a005.

[109] Howe NM, Shipman CW. A tentative model for rates of combustion in confined, turbulent flames. In: Symposium (international) on combustion. Tenth symposium (international) on combustion, vol.10, (no.1):1965, p. 1139–49. http://dx.doi.org/10.1016/S0082-0784(65)80251-X.

[110] Spalding DB. Mixing and chemical reaction in steady confined turbulent flames. In: Symposium (international) on combustion. Thirteenth symposium (international) on combustion, vol.13, (no.1):1971, p. 649–57. http://dx.doi.org/10.1016/S0082-0784(71)80067-X.

[111] Magnussen BF. The rate of combustion of soot in turbulent flames. In: Symposium (International) on Combustion. Thirteenth symposium (International) on Combustion, vol.13, (no.1):1971, p. 869–77. http://dx.doi.org/10.1016/S0082-0784(71)80088-7.

[112] Magnussen BF. An investigation into the behavior of soot in a turbulent free jet C2H2-flame. In: Symposium (international) on combustion. Fifteenth symposium (international) on combustion, vol.15, (no.1):1975, p. 1415–25. http://dx.doi.org/10.1016/S0082-0784(75)80400-0.

[113] Magnussen BF, Hjertager BH. On mathematical modeling of turbulent combustion with special emphasis on soot formation and combustion. In: Symposium (international) on combustion, Vol. 16, no. 1. 1977, p. 719–29. http://dx.doi.org/10.1016/S0082-0784(77)80366-4.

[114] Spalding DB. Development of the eddy-break-up model of turbulent combustion. In: Symposium (international) on combustion, Vol. 16, no. 1. 1977, p. 1657–63. http://dx.doi.org/10.1016/S0082-0784(77)80444-X.

[115] Meneveau C, Poinsot T. Stretching and quenching of flamelets in premixed turbulent combustion. Combust Flame 1991;86(4):311–32. http://dx.doi.org/10.1016/0010-2180(91)90126-V.

[116] Nicolleau F, Mathieu J. Eddy break-up model and fractal theory: comparisons with experiments. Int J Heat Mass Transfer 1994;37(18):2925–33. http://dx.doi.org/10.1016/0017-9310(94)90347-6.

[117] Ma A, Noseir M, Spalding D. An application of the ESCIMO theory of turbulent combustion. In: 18th aerospace sciences meeting. Pasadena,CA,U.S.A.: American Institute of Aeronautics and Astronautics; 1980, http://dx.doi.org/10.2514/6.1980-14.

[118] Magnussen BF, Hjertager BH, Olsen JG, Bhaduri D. Effects of turbulent structure and local concentrations on soot formation and combustion in C2H2 diffusion flames. In: Symposium (international) on combustion. Seventeenth symposium (international) on combustion, vol.17, (no.1):1979, p. 1383–93. http://dx.doi.org/10.1016/S0082-0784(79)80130-7.

[119] Magnussen BF. Modeling of reaction processes in turbulent flames with special emphasis on soot formation and combustion. In: Particulate carbon. Boston, MA: Springer US; 1980, p. 321–41. http://dx.doi.org/10.1007/978-1-4757-6137-5-12.

[120] Bray KNC, Moss JB. A unified statistical model of the premixed turbulent flame. Acta Astronaut 1977;4(3):291–319. http://dx.doi.org/10.1016/0094-5765(77)90053-4.

[121] Tanahashi M, Fujimura M, Miyauchi T. Coherent fine-scale eddies in turbulent premixed flames. Proc Combust Inst 2000;28(1):529–35. http://dx.doi.org/10.1016/S0082-0784(00)80252-0.

[122] Magnussen B. Modeling of NOx and soot formation by the eddy dissipation concept. In: Int. flame research foundation, 1st topic oriented technical meeting. Amsterdam, Holland; 1989, p. 17–9.

[123] Gran IR, Magnussen BF. A numerical study of a bluff-body stabilized diffusion flame. part 2. influence of combustion modeling and finite-rate chemistry. Combust Sci Technol 1996;119(1–6):191–217. http://dx.doi.org/10.1080/00102209608951999, Publisher: Taylor & Francis _eprint.

[124] Ertesvåg IS, Magnussen BF. The eddy dissipation turbulence energy cascade model. Combust Sci Technol 2000;159(1):213–35. http://dx.doi.org/10.1080/00102200008935784, Publisher: Taylor & Francis _eprint.

[125] Magnussen BF. The eddy dissipation concept: A bridge between science and technology, vol. 21. 2005, p. 25, Lisbon, Portugal.

[126] Ertesvåg IS. Scrutinizing proposed extensions to the eddy dissipation concept (EDC) at low turbulence Reynolds numbers and low damköhler numbers. Fuel 2022;309:122032. http://dx.doi.org/10.1016/j.fuel.2021.122032.

[127] Lewandowski MT, Ertesvåg IS. Analysis of the eddy dissipation concept formulation for MILD combustion modelling. Fuel 2018;224:687–700. http://dx.doi.org/10.1016/j.fuel.2018.03.110.

[128] Evans MJ, Petre C, Medwell PR, Parente A. Generalisation of the eddy-dissipation concept for jet flames with low turbulence and low Damköhler number. Proc Combust Inst 2019;37(4):4497–505. http://dx.doi.org/10.1016/j.proci.2018.06.017.

[129] Li Z, Cuoci A, Sadiki A, Parente A. Comprehensive numerical study of the adelaide jet in hot-coflow burner by means of RANS and detailed chemistry. Energy 2017;139:555–70. http://dx.doi.org/10.1016/j.energy.2017.07.132.

[130] Gran IR. Mathematical modeling and numerical simulation of chemical kinetics in turbulent combustion [Ph.D. thesis], Norway; 1994.

[131] Chomiak J. Combustion a study in theory, fact and application. Philadelphia, PA (USA): Abacus Press; 1990.

[132] Moule Y. Modélisation et simulation de la combustion dans les écoulements rapides [Ph.D. thesis], Chasseneuil-du-Poitou, Ecole nationale supérieure de mécanique et d'aérotechnique; 2013.

[133] De A, Dongre A. Assessment of turbulence-chemistry interaction models in MILD combustion regime. Flow Turbul Combust 2015;94(2):439–78. http://dx.doi.org/10.1007/s10494-014-9587-8.

[134] ANSYS. ANSYS fluent - CFD software | ANSYS. 2016.

[135] Vulis LA. Thermal regimes of combustion. New York: McGraw-Hill; 1961, OCLC, 927133.

[136] Karlsson A. Modeling auto-ignition, flame propagation and combustion in non-stationary turbulent sprays. 1995.

[137] Golovitchev VI, Nordin N, Chomiak J. Neat dimethyl ether: is it really diesel fuel of promise?. (SAE technical paper 982537). Warrendale, PA: SAE International; 1998, http://dx.doi.org/10.4271/982537, ISSN: 0148-7191, 2688-3627.

[138] Golovitchev VI. Revising "old" good models: detailed chemistry spray combustion modeling based on eddy dissipation concept. SAE Technical paper 2001-24-0002, Warrendale, PA: SAE International; 2001, http://dx.doi.org/10.4271/2001-24-0002, ISSN: 0148-7191, 2688-3627.

[139] Gonzalez M, Borghi R. A Lagrangian intermittent model for turbulent combustion; theoretical basis and comparisons with experiments. In: Durst F, Launder BE, Reynolds WC, Schmidt FW, Whitelaw JH, editors. Turbulent shear flows 7. Berlin, Heidelberg: Springer; 1991, p. 293–311. http://dx.doi.org/10.1007/978-3-642-76087-7-22.

[140] Fureby C. Comparison of flamelet and finite rate chemistry LES for premixed turbulent combustion. In: 45th AIAA aerospace sciences meeting and exhibit. American Institute of Aeronautics and Astronautics; 2007, http://dx.doi.org/10.2514/6.2007-1413, _eprint: https://arc.aiaa.org/doi/pdf/10.2514/6.2007-1413.

[141] Marzouk OA, Huckaby ED. A comparative study of eight finite-rate chemistry kinetics for co/H2 combustion. Eng Appl Comput Fluid Mech 2010;4(3):331–56. http://dx.doi.org/10.1080/19942060.2010.11015322, Publisher: Taylor & Francis _eprint.

[142] Duwig C, Nogenmyr K-J, Chan C-k, Dunn MJ. Large Eddy simulations of a piloted lean premix jet flame using finite-rate chemistry. Combust Theory Model 2011;15(4):537–68. http://dx.doi.org/10.1080/13647830.2010.548531, Publisher: Taylor & Francis _eprint.

[143] Duwig C, Iudiciani P. Large Eddy simulation of turbulent combustion in a stagnation point reverse flow combustor using detailed chemistry. Fuel 2014;123:256–73. http://dx.doi.org/10.1016/j.fuel.2014.01.072.

[144] Weller HG, Tabor G, Jasak H, Fureby C. A tensorial approach to computational continuum mechanics using object-oriented techniques. Comput Phys 1998;12(6):620–31. http://dx.doi.org/10.1063/1.168744, Publisher: American Institute of Physics.

[145] Grinstein FF, Kailasanath K. Three-dimensional numerical simulations of unsteady reactive square jets. Combust Flame 1995;100(1):2–10. http://dx.doi.org/10.1016/0010-2180(94)00095-A.

[146] Moule Y, Sabel'nikov V, Mura A. Modelling of self-ignition processes in supersonic non premixed coflowing jets based on a PaSR approach. In: 17th AIAA international space planes and hypersonic systems and technologies conference. American Institute of Aeronautics and Astronautics; 2011, http://dx.doi.org/10.2514/6.2011-2396, _eprint: https://arc.aiaa.org/doi/pdf/10.2514/6.2011-2396.

[147] Le Pichon T, Sabel'nikov V, Moule Y, Cochet A. Assessment of a partially stirred reactor combustion model to predict the lean blow-out limit of a ramjet combustor. In: 18th AIAA/3AF international space planes and hypersonic systems and technologies conference. American Institute of Aeronautics and Astronautics; 2012, http://dx.doi.org/10.2514/6.2012-5962, _eprint: https://arc.aiaa.org/doi/pdf/10.2514/6.2012-5962.

[148] Moule Y, Sabelnikov V, Mura A. Highly resolved numerical simulation of combustion in supersonic hydrogen–air coflowing jets. Combust Flame 2014;161(10):2647–68. http://dx.doi.org/10.1016/j.combustflame.2014.04.011.

[149] Moule Y, Sabel'nikov V, Mura A, Smart M. Computational fluid dynamics investigation of a mach 12 scramjet engine. J Propuls Power 2014;30(2):461–73. http://dx.doi.org/10.2514/1.B34992, Publisher: American Institute of Aeronautics and Astronautics _eprint.

[150] Ferrarotti M, Li Z, Parente A. On the role of mixing models in the simulation of MILD combustion using finite-rate chemistry combustion models. Proc Combust Inst 2019;37(4):4531–8. http://dx.doi.org/10.1016/j.proci.2018.07.043.

[151] Ferrarotti M, Fürst M, Cresci E, de Paepe W, Parente A. Key modeling aspects in the simulation of a quasi-industrial 20 kW moderate or intense low-oxygen dilution combustion chamber. Energy Fuels 2018;32(10):10228–41. http://dx.doi.org/10.1021/acs.energyfuels.8b01064, Publisher: American Chemical Society.

[152] Iavarone S, Cafiero M, Ferrarotti M, Contino F, Parente A. A multiscale combustion model formulation for NOx predictions in hydrogen enriched jet flames. Int J Hydrogen Energy 2019;44(41):23436–57. http://dx.doi.org/10.1016/j.ijhydene.2019.07.019.

[153] Amaduzzi R, Ferrarotti M, Parente A. Strategies for hydrogen-enriched methane flameless combustion in a quasi-industrial furnace. Front Energy Res 2021;8.

[154] Péquin A, Iavarone S, Malpica Galassi R, Parente A. The partially stirred reactor model for combustion closure in large eddy simulations: Physical principles, sub-models for the cell reacting fraction, and open challenges. Phys Fluids 2022;34(5):055122. http://dx.doi.org/10.1063/5.0090970, Publisher: American Institute of Physics.

[155] Senouci M, Bounif A, Abidat M, Belkaid NM, Mansour C, Gokalp I. Transported-PDF (IEM, EMST) micromixing models in a hydrogen-air nonpremixed turbulent flame. Acta Mech 2013;224(12):3111–24. http://dx.doi.org/10.1007/s00707-013-0911-5.

[156] Raman V, Pitsch H. A consistent LES/filtered-density function formulation for the simulation of turbulent flames with detailed chemistry. Proc Combust Inst 2007;31(2):1711–9. http://dx.doi.org/10.1016/j.proci.2006.07.152.

[157] Ye IK. Investigation of the scalar variance and scalar dissipation rate in URANS and LES [Ph.D. thesis], University of Waterloo; 2011, URL https://uwspace.uwaterloo.ca/handle/10012/5801. Accepted: 2011-02-22T15:32:52Z.

[158] Amaduzzi R, Péquin A, Parente A. Chapter 9 - large eddy simulation of MILD combustion. In: Hosseini SE, editor. Fundamentals of low emission flameless combustion and its applications. Academic Press; 2022, p. 261–310. http://dx.doi.org/10.1016/B978-0-323-85244-9.00005-8.

[159] Li Z, Cuoci A, Parente A. Large eddy simulation of MILD combustion using finite rate chemistry: Effect of combustion sub-grid closure. Proc Combust Inst 2019;37(4):4519–29. http://dx.doi.org/10.1016/j.proci.2018.09.033.

[160] Iavarone S, Péquin A, Chen ZX, Doan NAK, Swaminathan N, Parente A. An a priori assessment of the partially stirred reactor (PaSR) model for MILD combustion. Proc Combust Inst 2021;38(4):5403–14. http://dx.doi.org/10.1016/j.proci.2020.06.234.

[161] Wartha E-M, Bösenhofer M, Harasek M. Characteristic chemical time scales for reactive flow modeling. Combust Sci Technol 2021;193(16):2807–32. http://dx.doi.org/10.1080/00102202.2020.1760257, Publisher: Taylor & Francis _eprint.

[162] Correa SM. Turbulence-chemistry interactions in the intermediate regime of premixed combustion. Combust Flame 1993;93(1):41–60. http://dx.doi.org/10.1016/0010-2180(93)90083-F.

[163] Correa SM. Models for high-intensity turbulent combustion. Comput Syst Eng 1994;5(2):135–45. http://dx.doi.org/10.1016/0956-0521(94)90045-0.

[164] Chen J-Y. Stochastic modeling of partially stirred reactors. Combust Sci Technol 1997;122(1–6):63–94. http://dx.doi.org/10.1080/00102209708935605, Publisher: Taylor & Francis _eprint.

[165] Bhave A, Kraft M. Partially stirred reactor model: Analytical solutions and numerical convergence study of a PDF/Monte Carlo method. SIAM J Sci Comput 2006. http://dx.doi.org/10.1137/S1064827502411328, Publisher: Society for Industrial and Applied Mathematics.

[166] Villermaux J. Macro and micromixing phenomena in chemical reactors. In: Chemical reactor design and technology. Dordrecht: Springer Netherlands; 1986, p. 191–244. http://dx.doi.org/10.1007/978-94-009-4400-8-6.

[167] Borghi R. Turbulent combustion modelling. Prog Energy Combust Sci 1988;14(4):245–92. http://dx.doi.org/10.1016/0360-1285(88)90015-9.

[168] Borghi R, Gonzalez M. Applications of Lagrangian models to turbulent combustion. Combust Flame 1986;63(1):239–50. http://dx.doi.org/10.1016/0010-2180(86)90124-0.

[169] Trisjono P, Pitsch H. Systematic analysis strategies for the development of combustion models from DNS: A review. Flow Turbul Combust 2015;95(2):231–59. http://dx.doi.org/10.1007/s10494-015-9645-x.

[170] Oldenhof E, Tummers MJ, van Veen EH, Roekaerts DJEM. Role of entrainment in the stabilisation of jet-in-hot-coflow flames. Combust Flame 2011;158(8):1553–63. http://dx.doi.org/10.1016/j.combustflame.2010.12.018.

[171] Medwell PR, Kalt PAM, Dally BB. Simultaneous imaging of OH, formaldehyde, and temperature of turbulent nonpremixed jet flames in a heated and diluted coflow. Combust Flame 2007;148(1):48–61. http://dx.doi.org/10.1016/j.combustflame.2006.10.002.

[172] Medwell PR, Kalt PAM, Dally BB. Imaging of diluted turbulent ethylene flames stabilized on a jet in hot coflow (JHC) burner. Combust Flame 2008;152(1):100–13. http://dx.doi.org/10.1016/j.combustflame.2007.09.003.

[173] Ye J, Medwell PR, Evans MJ, Dally BB. Characteristics of turbulent n-heptane jet flames in a hot and diluted coflow. Combust Flame 2017;183:330–42. http://dx.doi.org/10.1016/j.combustflame.2017.05.027.

[174] Ihme M, Zhang J, He G, Dally B. Large-eddy simulation of a jet-in-hot-coflow burner operating in the oxygen-diluted combustion regime. Flow Turbul Combust 2012;89(3):449–64. http://dx.doi.org/10.1007/s10494-012-9399-7.

[175] De A, Oldenhof E, Sathiah P, Roekaerts D. Numerical simulation of delft-jet-in-hot-coflow (DJHC) flames using the eddy dissipation concept model for turbulence–chemistry interaction. Flow Turbul Combust 2011;87(4):537–67. http://dx.doi.org/10.1007/s10494-011-9337-0.

[176] Aminian J, Galletti C, Shahhosseini S, Tognotti L. Numerical investigation of a MILD combustion burner: Analysis of mixing field, chemical kinetics and turbulence-chemistry interaction. Flow Turbul Combust 2012;88(4):597–623. http://dx.doi.org/10.1007/s10494-012-9386-z.

[177] Evans MJ, Medwell PR, Tian ZF. Modeling lifted jet flames in a heated coflow using an optimized eddy dissipation concept model. Combust Sci Technol 2015;187(7):1093–109. http://dx.doi.org/10.1080/00102202.2014.1002836, Publisher: Taylor & Francis _eprint.

[178] Mardani A. Optimization of the eddy dissipation concept (EDC) model for turbulence-chemistry interactions under hot diluted combustion of CH4/H2. Fuel 2017;191:114–29. http://dx.doi.org/10.1016/j.fuel.2016.11.056.

[179] Aminian J, Galletti C, Tognotti L. Extended EDC local extinction model accounting finite-rate chemistry for MILD combustion. Fuel 2016;165:123–33. http://dx.doi.org/10.1016/j.fuel.2015.10.041.

[180] Farokhi M, Birouk M. A hybrid EDC/Flamelet approach for modelling biomass combustion of grate-firing furnace. Combust Theory Model 2019;23(4):716–47. http://dx.doi.org/10.1080/13647830.2019.1587177, Publisher: Taylor & Francis _eprint.

[181] Barlow RS, Karpetis AN. Scalar length scales and spatial averaging effects in turbulent piloted methane/air jet flames. Proc Combust Inst 2005;30(1):673–80. http://dx.doi.org/10.1016/j.proci.2004.08.139.

[182] Farokhi M, Birouk M. Assessment of fractal/wrinkling theories for describing turbulent reacting fine structures under MILD combustion regimes. Combust Sci Technol 2021;193(10):1798–825. http://dx.doi.org/10.1080/00102202.2020.1715963, Publisher: Taylor & Francis _eprint.

[183] Mardani A, Karimi Motaalegh Mahalegi H. Hydrogen enrichment of methane and syngas for MILD combustion. Int J Hydrogen Energy 2019;44(18):9423–37. http://dx.doi.org/10.1016/j.ijhydene.2019.02.072.

[184] Mardani A, Nazari A. Dynamic adjustment of the eddy dissipation concept model for turbulent/combustion interactions in mixed combustion regimes. Combust Flame 2022;241:111873. http://dx.doi.org/10.1016/j.combustflame.2021.111873.

[185] Romero-Anton N, Huang X, Bao H, Martin-Eskudero K, Salazar-Herran E, Roekaerts D. New extended eddy dissipation concept model for flameless combustion in furnaces. Combust Flame 2020;220:49–62. http://dx.doi.org/10.1016/j.combustflame.2020.06.025.

[186] Romero-Anton N, Martin-Escudero K, Ren M, Azkorra-Larrinaga Z. Consideration of the interactions between the reaction zones in the new extended eddy dissipation concept model. Comput & Fluids 2022;233:105203. http://dx.doi.org/10.1016/j.compfluid.2021.105203.

[187] He D, Yu Y, Kuang Y, Wang C. Analysis of EDC constants for predictions of methane MILD combustion. Fuel 2022;324:124542. http://dx.doi.org/10.1016/j.fuel.2022.124542.

[188] Lewandowski MT, Parente A, Pozorski J. Generalised eddy dissipation concept for MILD combustion regime at low local Reynolds and Damköhler numbers. part 1: Model framework development. Fuel 2020;278:117743. http://dx.doi.org/10.1016/j.fuel.2020.117743.

[189] Lewandowski MT, Li Z, Parente A, Pozorski J. Generalised eddy dissipation concept for MILD combustion regime at low local Reynolds and damköhler numbers. part 2: Validation of the model. Fuel 2020;278:117773. http://dx.doi.org/10.1016/j.fuel.2020.117773.

[190] Ferrarotti M, Amaduzzi R, Bascherini D, Galletti C, Parente A. Heat release rate markers for the adelaide jet in hot coflow flame. Front Mech Eng 2020. http://dx.doi.org/10.3389/fmech.2020.00005, Publisher: Frontiers.

[191] Li Z, Galassi RM, Ciottoli PP, Parente A, Valorani M. Characterization of jet-in-hot-coflow flames using tangential stretching rate. Combust Flame 2019;208:281–98. http://dx.doi.org/10.1016/j.combustflame.2019.06.023.

[192] Li Z, Ferrarotti M, Cuoci A, Parente A. Finite-rate chemistry modelling of non-conventional combustion regimes using a partially-stirred reactor closure: Combustion model formulation and implementation details. Appl Energy 2018;225:637–55. http://dx.doi.org/10.1016/j.apenergy.2018.04.085.

[193] Amaduzzi R, Bertolino A, Özden A, Galassi RM, Parente A. Impact of scalar mixing uncertainty on the predictions of reactor-based closures: Application to a lifted methane/air jet flame. Proc Combust Inst 2022. http://dx.doi.org/10.1016/j.proci.2022.06.028.

[194] Najm HN. Uncertainty quantification and polynomial chaos techniques in computational fluid dynamics. Annu Rev Fluid Mech 2009;41(1):35–52. http://dx.doi.org/10.1146/annurev.fluid.010908.165248, _eprint: http://dx.doi.org/10.1146/annurev.fluid.010908.165248.

[195] Iavarone S. Uncertainty quantification for scale-bridging modeling of multiphase reactive flows [Ph.D. thesis], Université libre de Bruxelles, Ecole polytechnique de Bruxelles, Vrije Universiteit Brussel; 2019.

[196] Cabra R, Chen JY, Dibble RW, Karpetis AN, Barlow RS. Lifted methane–air jet flames in a vitiated coflow. Combust Flame 2005;143(4):491–506. http://dx.doi.org/10.1016/j.combustflame.2005.08.019.

[197] Lam SH, Goussis DA. Understanding complex chemical kinetics with computational singular perturbation. In: Symposium (international) on combustion, Vol. 22, no. 1. 1989, p. 931–41. http://dx.doi.org/10.1016/S0082-0784(89)80102-X.

[198] Valorani M, Paolucci S. The G-scheme: A framework for multi-scale adaptive model reduction. J Comput Phys 2009;228(13):4665–701. http://dx.doi.org/10.1016/j.jcp.2009.03.011.

[199] Valorani M, Ciottoli PP, Galassi RM. Tangential stretching rate (TSR) analysis of non premixed reactive flows. Proc Combust Inst 2017;36(1):1357–67. http://dx.doi.org/10.1016/j.proci.2016.09.008.

[200] Valorani M, Ciottoli PP, Malpica Galassi R, Paolucci S, Grenga T, Martelli E. Enhancements of the G-scheme framework. Flow Turbul Combust 2018;101(4):1023–33. http://dx.doi.org/10.1007/s10494-018-9942-2.

[201] Peters N. Multiscale combustion and turbulence. Proc Combust Inst 2009;32(1):1–25. http://dx.doi.org/10.1016/j.proci.2008.07.044.

[202] Sutherland J. Evaluation of mixing and reaction models for large-eddy simulation of nonpremixed combustion using direct numerical simulation [Ph.D. thesis], Department of Chemical and Fuels Engineering: University of Utah; 2004.

[203] Quadarella E, Péquin A, Stagni A, Parente A, Faravelli T, Im HG. A generalized partially stirred reactor model for turbulent closure. Proc Combust Inst 2022. http://dx.doi.org/10.1016/j.proci.2022.08.061, S1540748922003583.

[204] Veríssimo AS, Rocha AMA, Costa M. Operational, combustion, and emission characteristics of a small-scale combustor. Energy Fuels 2011;25(6):2469–80. http://dx.doi.org/10.1021/ef200258t, Publisher: American Chemical Society.

[205] Chinnici A, Nathan GJ, Dally BB. Combined solar energy and combustion of hydrogen-based fuels under MILD conditions. Int J Hydrogen Energy 2018;43(43):20086–100. http://dx.doi.org/10.1016/j.ijhydene.2018.09.027.

[206] Sorrentino, Sabia, De Joannon, Cavaliere, Ragucci. Design and development of a lab-scale burner for mild/flameless combustion. Chem Eng Trans 2015;43:883–8. http://dx.doi.org/10.3303/CET1543148.

[207] Castela M, Veríssimo AS, Rocha AMA, Costa M. Experimental study of the combustion regimes occurring in a laboratory combustor. Combust Sci Technol 2012;184(2):243–58. http://dx.doi.org/10.1080/00102202.2011.630592, Publisher: Taylor & Francis _eprint.

[208] Xing F, Kumar A, Huang Y, Chan S, Ruan C, Gu S, et al. Flameless combustion with liquid fuel: A review focusing on fundamentals and gas turbine application. Appl Energy 2017;193:28–51. http://dx.doi.org/10.1016/j.apenergy.2017.02.010.

[209] Chinnici A, Nathan GJ, Dally BB. An experimental study of the stability and performance characteristics of a hybrid solar receiver combustor operated in the MILD combustion regime. Proc Combust Inst 2019;37(4):5687–95. http://dx.doi.org/10.1016/j.proci.2018.05.099.

[210] Chinnici A, Tian ZF, Lim JH, Nathan GJ, Dally BB. Thermal performance analysis of a syngas-fuelled hybrid solar receiver combustor operated in the MILD combustion regime. Combust Sci Technol 2019;191(1):2–17. http://dx.doi.org/10.1080/00102202.2018.1452381, Publisher: Taylor & Francis _eprint.

[211] Sorrentino G, Sabia P, de Joannon M, Bozza P, Ragucci R. Influence of preheating and thermal power on cyclonic burner characteristics under mild combustion. Fuel 2018;233:207–14. http://dx.doi.org/10.1016/j.fuel.2018.06.049.

[212] Graça M, Duarte A, Coelho PJ, Costa M. Numerical simulation of a reversed flow small-scale combustor. Fuel Process Technol 2013;107:126–37. http://dx.doi.org/10.1016/j.fuproc.2012.06.028.

[213] Li Z, Tomasch S, Chen ZX, Parente A, Ertesvåg IS, Swaminathan N. Study of MILD combustion using LES and advanced analysis tools. Proc Combust Inst 2021;38(4):5423–32. http://dx.doi.org/10.1016/j.proci.2020.06.298.

[214] Parente A, Sutherland JC, Dally BB, Tognotti L, Smith PJ. Investigation of the MILD combustion regime via principal component analysis. Proc Combust Inst 2011;33(2):3333–41. http://dx.doi.org/10.1016/j.proci.2010.05.108.

[215] D'Alessio G, Parente A, Stagni A, Cuoci A. Adaptive chemistry via pre-partitioning of composition space and mechanism reduction. Combust Flame 2020;211:68–82. http://dx.doi.org/10.1016/j.combustflame.2019.09.010.

[216] Amaduzzi R, Ceriello G, Ferrarotti M, Sorrentino G, Parente A. Evaluation of modeling approaches for MILD combustion systems with internal recirculation. Front Mech Eng 2020;6.

[217] Fang X, Wang H, Liu G, Tian X, Ding G, Zhang H. Industry application of digital twin: From concept to implementation. Int J Adv Manuf Technol 2022;121(7):4289–312. http://dx.doi.org/10.1007/s00170-022-09632-z.

[218] Aversano G, Bellemans A, Li Z, Coussement A, Gicquel O, Parente A. Application of reduced-order models based on PCA & Kriging for the development of digital twins of reacting flow applications. Comput Chem Eng 2019;121:422–41. http://dx.doi.org/10.1016/j.compchemeng.2018.09.022.

[219] Aversano G, Ferrarotti M, Parente A. Digital twin of a combustion furnace operating in flameless conditions: Reduced-order model development from CFD simulations. Proc Combust Inst 2021;38(4):5373–81. http://dx.doi.org/10.1016/j.proci.2020.06.045.

[220] Procacci A, Amaduzzi R, Coussement A, Parente A. Adaptive digital twins of combustion systems using sparse sensing strategies. Proc Combust Inst 2022. http://dx.doi.org/10.1016/j.proci.2022.07.029.

[221] Procacci A, Cafiero M, Sharma S, Kamal MM, Coussement A, Parente A. Digital twin for experimental data fusion applied to a semi-industrial furnace fed with H2-rich fuel mixtures. Energies 2023;16(2):662. http://dx.doi.org/10.3390/en16020662, Number: 2 Publisher: Multidisciplinary Digital Publishing Institute.

[222] Parente A, Sutherland JC. Principal component analysis of turbulent combustion data: Data pre-processing and manifold sensitivity. Combust Flame 2013;160(2):340–50. http://dx.doi.org/10.1016/j.combustflame.2012.09.016.

[223] Zdybał K, Armstrong E, Parente A, Sutherland JC. PCAfold: Python software to generate, analyze and improve PCA-derived low-dimensional manifolds. SoftwareX 2020;12:100630. http://dx.doi.org/10.1016/j.softx.2020.100630.

[224] Weber R, Orsino S, Lallemant N, Verlaan A. Combustion of natural gas with high-temperature air and large quantities of flue gas. Proc Combust Inst 2000;28(1):1315–21. http://dx.doi.org/10.1016/S0082-0784(00)80345-8.

[225] Weber R, Smart JP, Kamp Wv. On the (MILD) combustion of gaseous, liquid, and solid fuels in high temperature preheated air. Proc Combust Inst 2005;30(2):2623–9. http://dx.doi.org/10.1016/j.proci.2004.08.101.

[226] Landfahrer M, Schluckner C, Gerhardter H, Zmek T, Klarner J, Hochenauer C. Numerical model incorporating different oxidizer in a reheating furnace fired with natural gas. Fuel 2020;268:117185. http://dx.doi.org/10.1016/j.fuel.2020.117185.

[227] Mayr B, Prieler R, Demuth M, Moderer L, Hochenauer C. CFD analysis of a pusher type reheating furnace and the billet heating characteristic. Appl Therm Eng 2017;115:986–94. http://dx.doi.org/10.1016/j.applthermaleng.2017.01.028.

[228] Tan P, Ma L, Fang Q, Zhang C, Chen G. Application of different combustion models for simulating the co-combustion of sludge with coal in a 100 MW tangentially coal-fired utility boiler. Energy Fuels 2016;30(3):1685–92. http://dx.doi.org/10.1021/acs.energyfuels.5b02236, Publisher: American Chemical Society.

[229] Fang Q, Musa AAB, Wei Y, Luo Z, Zhou H. Numerical simulation of multi-fuel combustion in a 200 MW tangentially fired utility boiler. Energy Fuels 2012;26(1):313–23. http://dx.doi.org/10.1021/ef201149p, Publisher: American Chemical Society.

[230] Kang Z, Ding X. Numerical analysis on combustion process and sodium transformation behavior in a 660 MW supercritical face-fired boiler purely burning high sodium content Zhundong coal. J Energy Inst 2020;93(2):450–62. http://dx.doi.org/10.1016/j.joei.2019.07.006.

[231] Schaffel-Mancini N, Mancini M, Szlek A, Weber R. Novel conceptual design of a supercritical pulverized coal boiler utilizing high temperature air combustion (HTAC) technology. Energy 2010;35(7):2752–60. http://dx.doi.org/10.1016/j.energy.2010.02.014.

[232] Nadziakiewicz J, Kozioł M. Co-combustion of sludge with coal. Appl Energy 2003;75(3):239–48. http://dx.doi.org/10.1016/S0306-2619(03)00037-0.

[233] Perrone D, Castiglione T, Klimanek A, Morrone P, Amelio M. Numerical simulations on oxy-MILD combustion of pulverized coal in an industrial boiler. Fuel Process Technol 2018;181:361–74. http://dx.doi.org/10.1016/j.fuproc.2018.09.001.

[234] Zhao J, Ma L, Zayed ME, Elsheikh AH, Li W, Yan Q, et al. Industrial reheating furnaces: A review of energy efficiency assessments, waste heat recovery potentials, heating process characteristics and perspectives for steel industry. Process Saf Environ Protect 2021;147:1209–28. http://dx.doi.org/10.1016/j.psep.2021.01.045.

[235] Chen JH. Petascale direct numerical simulation of turbulent combustion—fundamental insights towards predictive models. Proc Combust Inst 2011;33(1):99–123. http://dx.doi.org/10.1016/j.proci.2010.09.012.

[236] Shamooni A, Cuoci A, Faravelli T, Sadiki A. An a priori DNS analysis of scale similarity based combustion models for LES of non-premixed jet flames. Flow Turbul Combust 2020;104(2):605–24. http://dx.doi.org/10.1007/s10494-019-00099-9.

[237] Freitas RS, Péquin A, Galassi RM, Attili A, Parente A. Model identification in reactor-based combustion closures using sparse symbolic regression. Combust Flame 2023;255:112925. http://dx.doi.org/10.1016/j.combustflame.2023.112925.

[238] Péquin A. Direct numerical simulation analysis of the partially stirred reactor model for turbulent reacting flows. 2023, http://dx.doi.org/10.13140/RG.2.2.24133.83688, Publisher: Unpublished.

[239] Martinez-Sanchis D, Sternin A, Shvab J, Haidn O, Hu X. An eddy dissipation concept performance study for space propulsion applications. Aerospace 2022;9(9):476. http://dx.doi.org/10.3390/aerospace9090476, Number: 9 Publisher: Multidisciplinary Digital Publishing Institute.

[240] Jigjid K, Minamoto Y, Doan NAK, Tanahashi M. SGS reaction rate modelling for MILD combustion based on machine-learning combustion mode classification: Development and a priori study. Proc Combust Inst 2022. http://dx.doi.org/10.1016/j.proci.2022.07.020.

[241] Péquin A, Iavarone S, Malpica Galassi R, Parente A. Supervised clustering for optimal sub-model selection in reactor-based models. Flow Turbul Combust 2023. http://dx.doi.org/10.1007/s10494-023-00442-1.

[242] Brunton SL, Kutz JN. Data-driven science and engineering: machine learning, dynamical systems, and control. 1st ed.. Cambridge University Press; 2019, http://dx.doi.org/10.1017/9781108380690.

[243] Ihme M, Chung WT, Mishra AA. Combustion machine learning: Principles, progress and prospects. Prog Energy Combust Sci 2022;91:101010. http://dx.doi.org/10.1016/j.pecs.2022.101010.

[244] Swaminathan N, Parente A, editors. Machine learning and its application to reacting flows: ML and combustion. Lecture notes in energy, vol. 44, Cham: Springer International Publishing; 2023, http://dx.doi.org/10.1007/978-3-031-16248-0.

[245] Xing V, Lapeyre C, Jaravel T, Poinsot T. Generalization capability of convolutional neural networks for progress variable variance and reaction rate subgrid-scale modeling. Energies 2021;14(16):5096. http://dx.doi.org/10.3390/en14165096.

[246] Lapeyre CJ, Misdariis A, Cazard N, Veynante D, Poinsot T. Training convolutional neural networks to estimate turbulent sub-grid scale reaction rates. Combust Flame 2019;203:255–64. http://dx.doi.org/10.1016/j.combustflame.2019.02.019.

[247] LeCun Y, Bengio Y, Hinton G. Deep learning. Nature 2015;521(7553):436–44. http://dx.doi.org/10.1038/nature14539, Number: 7553 Publisher: Nature Publishing Group.

[248] Chen ZX, Iavarone S, Ghiasi G, Kannan V, D'Alessio G, Parente A, et al. Application of machine learning for filtered density function closure in MILD combustion. Combust Flame 2021;225:160–79. http://dx.doi.org/10.1016/j.combustflame.2020.10.043.

[249] Nakazawa R, Minamoto Y, Inoue N, Tanahashi M. Species reaction rate modelling based on physics-guided machine learning. Combust Flame 2022;235:111696. http://dx.doi.org/10.1016/j.combustflame.2021.111696.

[250] Brunton SL, Proctor JL, Kutz JN. Discovering governing equations from data by sparse identification of nonlinear dynamical systems. Proc Natl Acad Sci 2016;113(15):3932–7. http://dx.doi.org/10.1073/pnas.1517384113.

[251] Law CK. Combustion physics. Cambridge, New York: Cambridge University Press; 2006, OCLC, ocm65978625.